In vivo and *ex vivo* vessel wall MRI of the circle of Willis

Anita Harteveld

***In vivo* and *ex vivo* vessel wall MRI of the circle of Willis**

PhD thesis, Utrecht University, The Netherlands

ISBN: 978-90-393-6775-9
Cover design: Proefschriftmaken
Lay-out: Roy Sanders and Anita Harteveld
Printed by: Proefschriftmaken

In vivo and *ex vivo* vessel wall MRI of the circle of Willis

In vivo en *ex vivo* MRI-metingen
van de vaatwand van de hersenslagaders
(met een samenvatting in het Nederlands)

Proefschrift

ter verkrijging van de graad van doctor aan de Universiteit Utrecht op
gezag van de rector magnificus, prof.dr. G.J. van der Zwaan, ingevolge
het besluit van het college voor promoties
in het openbaar te verdedigen
op dinsdag 30 mei 2017 des middags te 2.30 uur

door

Anna Adriaantje Harteveld
geboren op 28 februari 1985 te Rotterdam

Promotoren:	Prof.dr. J. Hendrikse Prof.dr. P.R. Luijten
Copromotoren:	Dr. A.G. van der Kolk Dr.ir. J.J.M. Zwanenburg

This research was supported by the Netherlands Organization for Scientific Research (NWO) under grant n°91712322 and the European Research Council under grant n°637024

Financial support by the Dutch Heart Foundation for the publication of this thesis is gratefully acknowledged

Additional financial support was generously provided by Philips Healthcare

‘Inch by inch
play by play
till we’re finished.’

~ Al Pacino (movie *Any Given Sunday*)

Contents

Chapter 1

General introduction

Ischemic stroke

Stroke is among the leading causes of death worldwide, and a major global cause of (long-term) disability in adults.[1-4] There are two main pathologic types of stroke: ischemic and hemorrhagic (intracerebral or subarachnoid) stroke. Ischemic stroke, the most common type of stroke accounting for 87% of all strokes[1], is caused by the occlusion or stenosis of an artery supplying blood to the brain. Sometimes, an artery is only temporarily blocked causing transient stroke symptoms (typically lasting < 1h) without evidence of acute ischemic stroke. This is referred to as a transient ischemic attack (TIA). Clinical symptoms of stroke are highly dependent on the brain region that is supplied by blood from the blocked cerebral artery. Ischemic strokes are most common in the territory of the anterior circulation, accounting for approximately 70% of all cases.[5,6] The TOAST classification system[7] has been developed for diagnosis of ischemic stroke subtype, including five categories mainly based on etiology: (1) large-artery atherosclerosis, (2) cardioembolism, (3) small-artery occlusion (lacune), (4) stroke of other determined etiology, and (5) stroke of undetermined etiology. Diagnosis are based on clinical features and on data collected by tests such as brain imaging (CT/MRI).[7] Identifying the cause of ischemic stroke is of great clinical importance, not only for deciding which treatment options are best for the individual patient, but also with regard to possible prevention of future ischemic events, both recurrent and new. However, in current clinical practice it can be difficult to determine the cause of ischemic stroke, with many stroke patients being diagnosed with an undetermined cause.

Imaging of intracranial arteries

For diagnosis of stroke secondary to large-artery atherosclerosis conventional imaging techniques, like computed tomography angiography (CTA) or magnetic resonance angiography (MRA), are used to detect a significant (>50%) stenosis or occlusion of an appropriate intracranial or extracranial artery. Conventional imaging techniques are based on visualizing the lumen of the intracranial vasculature, thereby giving indirect information about underlying vessel wall abnormalities

caused by atherosclerosis. Due to compensatory arterial remodeling, in which the luminal diameter remains equal despite the presence of an underlying atheroma[8], these conventional techniques may result in underestimation of the extent of intracranial atherosclerosis[9,10]. Intracranial atherosclerosis has been established as a major risk factor for ischemic stroke, and its presence is associated with an increased risk of stroke recurrence.[11-14] Development of atherosclerotic lesions occurs silently over a long period, before they become symptomatic. Therefore, early detection of atherosclerotic lesions and a better understanding of the role of intracranial atherosclerosis in the development of cerebral ischemic events necessitates an imaging technique that enables direct visualization of the intracranial vessel wall.

Intracranial vessel wall MRI

MRI, with its superior soft tissue contrast, has already been used extensively for visualization of extracranial arterial vessel walls.[15-18] In recent years, also several MRI sequences have been developed for direct evaluation of the intracranial vessel wall and its pathology *in vivo*.[19] These MRI sequences enable detection of intracranial vessel wall abnormalities, including those that have not yet caused luminal narrowing.[20,21] Intracranial vessel wall MRI is likely a useful addition to conventional imaging to differentiate between causes of intracranial arterial narrowing, and to identify symptomatic nonstenotic disease of the intracranial arteries.[22,23] For each TOAST subtype, different expected vessel wall abnormalities have been proposed.[19]

There are several technical requirements for intracranial vessel wall MRI that need to be met for proper assessment of the major arteries of the circle of Willis and its primary branches.[19,23] First of all, both black blood and complete CSF suppression are necessary for clear visualization of the inner and outer boundary of the vessel wall with highest image contrast. Also, a whole brain sequence with isotropic spatial resolution is preferred, enabling reconstructions to assess all major arteries of the circle of Willis and its branches with their tortuous orientations. Furthermore, the intracranial vessel walls are typically very thin (<1.0 mm), which requires a high spatial resolution. Therefore, intracranial vessel wall MRI has been

performed mainly on 3T and 7T field strengths. At these higher magnetic field strengths the increased signal-to-noise (SNR) and contrast-to-noise ratios (CNR) can be exploited to most closely approximate the technical requirements within reasonable scan times to clearly show the thin arterial vessel walls.

The research field devoted to visualization of the intracranial vessel wall with high-resolution vessel wall MRI has seen a tremendous growth in the last few years. Intracranial vessel wall MR sequences are already used on a clinical basis at many centers. However, considerable gaps in knowledge still remain.[23] Currently, the main limitation of intracranial vessel wall MRI is the lack of validation of *in vivo* imaging findings with a gold standard (histology), due to poor accessibility of the intracranial arteries. For usability and translation of vessel wall imaging findings to clinical practice, this validation step is essential. As a first step towards MR validation, studies can be performed using post-mortem circle of Willis specimens.[24,25] Important other topics that require further investigation are for instance the identification and characterization of possible culprit lesions. Also, the exact mechanism and meaning of contrast enhancement of the intracranial vessel wall is still largely unknown. Furthermore, intracranial vessel wall MR sequences have been developed mainly at 3T and 7T. However, a head-to-head comparison between both field strengths to investigate potential differences in vessel wall visualization and lesion detection has not been performed yet. Also, a direct comparison of vessel wall lesion burden and contrast enhancement between symptomatic patients and healthy volunteers to further understand the pathogenesis and natural history of intracranial atherosclerosis is still lacking.

Outline of this thesis

The studies described in this thesis are a continuation of work previously performed within our research lab dedicated to visualization of the intracranial arteries using (ultra)high field MRI, with special focus on imaging of the vessel wall[26,27]. The main goal was to perform further histological validation of intracranial vessel wall MRI and to further evaluate its application in patients.

In **Part I**, an overview is given of key developments of 7T MRI in cerebrovascular diseases over the last decade (***Chapter 2***). One of these developments is described in the subsequent chapter, where small perforating arteries are visualized using MRA after administration of a contrast agent (***Chapter 3***). **Part II** and **III** specifically focus on visualization of the intracranial vessel wall using (ultra)high field MRI. In **Part II**, vessel wall sequences developed within our research lab[21,28,29] are evaluated *in vivo* in patients with recent ischemic stroke / TIA and elderly healthy volunteers. First, 3T and 7T intracranial vessel wall MRI are compared in visualizing the intracranial vessel wall and possible vessel wall lesions in asymptomatic elderly volunteers (***Chapter 4***). Next, presence of vessel wall lesions within intracranial arteries of patients with recent posterior circulation ischemia versus matched healthy volunteers are assessed using 7T MRI (***Chapter 5***). For clinical application of intracranial vessel wall imaging, validation of the MRI findings with a gold standard (histology) is a prerequisite. Therefore, in **Part III** validation of vessel wall MRI with histology is performed using *ex vivo* circle of Willis specimens. First, a quantitative MRI protocol was developed to identify MR signal characteristics of different intracranial atherosclerotic plaque components (***Chapter 6***). Next, *ex vivo* circle of Willis specimens are used for vessel wall thickness measurements of different major intracranial arteries using MR images with ultrahigh-resolution, to obtain more detailed information about wall thickness variations of the intracranial arteries (***Chapter 7***). In the final chapter, main findings described in this thesis are discussed (***Chapter 8***).

References

1. Go AS, Mozaffarian D, Roger VL, et al: Heart disease and stroke statistics--2014 update: a report from the American Heart Association. Circulation 129:e28-e292, 2014.
2. Lozano R, Naghavi M, Foreman K, et al: Global and regional mortality from 235 causes of death for 20 age groups in 1990 and 2010: a systematic analysis for the Global Burden of Disease Study 2010. Lancet 380:2095-2128, 2012.
3. Mozaffarian D, Benjamin EJ, Go AS, et al: Heart Disease and Stroke Statistics-2016 Update: A Report From the American Heart Association. Circulation 133:e38-360, 2016.
4. Tsai CF, Thomas B, Sudlow CL: Epidemiology of stroke and its subtypes in Chinese vs white populations: a systematic review. Neurology 81:264-272, 2013.
5. Bamford J, Sandercock P, Dennis M, et al: Classification and natural history of clinically identifiable subtypes of cerebral infarction. Lancet 337:1521-1526, 1991.
6. Bogousslavsky J, Van Melle G, Regli F: The Lausanne Stroke Registry: analysis of 1,000 consecutive patients with first stroke. Stroke 19:1083-1092, 1988.
7. Adams HP, Jr., Bendixen BH, Kappelle LJ, et al: Classification of subtype of acute ischemic stroke. Definitions for use in a multicenter clinical trial. TOAST. Trial of Org 10172 in Acute Stroke Treatment. Stroke 24:35-41, 1993.
8. Glagov S, Weisenberg E, Zarins CK, et al: Compensatory enlargement of human atherosclerotic coronary arteries. N Engl J Med 316:1371-1375, 1987.
9. Leng X, Wong KS, Liebeskind DS: Evaluating intracranial atherosclerosis rather than intracranial stenosis. Stroke 45:645-651, 2014.
10. Mazighi M, Labreuche J, Gongora-Rivera F, et al: Autopsy prevalence of intracranial atherosclerosis in patients with fatal stroke. Stroke 39:1142-1147, 2008.
11. Arenillas JF: Intracranial atherosclerosis: current concepts. Stroke 42:S20-23, 2011.
12. Bos D, Portegies ML, van der Lugt A, et al: Intracranial carotid artery atherosclerosis and the risk of stroke in whites: the Rotterdam Study. JAMA Neurol 71:405-411, 2014.
13. Gorelick PB, Wong KS, Bae HJ, et al: Large artery intracranial occlusive disease: a large worldwide burden but a relatively neglected frontier. Stroke 39:2396-2399, 2008.
14. Qureshi AI, Caplan LR: Intracranial atherosclerosis. Lancet 383:984-998, 2014.
15. Hellings WE, Peeters W, Moll FL, et al: Composition of carotid atherosclerotic plaque is associated with cardiovascular outcome: a prognostic study. Circulation 121:1941-1950, 2010.
16. Saam T, Hatsukami TS, Takaya N, et al: The vulnerable, or high-risk, atherosclerotic plaque: noninvasive MR imaging for characterization and assessment. Radiology 244:64-77, 2007.

17. Saba L, Anzidei M, Sanfilippo R, et al: Imaging of the carotid artery. Atherosclerosis 220:294-309, 2012.
18. Takaya N, Yuan C, Chu B, et al: Association between carotid plaque characteristics and subsequent ischemic cerebrovascular events: a prospective assessment with MRI--initial results. Stroke 37:818-823, 2006.
19. Dieleman N, van der Kolk AG, Zwanenburg JJ, et al: Imaging intracranial vessel wall pathology with magnetic resonance imaging: current prospects and future directions. Circulation 130:192-201, 2014.
20. Bodle JD, Feldmann E, Swartz RH, et al: High-resolution magnetic resonance imaging: an emerging tool for evaluating intracranial arterial disease. Stroke 44:287-292, 2013.
21. van der Kolk AG, Zwanenburg JJ, Brundel M, et al: Intracranial vessel wall imaging at 7.0-T MRI. Stroke 42:2478-2484, 2011.
22. Dieleman N, van der Kolk AG, van Veluw SJ, et al: Patterns of intracranial vessel wall changes in relation to ischemic infarcts. Neurology 83:1316-1320, 2014.
23. Mandell DM, Mossa-Basha M, Qiao Y, et al: Intracranial Vessel Wall MRI: Principles and Expert Consensus Recommendations of the American Society of Neuroradiology. AJNR Am J Neuroradiol, 2016.
24. Majidi S, Sein J, Watanabe M, et al: Intracranial-derived atherosclerosis assessment: an in vitro comparison between virtual histology by intravascular ultrasonography, 7T MRI, and histopathologic findings. AJNR Am J Neuroradiol 34:2259-2264, 2013.
25. van der Kolk AG, Zwanenburg JJ, Denswil NP, et al: Imaging the Intracranial Atherosclerotic Vessel Wall Using 7T MRI: Initial Comparison with Histopathology. AJNR Am J Neuroradiol, 2014.
26. Dieleman N: MR imaging of intracranial vessel wall pathologies and parenchymal brain damage. PhD thesis, Utrecht University, The Netherlands ISBN: 978-90-393-6638-7, 2016.
27. van der Kolk AG: Intracranial vessel wall imaging at 7.0 tesla MRI. PhD thesis, Utrecht University, The Netherlands ISBN: 978-94-6259-143-1, 2014.
28. Dieleman N, Yang W, van der Kolk AG, et al: Qualitative Evaluation of a High-Resolution 3D Multi-Sequence Intracranial Vessel Wall Protocol at 3 Tesla MRI. PLoS One 11:e0160781, 2016.
29. van der Kolk AG, Hendrikse J, Brundel M, et al: Multi-sequence whole-brain intracranial vessel wall imaging at 7.0 tesla. Eur Radiol 23:2996-3004, 2013.

PART I

7T MRI in cerebrovascular diseases

Chapter 2

7T MRI in cerebrovascular diseases: challenges to overcome and initial results

Anita A. Harteveld[1], Anja G. van der Kolk[1], Jaco J.M. Zwanenburg[1,2], Peter R. Luijten[1], Jeroen Hendrikse[1]

[1]Department of Radiology; [2]Image Sciences Institute; University Medical Center Utrecht, Utrecht, the Netherlands

Published in *Topics in Magnetic Resonance Imaging* 2016

MRI plays a key role in the investigation of cerebrovascular diseases. Compared with computed tomography (CT) and digital subtraction angiography (DSA), its advantages in diagnosing cerebrovascular pathology include its superior tissue contrast, its ability to visualize blood vessels without the use of a contrast agent, and its use of magnetic fields and radiofrequency pulses instead of ionizing radiation. In recent years, ultrahigh field MRI at 7T has shown promise in the diagnosis of many cerebrovascular diseases. The increased signal-to-noise ratio (SNR; 2.3x and 4.7x increase compared with resp. 3T and 1.5T) and contrast-to-noise ratio (CNR) at this higher field strength can be exploited to obtain a higher spatial resolution and higher lesion conspicuousness, enabling assessment of smaller brain structures and lesions.

Cerebrovascular diseases can be assessed at different tissue levels; for instance, changes of the arteries feeding the brain can be visualized to determine the cause of ischemic stroke, regional changes in brain perfusion can be mapped to predict outcome after revascularization, and tissue damage, including old and recent ischemic infarcts, can be evaluated as marker of ischemic burden. For the purpose of this review, we will discriminate three levels of assessment of cerebrovascular diseases using MRI: **P**ipes, **P**erfusion and **P**arenchyma (3 **P**s). The term Pipes refers to the brain feeding arteries from the heart and aortic arch, upwards to the carotid arteries, vertebral arteries, circle of Willis and smaller intracranial arterial branches. Perfusion is the amount of blood arriving at the brain tissue level, and includes the vascular reserve and perfusion territories. Parenchyma refers to the acute and chronic burden of brain tissue damage, which includes larger infarcts, smaller microinfarcts, and SVD manifestations such as white matter lesions, lacunar infarcts and microbleeds.

In this review, we will describe the key developments in the last decade of 7T MRI of cerebrovascular diseases, subdivided for these three levels of assessment.

Pipes

Extracranial arteries

In the last decade, many developments have taken place in the field of 7T MR imaging of the extracranial brain feeding vasculature, and these can be grossly subdivided into developments in vessel lumen imaging and vessel wall imaging.

The vessel lumen

Imaging of the vessel lumen in cerebrovascular diseases is mainly performed using either phase contrast (PC-)MR angiography (MRA) or time-of-flight (TOF-)MRA. The advantage of ultrahigh field MRI (like 7T) in this regard is the longer T_1 relaxation time at these higher field strengths.[1] In TOF-MRA, static spins present in tissues within an excited volume become saturated during repetitive radiofrequency (RF) pulses within their relaxation time T_1, while flowing spins – like in blood – will only experience a limited number of excitations within this excited volume – being there for only a short period of time – and will therefore result in a high signal. When the T_1 relaxation time becomes longer, the static spins will relax less between RF pulses, thereby achieving faster and better suppression of these tissues and more contrast between flowing blood and the surrounding tissues.[2-8]

It might be assumed that this advantage, combined with the increased spatial resolution attainable at 7T, may result in detailed assessment of the extracranial arteries from the aortic arch upwards to the skull base, including clearer depiction of the arterial lumen and luminal stenosis. However, so far limited availability of dedicated coils (see next paragraph) for visualization of the neck region currently makes 7T less useful for 'one-stop-shop' imaging of the extracranial arteries. Furthermore, the increased magnetic field inhomogeneities and susceptibility artefacts make the neck region especially challenging for robust imaging of the extracranial arteries at ultrahigh field strength.[9]

The vessel wall

At 1.5T, extracranial atherosclerotic plaque (and vessel wall) imaging has been the mainstay of research for the last decade.[10] Most attention has been focused on characterization of atherosclerotic plaques in the proximal internal carotid artery as a possible way of selecting high-risk patients for carotid surgery (carotid endarterectomy). The increased SNR at 7T can be exploited for imaging at a higher spatial resolution, for more detailed assessment of atherosclerotic plaque composition.[11-14] Increasing spatial resolution has been shown to improve reproducibility of carotid arterial wall dimension measurements at 3T.[15] Typically, dedicated surface coils are used for measurement of carotid artery vessel wall thickness and characterization of carotid atherosclerotic plaques. At 7T, dedicated MR coils have been developed as well[9,16], and used in control subjects and patients for carotid vessel wall imaging and plaque characterization (**Figure 1**).[17,18] An approximately 2-fold higher SNR was measured in the carotid vessel wall at 7T compared to 3T, therefore potentially a more detailed assessment of carotid atherosclerosis may be achieved at 7T.[17-19] However, imaging of plaque components remains challenging at 7T MRI, which was shown in a first study at 7T where the feasibility of carotid vessel wall imaging was assessed in a series of patients with a symptomatic

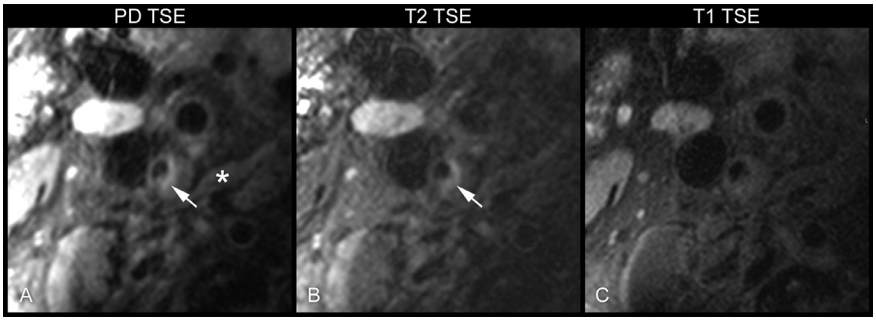

Figure 1 | Carotid plaque imaging with different contrast weightings at 7T MRI. A proton-density-weighted turbo spin echo (TSE) (**A**), T_2-weighted TSE (**B**), and T_1-weighted TSE (**C**) sequence of 75-year-old patient with transient ischemic symptoms in the right hemisphere based on a stenosis (>70%) of the right internal carotid artery. A hyperintense signal, relative to the adjacent muscle (*), is visible on the plaque-lumen interface (arrow). This hyperintense signal might be suggestive of a fibrous cap on top of a lipid-rich necrotic core. Reproduced from De Rotte *et al*. Investigative Radiology 2014[17] with permission.

stenosis of the internal carotid artery.[17] One of the current limitations is the absence of a body transmit coil which complicates suppression of the MR signal in the arterial lumen. Another limitation is that not all MR image contrast sequences are yet available at 7T that are conventionally used for full characterization of carotid plaques at 1.5T and 3T.

Intracranial arteries

Compared with the extracranial feeding arteries of the brain, advantages of ultrahigh field MRI are more obvious when used for the intracranial vasculature. Intracranial arteries are smaller than their extracranial counterparts, and detailed visualization of these arteries will therefore require a higher spatial resolution, which is more easily accomplished within reasonable scan times at ultrahigh field strengths. Developments within this field can be subdivided in the same way as for the extracranial arteries, namely vessel lumen and vessel wall.

The vessel lumen

Improved visualization of the intracranial arteries at higher field strengths becomes especially obvious for the small perforating arteries. These arteries are hardly visible at 1.5T and become clearly visible with TOF-MRA at 3T and 7T (**Figure 2**). 7T TOF-MRA has been shown to give improved vessel contrast, especially for the smaller arteries[20-24], increase the number visualized and trajectory of detected arteries compared to lower field strengths[25,26], and improve assessment of intracranial aneurysms[7,27,28]. Multiple studies have shown the ability of 7T MRI in visualizing different perforating arteries, including the lenticulostriate arteries[2,3,8,29], basilar artery perforators[30], and perforating arteries originating from the posterior communicating artery[6]. The lenticulostriate arteries have already been studied in more detail at 7T for patients with stroke[31], vascular dementia[32], CADASIL (cerebral autosomal-dominant arteriopathy with subcortical infarcts and leukoencephalopathy)[33], hypertension[34], and asymptomatic middle cerebral artery (MCA) steno-occlusion[35]. For instance, in a study in patients with a large small vessel disease (SVD) burden related to CADASIL, no difference in the luminal diameters of lenticulostriate arteries was found on 7T TOF-MRA compared with a control group. Other studies have focused on optimization of the currently used 7T (TOF-)MRA sequences

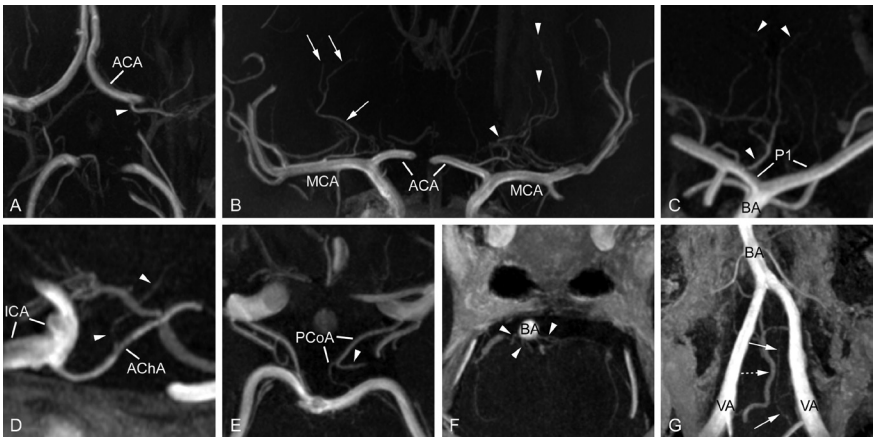

Figure 2 | TOF-MRA at 7T of the intracranial perforating arteries (postcontrast). (**A**) A medial lenticulostriate artery (arrowhead), arising from the A1 segment of the anterior cerebral artery (ACA; transverse slab maximum intensity projection (MIP), thickness 10 mm), (**B**) lateral lenticulostriate arteries arising from the right middle cerebral artery (MCA; arrows) and medial lenticulostriate arteries arising from the left ACA (arrowheads; coronal slab MIP, thickness 10 mm), (**C**) artery of Percheron (arrowheads), arising from the P1 segment of the posterior cerebral artery (PCA; coronal slab MIP, thickness 10 mm), (**D**) perforating branch (arrowheads) arising from the right anterior choroideal artery (sagittal slab MIP, thickness 10 mm), (**E**) thalamoperforating artery (arrowhead), arising from the left posterior communicating artery (transverse slab MIP, thickness 6 mm), (**F**) pontine arteries (arrowheads) arising from the basilar artery (BA; transverse slab MIP, thickness 4 mm), and (**G**) the intracranial feeders of the anterior spinal artery (arrows) with an adjacent vein (dashed arrow, transverse slab MIP angulated anterior-posterior in line with the BA, thickness 10 mm). Reproduced from Harteveld *et al*. PLoS One 2015[41] with permission.

for better visualization of the intracranial vessel lumen, by tackling some of the limitations of scanning at an ultrahigh field strength[36-40]. Also, the effect of injecting a gadolinium-based contrast agent on vessel lumen visualization has been evaluated[41,42], since this might improve the CNR between blood and surrounding tissue due to the shortened T_1 relaxation time of the blood.

In addition to TOF-MRA, 3D PC-MRA has also been performed at 7T for visualization and quantification of blood flow in the arteries of the circle of Willis (**Figure 3**).[43,44] Besides normal intracranial arteries, 7T PC-MRA may especially be useful in showing flow patterns in the smaller blood vessels that require a high spatial resolution.[43] In addition to anatomical imaging

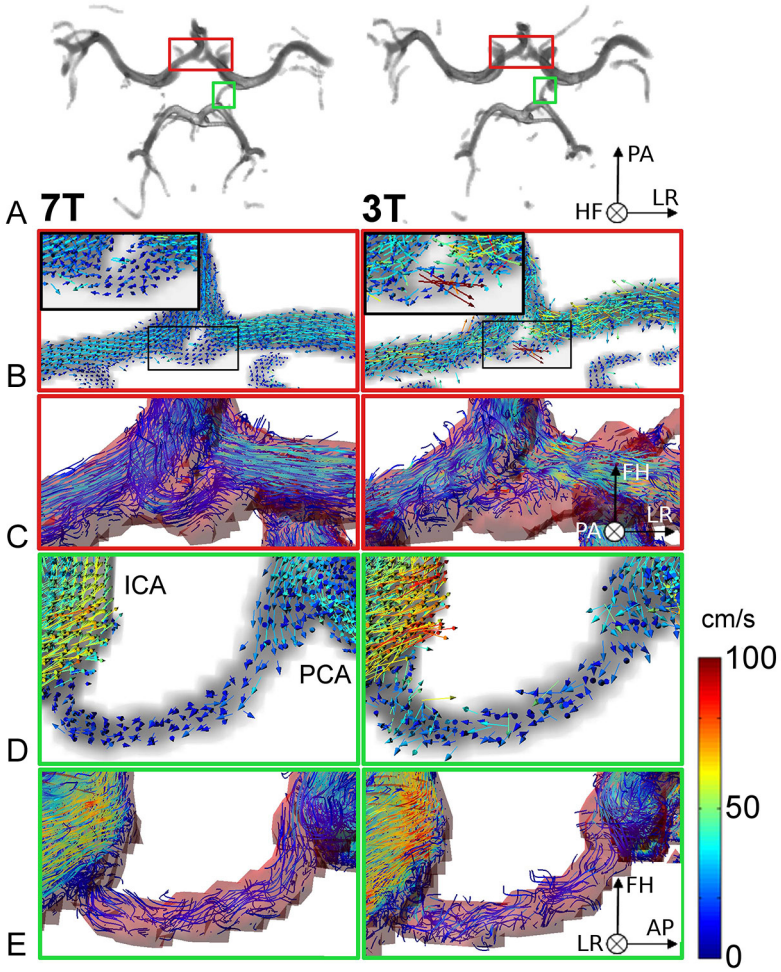

Figure 3 | 3D phase contrast (PC-)MRI for visualization and quantification of the blood flow in the arteries of the circle of Willis at 7T (left column) and 3T (right column). In row (**A**), the top view of the 3D circle of Willis after segmentation of the PC magnitude images is shown at peak systole. The anterior communicating artery (ACoA) is shown in the red square and the right posterior communicating artery (PCoA) in the green square. The neurological convention is used here where the circle of Willis is viewed from the top and left and right is not reversed. In row (**B**), a velocity vector visualization of the flow in the ACoA at begin diastole is presented. In row (**C**), streamlines in the ACoA at the same cardiac phase are displayed. In row (**D**) and (**E**), velocity vectors and streamlines at peak systole are shown in the right PCoA. Gray areas in the figures with vectors represent the PC magnitude segmentation, the pink area in the streamline figures displays the kernel used for the streamline calculation and is slightly larger than the segmented vessel area. Reproduced from Van Ooij *et al*. MRM 2013[43] with permission.

of the perforating arteries, novel innovative methods using phase contrast 7T MRI have recently been optimized for functional assessment of these small vessels by measuring blood flow velocity and pulsatility in perforating arteries of the basal ganglia and the semioval center (**Figure 4**).[44,45] It is currently hypothesized that functional assessment, including PC-MRI for measurements of blood flow and pulsatility, may be a better feature to discriminate diseased from healthy arteries than anatomical imaging alone.[46] In this respect, 7T MRI may start to bridge the gap between vascular pathology of the larger extra- and intracranial arteries causing mainly larger ischemic infarcts, and pathology at the arteriolar level causing SVD. Still, currently these arterioles themselves remain under the detection limit for direct visualization with MRA methods.

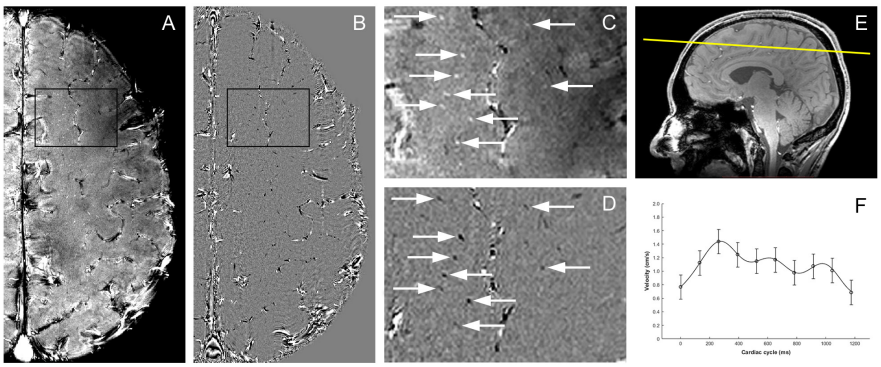

Figure 4 | Blood flow velocity measurements at 7T in perforating arteries of the semioval center.[45] Mean magnitude image over all cardiac time points (**A, C**) and mean velocity map (**B, D**) of the left brain hemisphere of a healthy volunteer. The slice location (15 mm above the corpus callosum) is shown on the T_1-weighted image (**E**). Arrows indicate the location of a perforting artery (**C**) with blood flow velocity (**D**). An example of a blood flow velocity curve for a single perforating artery is shown in (**F**). Image courtesy of Lennart J. Geurts (University Medical Center Utrecht, The Netherlands)

The vessel wall

The research field devoted to visualization of the intracranial vessel wall and its pathology has seen a tremendous growth in the last few years. Because intracranial arterial vessel walls are very thin, they typically

remain under the detection limit at 1.5T MRI. Therefore, most intracranial vessel wall MRI sequences have been developed at both 3T and 7T, where a higher spatial resolution can be achieved within a reasonable scan time to clearly show these thin arterial vessel walls.[47] The MRI sequences used for imaging intracranial arterial vessel walls typically suppress the arterial signal in the arteries based on outflow, thereby creating increased contrast between flowing blood and the inner vessel wall. Care should be taken to suppress as much of the blood pool signal as possible, because remaining slow flow next to the arterial vessel wall might result in diagnostic errors, by mistakenly being interpreted as thickening or postcontrast enhancement of the arterial vessel wall.[48] In addition to suppression of the arterial signal, suppression of the surrounding cerebrospinal fluid (CSF) signal can be used to optimally visualize the outer wall of the intracranial arteries. CSF suppression results in an increased acquisition time and decreased signal from the vessel wall; therefore, most of the methods that are currently used at 3T do not achieve complete suppression of the CSF signal. At 7T, complete CSF suppression can be achieved within reasonable scan times and with remaining sufficient vessel wall signal, due to the inherent increased SNR (**Figure 5**).[49,50] With complete CSF suppression, thickness of the arterial vessel walls can be appreciated more clearly, which could benefit detection of generalized intracranial atherosclerosis, in which arterial vessel wall thickening can be more diffuse. However, studies comparing different types of intracranial vessel wall sequences (both between different field strengths and between for instance sequences with and without complete CSF suppression) have not yet been published, so the question remains if CSF suppression is really necessary. It is not unthinkable that CSF suppression would be less needed for detection of vessel wall enhancement after injection of a contrast agent.

The increased spatial resolution combined with the inherent increased CNR that can be obtained at 7T in theory enables better depiction of specific plaque features compared with a lower spatial resolution. However, there is always a trade-off between spatial resolution and MR signal: the higher the spatial resolution, the lower the MR signal in a given voxel will be. Typically, the in-plane spatial resolution of intracranial arterial vessel wall imaging is chosen to be <1.0 mm. The slice thickness, especially

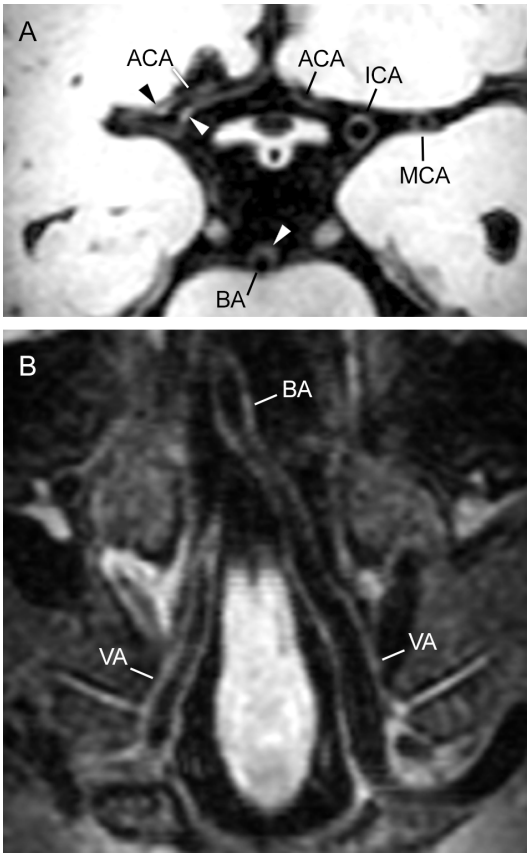

Figure 5 | Intracranial vessel wall imaging at 7T. Whole-brain 3D T_1-weighted magnetization prepared inversion recovery (MPIR) TSE images[50] before contrast administration (voxel sizes 0.8x0.8x0.8 mm^3) in a 55-year-old patient with ischemic stroke in the left thalamus. Vessel walls of arteries of the anterior (**A**; transverse slice) and posterior circulation (**B**; coronal slice, angulated anterior-posterior in line with the basilar and vertebral arteries) are shown. Arrowheads indicate the locations of focal thickening of the vessel wall.

at 3T MRI, is often chosen to be around 1.0 mm, to avoid too much MR signal loss within each voxel. Using multi-planar reconstructions of axially acquired images, will result in blurring and less detail in the sagittal and coronal reconstructions. Due to the increased SNR at 7T, whole-brain sequences with acquired isotropic voxels <1.0 mm^3 are possible within reasonable scan times and with sufficient SNR. At 3T some recent studies have shown results on this as well.[51,52] The advantage of isotropic voxels is that reconstructions can be made in all directions without losing detail. A disadvantage is that scan time increases, especially when combined with adequate suppression of the signal of blood within and CSF surrounding the arteries.

In accordance with developments for the extracranial vasculature, plaque characterization has become of interest for intracranial arteries as well. The most obvious way to characterize intracranial arterial plaques is by injection of a contrast agent to detect contrast uptake within the plaque. Different studies at 7T MRI in patients with ischemic stroke and TIA have shown that contrast uptake was present in 20-35% of all visualized intracranial arterial lesions.[49,53,54] The presence of vasa vasorum are thought to be the main underlying cause of contrast uptake of intracranial arterial lesions.[55] Another potential method of characterization is the detection of intraplaque hemorrhage[56], although this plaque complication is much less common in the intracranial arteries compared with for instance extracranial internal carotid artery plaques.[57] Furthermore, intracranial plaque calcifications can be detected based on their low signal intensity on high-resolution T_2^*-weighted images. Also, other intracranial plaque characteristics like thickening pattern or configuration may be appreciated with high-resolution vessel wall imaging at 7T MRI.[58] However, due to poor accessibility of the intracranial arteries it is difficult to validate the *in vivo* vessel wall imaging findings with histology. Recently, post-mortem correlation studies have been performed at 7T MRI with circle of Willis specimens that showed focal thickening and identified plaque components with different image contrast weightings.[59,60] Thus far, for *in vivo* intracranial vessel wall imaging at 7T, one study already developed whole-brain intracranial vessel wall sequences with different image contrast weightings to potentially assess different vessel wall tissue components.[50]

At 7T, intracranial vessel wall imaging has so far been performed in a number patients with ischemic stroke and TIA for the assessment of the intracranial vessel wall and identification of possible vessel wall lesions[49,53,54,58], as well as in patients with intracranial aneurysms for visualization of the aneurysm wall[61,62] (**Figure 6**). In the future, head-to-head comparison studies are warranted which compare all the different aspects of the MRI sequences used at different field strengths, including in-plane spatial resolution, slice thickness, 2D versus 3D and SNR and CNR of both intracranial arterial vessel walls and atherosclerotic plaques.

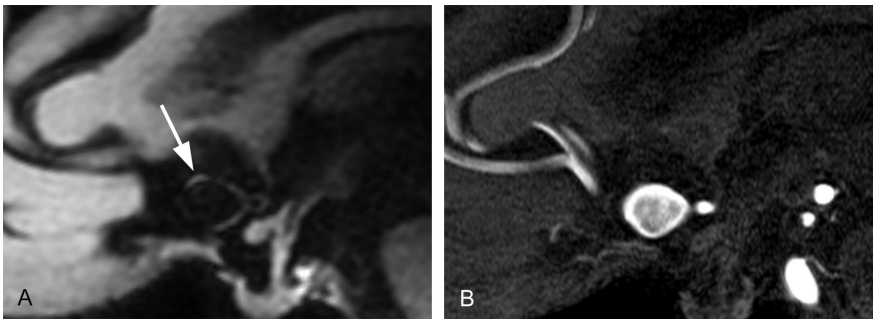

Figure 6 | Visualization of the aneurysm vessel wall at 7T. Images show the wall of an anterior communicating artery aneurysm on a T_1-weighted magnetization prepared inversion recovery (MPIR) TSE scan (**A**; sagittal slice) and the aneurysm lumen on the corresponding slice of the time-of-flight MRA scan (**B**).[61] Image courtesy of Rachel Kleinloog (University Medical Center Utrecht, The Netherlands).

Intracranial veins

In addition to arteries, intracranial veins are also better visualized; for instance, smaller veins in the semioval center have become clearly visible at 7T compared with lower field strengths. The increased conspicuousness of intracranial veins at 7T is due to the higher spatial resolution that can be achieved and the increased susceptibility effects at high field strengths, which causes structures with for instance deoxyhemoglobin, like veins, to stand out on T_2^*-weighted images as areas of signal loss on a hyperintense background.[63] MRI sequences have been developed that specifically utilize these benefits at ultrahigh field.[64]

7T MRI has been used to visualize veins in different brain structures, like the pineal gland[65], the nucleus dentatus[66], and cerebral cavernous malformations[67-69]. Another application at 7T is the detection of small central veins within multiple sclerosis lesions[70], which has been shown to be significantly better compared with 3T because of the increased paramagnetic effect of deoxyhemoglobin in the veins at 7T.[71,72]. In patients with white matter lesions due to multiple sclerosis a central vein was observed significantly more often in white matter lesions compared to control subjects with incidental asymptomatic white matter lesions. It has been suggested that based on T_2^*-weighted 7T MRI, patients with clinically definite MS can be reliably distinguished from patients without clinical MS.[73,74]

Currently, many efforts are made to quantify the information detected with T_2^*-weighted imaging at 7T; for instance, recent studies have developed analysis methods to automatically detect and quantify small (periventricular) veins visualized with these methods.[75-77]

Perfusion

MR perfusion imaging in cerebrovascular diseases grossly entails two main techniques: arterial spin labeling (ASL) and blood oxygenation level-dependent (BOLD) functional MRI (fMRI). Application of these techniques at 7T MRI will be discussed below. Other techniques to quantify cerebrovascular function have also been performed at 7T MRI, like measurement of oxygen extraction fraction (OEF)[78,79], vascular space occupancy (VASO) mapping[80], and simultaneous acquisition of VASO maps, perfusion images and BOLD images[81].

ASL

7T MRI has potential advantages over lower field strengths in the quantification of brain perfusion. Especially, arterial spin labeling (ASL) MRI may benefit from ultrahigh field strength due to both the inherent increase in SNR and the longer T_1 relaxation times of blood which will result in a stronger magnetic label compared to ASL at lower field strengths. The longer T_1 allows for using longer post labeling delays, which are necessary to assess perfusion in areas with long blood transit times.[82] Since ASL MRI uses a subtraction step between label and control images the method has an inherently low SNR. At lower field strengths (1.5T and 3T), a large series of label-control pairs need to be averaged to obtain perfusion images with an acceptable SNR. The low SNR also limits the spatial resolution that can be achieved within feasible scan times. Potential increases in SNR at ultrahigh field strength are therefore warranted. Still, in the last decade the promises of SNR improvements for ASL imaging at 7T have not been fully fulfilled.[83-85] The lack of a body transmit coil at 7T makes it challenging to perform labeling of the arterial blood in the arteries below the circle of Willis. As a potential solution, local labeling coils have been used in the neck region (**Figure 7**).[86] Although this approach is feasible, the transmit field is still inhomogeneous, which can result in variable

labeling of the arteries (both internal carotid and vertebral arteries) in the neck region and thus in variable perfusion measurements between subjects and between labeling territories. When labeling is performed in the lower part of the brain region and image readout is performed higher up in the brain, high SNR perfusion images can be obtained. However, the ASL perfusion images will only have partial brain coverage. Still, ASL imaging can be performed with a high spatial resolution[84] and some studies have used this method in for instance high-resolution functional MRI.[87] Currently, for perfusion imaging, and especially perfusion imaging with group analysis, lower MR field strengths are preferred over ultrahigh field MRI. However, with the ongoing technical improvements of head and neck coil technology with larger coverage and better homogeneity of the magnetic field, as well as MRI sequence developments[88], ASL might become better feasible in the near future at 7T.

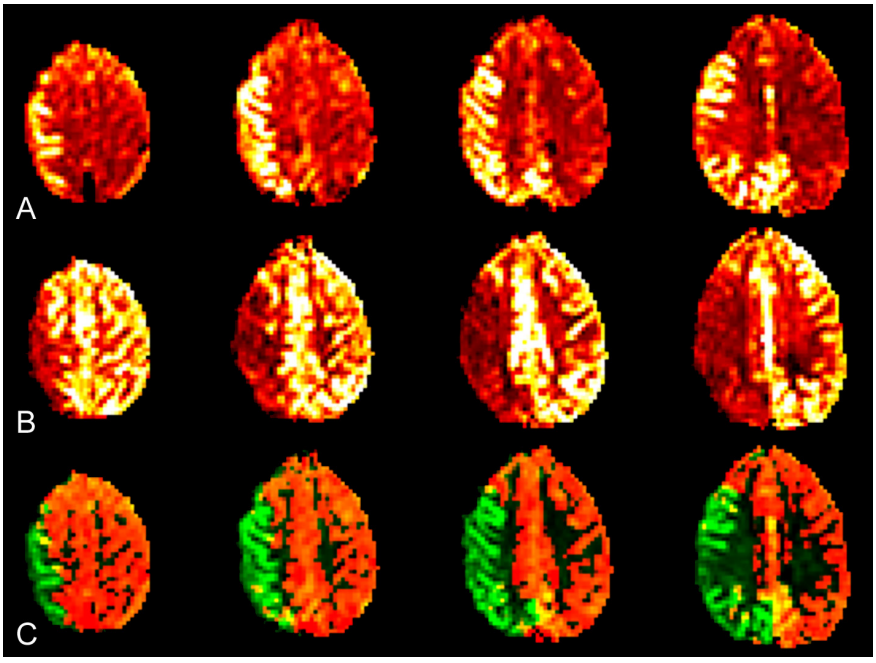

Figure 7 | Arterial spin labeling (ASL) at 7T MRI. Whole-brain perfusion maps using a PULSAR pulsed ASL sequence with local labeling coils in the neck region.[86] Summed subtraction images, with spatially selective labeling of the right (**A**) and left (**B**) hemisphere, and the colored combination of both hemispheres (**C**). Image courtesy of Wouter Koning (University Medical Center Utrecht, The Netherlands).

BOLD fMRI

Another method that benefits from ultrahigh field MRI is BOLD fMRI. The BOLD image contrast is the workhorse used for functional MRI, both task-based and resting state fMRI. In addition to the classic BOLD fMRI measurements, there has been an increased interest lately in measuring the cerebrovascular reactivity (CVR) using BOLD before and after a certain vascular challenge.[89] The most often used vascular challenge is the inhalation of carbon dioxide, which will result in an increased blood flow to the brain and a decrease of the BOLD signal. Other challenges that may be used are for instance breath-holding or medication administration (acetazolamide), which also increase the cerebral blood flow. It is generally believed that brain areas that have a lower signal change upon a certain challenge have a lower cerebrovascular reserve and are at higher risk of future ischemia.

For these functional hemodynamic measures, 7T MRI has the advantage of an increased SNR, as well as increased susceptibility effects resulting in stronger BOLD signal changes related to changes in deoxyhemoglobin.[90] The increased BOLD signal in an individual patient can be used to assess cerebral hemodynamics in much more detail. BOLD fMRI studies at 7T with high spatial resolution are currently capable of discriminating the functional response between different cortical layers.[91-95] Another application of BOLD fMRI at 7T has been focused on mapping detailed (sub-millimeter) patterns of neuronal population activity in individual subjects (**Figure 8**).[96-102] Until now, BOLD imaging at 7T with a vascular challenge has been performed using carbon dioxide inhalation to investigate the regional CVR response to progressive hypercapnia[103,104] (**Figure 9**), and breath-holding to examine the association of CVR with lacunar infarcts, white matter lesions and microbleeds[105].

The drawback of BOLD imaging at 7T is the presence of magnetic field inhomogeneities which may result in difficulties for whole brain hemodynamic measurements. Especially the temporal lobes remain sensitive to field inhomogeneities. In addition to problems with whole brain hemodynamic measures with similar sensitivity in all regions, group analysis and group averaging may also be more difficult at ultrahigh field MRI due to these field inhomogeneities. Currently, several technical

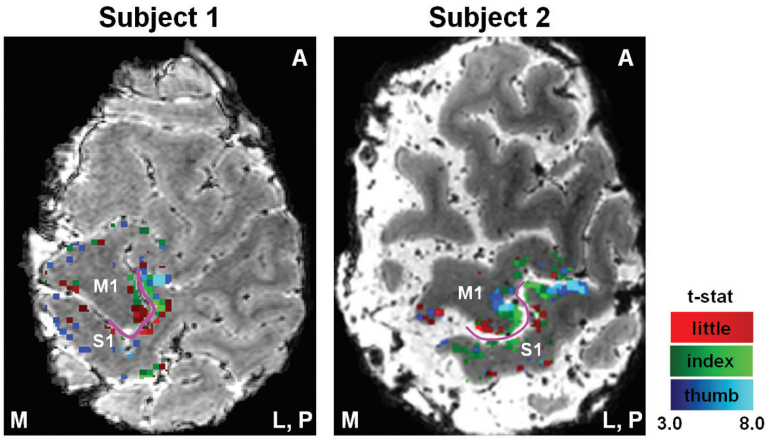

Figure 8 | Blood oxygenation level-dependent functional MRI (BOLD fMRI) activation measured at 7T in sensorimotor cortex elicited by individual finger movements for two subjects. BOLD differential contrast maps (t-values) of the movement of one finger versus movement of the other fingers for the index (green), thumb (blue) and little finger (red) are superimposed on the high-resolution T_2*-weighted images. Distinct activation foci are observed in the BOLD differential contrast map for the individual fingers. The medial, lateral, anterior and posterior side of the brain are indicated by the letters (M), (L), (A), and (P) respectively, for both subjects. The area of the hand knob is indicated by the line in magenta. M1 = primary motor cortex; S1 = primary sensory cortex. Reproduced from Siero *et al*. NeuroImage 2014[96] with permission.

developments have been studied at 7T to further improve the SNR, (whole brain) BOLD sensitivity and temporal resolution, like the development of dedicated coils[106] and alternative BOLD fMRI pulse sequences[107-111].

Parenchyma

For the detection of small brain parenchymal lesions 7T MRI has potential advantages over lower field strengths, enabling visualization of (very) small brain tissue lesions due to the increased SNR and CNR. Recent studies have shown that 7T MRI can detect both cerebral microbleeds and cortical microinfarcts.[112,113]

Microbleeds are clearly visualized with high sensitivity at 7T using T_2*-weighted MRI sequences, due to the increased susceptibility effects at higher field strengths.[114-116] Due to these susceptibility effects, microbleeds can also be seen at short echo times at which the microbleeds are

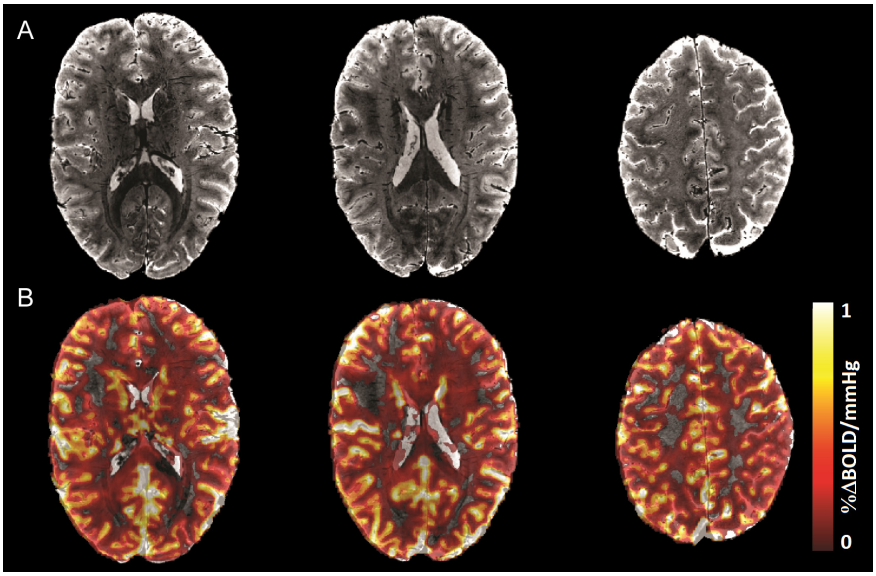

Figure 9 | Cerebrovascular reactivity (CVR) mapping using BOLD at 7T after a vascular challenge. CVR maps were calculated using BOLD images acquired during a hypo- to hypercapnic breathing challenge delivered using a RespirActTM device (Thornhill Research Inc, Toronto, Canada).[103] (**A**) T_2^*-weighted anatomical images of selected slices from one subject. (**B**) Reactivity maps calculated based on the linear slope of the BOLD response to progressive hypercapnia (ΔBOLD/mmHg $PetCO_2$). The parameter maps are overlaid on the corresponding T_2^*-weighted anatomical images. Image courtesy of Alex A. Bhogal (University Medical Center Utrecht, The Netherlands).

hypointense and easily discernible due to the more homogeneous hyperintense background signal of brain tissue and vessels (**Figure 10**). It has been shown that the number of detected microbleeds increases with field strength.[116,117] However, visual rating of microbleeds is more challenging at 7T compared to lower field strengths due to the limited size of some lesions and the susceptibility effects of overlapping structures that are also increased, like veins.[118] Also, since many small microbleeds can potentially be visualized, the detection is often time-consuming and microbleeds can easily be missed. Recently, semi-automated detection methods of microbleeds have been developed to do an automated search first, after which an observer checks the detected lesions.[119] This two-step approach both shortens the time for detection of microbleeds

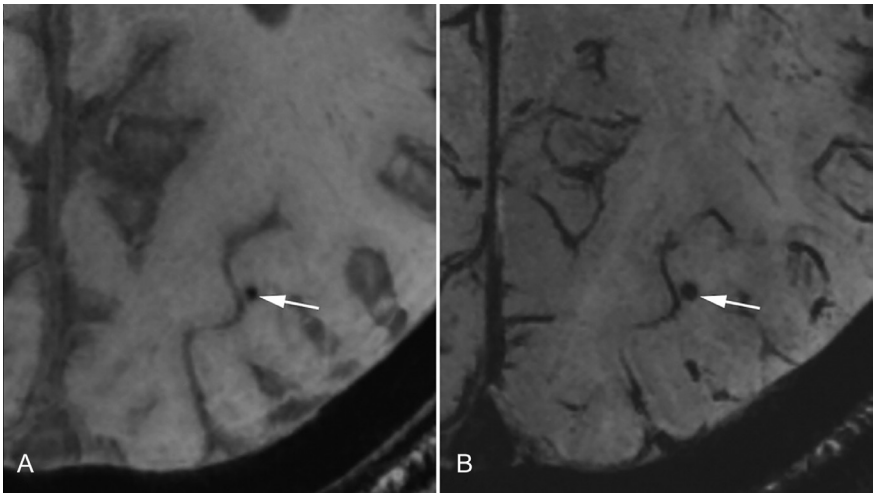

Figure 10 | Dual-echo T_2*-weighted sequence to visualize cerebral microbleeds. Minimum intensity projection (minIP) images of the first echo (**A**; TE 2.5 ms) and the second echo (**B**; TE 15.0 ms) are shown. The microbleed (arrow) appears larger on the minIP of the second echo image (**B**). Reproduced from Conijn *et al*. JMRI 2010[114] with permission.

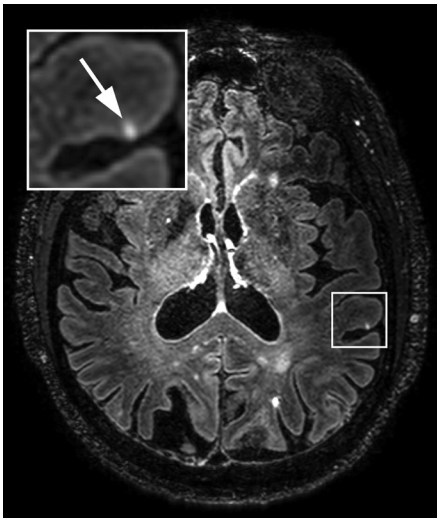

Figure 11 | Detection of cerebral microinfarcts at 7T MRI. One cortical microinfarct is shown on a transverse fluid attenuated inversion recovery (FLAIR) image (voxel sizes 0.8x0.8x0.8 mm^3) of a 75-year-old patient with ischemic stroke in multiple vascular territories. A zoomed view of the box at the location of the microinfarct is shown in the insert (arrow indicates microinfact). Image courtesy of Nikki Dieleman (University Medical Center Utrecht, The Netherlands).

and increases the number of detected microbleeds. To further investigate the clinical relevance of detected microbleeds on 7T MRI, studies have been performed recently in patients with dementia[116,120], cerebral amyloid angiopathy[121], and ALS[122].

In the last five years, 7T MRI has also shown the ability to detect cortical microinfarcts which were, until then, only visible on post-mortem histopathological examinations.[123] Especially, 3D fluid attenuated inversion recovery (FLAIR) MRI has shown these small cortical microinfarcts with a relatively high prevalence (**Figure 11**). Often a combination of FLAIR MRI and other sequences such as T_1-weighted MRI is used to confirm the presence of a cortical microinfarct.[124] The microinfarcts often show as small cortical-based areas of gliosis. However, care should be taken to distinguish these cortical microinfarcts from perivascular spaces. MRI studies with histopathological validation have been performed to confirm that the lesions detected with MRI were indeed microinfarcts.[125,126] Recently, several studies have been performed on 7T to take a closer look at the relation between cortical microinfarcts and certain cerebrovascular diseases, like intracerebral hemorrhage[127], ischemic stroke or TIA[54], and Alzheimer's disease[128]. Another study evaluated the presence of cortical microinfarcts in patients with a symptomatic high-grade stenosis of the carotid artery.[129] Based on the knowledge obtained at 7T MRI, nowadays microinfarcts are also being observed at 3T MRI[130,131] The advantage of 3T MRI is the more widely availability compared to 7T, however, the sensitivity of 3T to detect cortical microinfarcts is much lower than 7T.[130] Still, the number of microinfarcts detected on MRI so far remains lower compared to the number of microinfarcts reported in post-mortem histopathological studies, suggesting that even at 7T using high spatial resolutions, we are still only tentatively approaching histopathological sensitivity.

In addition to microbleeds and microinfarcts, 7T MRI sequences are also used to investigate other small brain structures related to SVD, such as white matter lesions, the deep gray matter regions, and perivascular spaces. Imaging at higher field strength has been shown to increase the detection rate of white matter lesions[132,133], however, the distribution pattern was not different between field strengths[116]. Another study showed improved differentiation between MS and vascular brain lesions with the use of a novel MRI sequence at 7T (FLAIR*).[134] For the perivascular spaces it is nowadays possible with 7T MRI to actually show the perforating artery, which is known to be present in these spaces based on post-mortem histology studies.[135] As said before, functional pulsatility measurements of

the blood flow velocity in these small penetrating arteries are also possible, based on the increased SNR at ultrahigh field. Apart from visualization of perivascular spaces and manual measurements of their sizes[135,136] also several studies showed (semi-)automatic measurement methods for characterization of morphological features of perivascular spaces using 7T MRI[137,138]. However, as shown by numerical simulations, diameters of the perivascular spaces cannot be assessed below approximately 2 times the image resolution.[135] As only the largest perivascular spaces exceed 1 mm in diameter, while the smallest are in the micrometer range, further work is needed to develop valid quantitative measures of the perivascular spaces at MRI.

Discussion

In the last decade, much progress has been made in the field of 7T MRI for imaging cerebrovascular diseases. Both at the level of the arteries (**P**ipes), the brain tissue function (**P**erfusion) and the brain tissue itself (**P**arenchyma), small lesions can be visualized that provide additional information, not only about the total burden of cerebrovascular disease, but also about the possible causes and prognosis of individual patients. Intracranial arterial atherosclerotic lesions can be detected that until now remained mainly unnoticed. The exact relationship between these intracranial arterial lesions and brain tissue lesions is still to be elucidated. Because intracranial atherosclerosis is the most important cause of stroke worldwide, imaging methods that can show the location, burden and characteristics of intracranial plaques are of crucial importance for understanding the mechanisms underlying stroke with an intracranial arterial cause. Also, other causes of cerebrovascular disease and mechanisms of lesion development may be unraveled by combining different innovative methods at 7T. For instance, the relation between perforating arteries and microbleeds was shown with a combination of MRA and T_2^*-weighted imaging at 7T.[139] Functional imaging methods that can show brain tissue function and – indirectly – tissue perfusion at 7T are primarily BOLD fMRI and OEF techniques, which exploit the increased susceptibility effects of deoxyhemoglobin in the veins at higher field

strengths; ASL perfusion techniques at 7T are still in their developmental phase. Finally, at the brain tissue level the increased SNR at 7T has been exploited for breakthroughs in the detection of small brain tissue lesions such as microbleeds and microinfarcts. At all three levels (**P**ipes, **P**erfusion, **P**arenchyma) the new sequences developed and knowledge obtained at 7T MRI have been used for successful development of similar methods at lower field strengths. For instance, cortical microinfarcts can nowadays also be detected at 3T, due to successful translation to 3T of the cortical microinfarct rating developed on 7T MRI. Several limitations of 7T MRI - like inhomogeneity of the magnetic fields - still remain and currently hamper further technical developments. The effects of these limitations are most apparent for functional MRI techniques and for anatomical scans in the area of the temporal lobes and the cerebellum. However, with the almost exponential growth in developments at 7T MRI over the last decade, these restrictions may well be partially or even totally resolved or bypassed in the near future.

Conclusion

In less than a decade, 7T MRI has provided innovative methods to assess both the small intracranial arteries (**P**ipes), the brain function (**P**erfusion) and the brain tissue lesions (**P**arenchyma). In the next decade these methods will become more widely available in patient studies with cerebrovascular disease and even on an individual basis in clinical practice, while the most successful methods can – if possible – be translated to widely available clinical MR field strengths (3T and 1.5T MRI).

References

1. van der Kolk AG, Hendrikse J, Zwanenburg JJ, et al: Clinical applications of 7 T MRI in the brain. Eur J Radiol 82:708-718, 2013.
2. Hendrikse J, Zwanenburg JJ, Visser F, et al: Noninvasive depiction of the lenticulostriate arteries with time-of-flight MR angiography at 7.0 T. Cerebrovasc Dis 26:624-629, 2008.
3. Cho ZH, Kang CK, Han JY, et al: Observation of the lenticulostriate arteries in the human brain *in vivo* using 7.0T MR angiography. Stroke 39:1604-1606, 2008.
4. Johst S, Wrede KH, Ladd ME, et al: Time-of-flight magnetic resonance angiography at 7 T using venous saturation pulses with reduced flip angles. Invest Radiol 47:445-450, 2012.
5. Bae KT, Park SH, Moon CH, et al: Dual-echo arteriovenography imaging with 7T MRI. J Magn Reson Imaging 31:255-261, 2010.
6. Conijn MM, Hendrikse J, Zwanenburg JJ, et al: Perforating arteries originating from the posterior communicating artery: a 7.0-Tesla MRI study. Eur Radiol 19:2986-2992, 2009.
7. Wrede KH, Dammann P, Monninghoff C, et al: Non-enhanced MR imaging of cerebral aneurysms: 7 Tesla versus 1.5 Tesla. PLoS One 9:e84562, 2014.
8. Zwanenburg JJ, Hendrikse J, Takahara T, et al: MR angiography of the cerebral perforating arteries with magnetization prepared anatomical reference at 7 T: comparison with time-of-flight. J Magn Reson Imaging 28:1519-1526, 2008.
9. Koning W, Bluemink JJ, Langenhuizen EA, et al: High-resolution MRI of the carotid arteries using a leaky waveguide transmitter and a high-density receive array at 7 T. Magn Reson Med 69:1186-1193, 2013.
10. den Hartog AG, Bovens SM, Koning W, et al: Current status of clinical magnetic resonance imaging for plaque characterisation in patients with carotid artery stenosis. Eur J Vasc Endovasc Surg 45:7-21, 2013.
11. Underhill HR, Yarnykh VL, Hatsukami TS, et al: Carotid plaque morphology and composition: initial comparison between 1.5- and 3.0-T magnetic field strengths. Radiology 248:550-560, 2008.
12. Yarnykh VL, Terashima M, Hayes CE, et al: Multicontrast black-blood MRI of carotid arteries: comparison between 1.5 and 3 tesla magnetic field strengths. J Magn Reson Imaging 23:691-698, 2006.
13. Balu N, Yarnykh VL, Chu B, et al: Carotid plaque assessment using fast 3D isotropic resolution black-blood MRI. Magn Reson Med 65:627-637, 2011.
14. den Hartog AG, Bovens SM, Koning W, et al: PLACD-7T Study: Atherosclerotic Carotid

Plaque Components Correlated with Cerebral Damage at 7 Tesla Magnetic Resonance Imaging. Curr Cardiol Rev 7:28-34, 2011.

15. van Wijk DF, Strang AC, Duivenvoorden R, et al: Increasing spatial resolution of 3T MRI scanning improves reproducibility of carotid arterial wall dimension measurements. MAGMA 27:219-226, 2014.
16. Kraff O, Bitz AK, Breyer T, et al: A transmit/receive radiofrequency array for imaging the carotid arteries at 7 Tesla: coil design and first *in vivo* results. Invest Radiol 46:246-254, 2011.
17. de Rotte AA, Koning W, Truijman MT, et al: Seven-tesla magnetic resonance imaging of atherosclerotic plaque in the significantly stenosed carotid artery: a feasibility study. Invest Radiol 49:749-757, 2014.
18. Koning W, de Rotte AA, Bluemink JJ, et al: MRI of the carotid artery at 7 Tesla: quantitative comparison with 3 Tesla. J Magn Reson Imaging 41:773-780, 2015.
19. Kroner ES, van Schinkel LD, Versluis MJ, et al: Ultrahigh-field 7-T magnetic resonance carotid vessel wall imaging: initial experience in comparison with 3-T field strength. Invest Radiol 47:697-704, 2012.
20. von Morze C, Xu D, Purcell DD, et al: Intracranial time-of-flight MR angiography at 7T with comparison to 3T. J Magn Reson Imaging 26:900-904, 2007.
21. Stamm AC, Wright CL, Knopp MV, et al: Phase contrast and time-of-flight magnetic resonance angiography of the intracerebral arteries at 1.5, 3 and 7 T. Magn Reson Imaging 31:545-549, 2013.
22. Heverhagen JT, Bourekas E, Sammet S, et al: Time-of-flight magnetic resonance angiography at 7 Tesla. Invest Radiol 43:568-573, 2008.
23. Madai VI, von Samson-Himmelstjerna FC, Sandow N, et al: Ultrahigh-field MPRAGE Magnetic Resonance Angiography at 7.0T in patients with cerebrovascular disease. Eur J Radiol 84:2613-2617, 2015.
24. Wrede KH, Dammann P, Johst S, et al: Non-Enhanced MR Imaging of Cerebral Arteriovenous Malformations at 7 Tesla. Eur Radiol, 2015.
25. Nowinski WL, Puspitasaari F, Volkau I, et al: Comparison of magnetic resonance angiography scans on 1.5, 3, and 7 Tesla units: a quantitative study of 3-dimensional cerebrovasculature. J Neuroimaging 23:86-95, 2013.
26. Deng X, Zhang Z, Zhang Y, et al: Comparison of 7.0- and 3.0-T MRI and MRA in ischemic-type moyamoya disease: preliminary experience. J Neurosurg:1-10, 2015.

27. Monninghoff C, Maderwald S, Wanke I: Pre-interventional assessment of a vertebrobasilar aneurysm with 7 tesla time-of-flight MR angiography. Rofo 181:266-268, 2009.
28. Monninghoff C, Maderwald S, Theysohn JM, et al: Evaluation of intracranial aneurysms with 7 T versus 1.5 T time-of-flight MR angiography - initial experience. Rofo 181:16-23, 2009.
29. Kang CK, Park CW, Han JY, et al: Imaging and analysis of lenticulostriate arteries using 7.0-Tesla magnetic resonance angiography. Magn Reson Med 61:136-144, 2009.
30. Kang CK, Park CA, Kim KN, et al: Non-invasive visualization of basilar artery perforators with 7T MR angiography. J Magn Reson Imaging 32:544-550, 2010.
31. Kang CK, Park CA, Park CW, et al: Lenticulostriate arteries in chronic stroke patients visualised by 7 T magnetic resonance angiography. Int J Stroke 5:374-380, 2010.
32. Seo SW, Kang CK, Kim SH, et al: Measurements of lenticulostriate arteries using 7T MRI: new imaging markers for subcortical vascular dementia. J Neurol Sci 322:200-205, 2012.
33. Liem MK, van der Grond J, Versluis MJ, et al: Lenticulostriate arterial lumina are normal in cerebral autosomal-dominant arteriopathy with subcortical infarcts and leukoencephalopathy: a high-field *in vivo* MRI study. Stroke 41:2812-2816, 2010.
34. Kang CK, Park CA, Lee H, et al: Hypertension correlates with lenticulostriate arteries visualized by 7T magnetic resonance angiography. Hypertension 54:1050-1056, 2009.
35. Cho ZH, Lee YB, Kang CK, et al: Microvascular imaging of asymptomatic MCA steno-occlusive patients using ultra-high-field 7T MRI. J Neurol 260:144-150, 2013.
36. Schmitter S, Wu X, Adriany G, et al: Cerebral TOF angiography at 7T: Impact of B1 (+) shimming with a 16-channel transceiver array. Magn Reson Med 71:966-977, 2014.
37. Wrede KH, Johst S, Dammann P, et al: Improved cerebral time-of-flight magnetic resonance angiography at 7 Tesla--feasibility study and preliminary results using optimized venous saturation pulses. PLoS One 9:e106697, 2014.
38. von Morze C, Purcell DD, Banerjee S, et al: High-resolution intracranial MRA at 7T using autocalibrating parallel imaging: initial experience in vascular disease patients. Magn Reson Imaging 26:1329-1333, 2008.
39. Maderwald S, Ladd SC, Gizewski ER, et al: To TOF or not to TOF: strategies for non-contrast-enhanced intracranial MRA at 7 T. MAGMA 21:159-167, 2008.
40. Zhang Z, Deng X, Weng D, et al: Segmented TOF at 7T MRI: Technique and clinical applications. Magn Reson Imaging 33:1043-1050, 2015.

41. Harteveld AA, De Cocker LJ, Dieleman N, et al: High-resolution postcontrast time-of-flight MR angiography of intracranial perforators at 7.0 Tesla. PLoS One 10:e0121051, 2015.
42. Umutlu L, Theysohn N, Maderwald S, et al: 7 Tesla MPRAGE imaging of the intracranial arterial vasculature: nonenhanced versus contrast-enhanced. Acad Radiol 20:628-634, 2013.
43. van Ooij P, Zwanenburg JJ, Visser F, et al: Quantification and visualization of flow in the Circle of Willis: time-resolved three-dimensional phase contrast MRI at 7 T compared with 3 T. Magn Reson Med 69:868-876, 2013.
44. Kang CK, Park CA, Lee DS, et al: Velocity measurement of microvessels using phase-contrast magnetic resonance angiography at 7 tesla MRI. Magn Reson Med, 2015.
45. Bouvy WH, Geurts LJ, Kuijf HJ, et al: Assessment of blood flow velocity and pulsatility in cerebral perforating arteries with 7-T quantitative flow MRI. NMR Biomed, 2015.
46. Mitchell GF: Effects of central arterial aging on the structure and function of the peripheral vasculature: implications for end-organ damage. J Appl Physiol (1985) 105:1652-1660, 2008.
47. Dieleman N, van der Kolk AG, Zwanenburg JJ, et al: Imaging intracranial vessel wall pathology with magnetic resonance imaging: current prospects and future directions. Circulation 130:192-201, 2014.
48. Ryoo S, Cha J, Kim SJ, et al: High-resolution magnetic resonance wall imaging findings of Moyamoya disease. Stroke 45:2457-2460, 2014.
49. van der Kolk AG, Zwanenburg JJ, Brundel M, et al: Intracranial vessel wall imaging at 7.0-T MRI. Stroke 42:2478-2484, 2011.
50. van der Kolk AG, Hendrikse J, Brundel M, et al: Multi-sequence whole-brain intracranial vessel wall imaging at 7.0 tesla. Eur Radiol 23:2996-3004, 2013.
51. Qiao Y, Steinman DA, Qin Q, et al: Intracranial arterial wall imaging using three-dimensional high isotropic resolution black blood MRI at 3.0 Tesla. J Magn Reson Imaging 34:22-30, 2011.
52. Wang J, Helle M, Zhou Z, et al: Joint blood and cerebrospinal fluid suppression for intracranial vessel wall MRI. Magn Reson Med, 2015.
53. van der Kolk AG, Zwanenburg JJ, Brundel M, et al: Distribution and natural course of intracranial vessel wall lesions in patients with ischemic stroke or TIA at 7.0 Tesla MRI. Eur Radiol 25:1692-1700, 2015.
54. Dieleman N, van der Kolk AG, Zwanenburg JJ, et al: Relations between location and type of intracranial atherosclerosis and parenchymal damage. J Cereb Blood Flow Metab, 2015.

55. Portanova A, Hakakian N, Mikulis DJ, et al: Intracranial vasa vasorum: insights and implications for imaging. Radiology 267:667-679, 2013.
56. Moody AR, Murphy RE, Morgan PS, et al: Characterization of complicated carotid plaque with magnetic resonance direct thrombus imaging in patients with cerebral ischemia. Circulation 107:3047-3052, 2003.
57. Ritz K, Denswil NP, Stam OC, et al: Cause and mechanisms of intracranial atherosclerosis. Circulation 130:1407-1414, 2014.
58. Dieleman N, van der Kolk AG, van Veluw SJ, et al: Patterns of intracranial vessel wall changes in relation to ischemic infarcts. Neurology 83:1316-1320, 2014.
59. Majidi S, Sein J, Watanabe M, et al: Intracranial-derived atherosclerosis assessment: an in vitro comparison between virtual histology by intravascular ultrasonography, 7T MRI, and histopathologic findings. AJNR Am J Neuroradiol 34:2259-2264, 2013.
60. van der Kolk AG, Zwanenburg JJ, Denswil NP, et al: Imaging the Intracranial Atherosclerotic Vessel Wall Using 7T MRI: Initial Comparison with Histopathology. AJNR Am J Neuroradiol, 2014.
61. Kleinloog R, Korkmaz E, Zwanenburg JJ, et al: Visualization of the aneurysm wall: a 7.0-tesla magnetic resonance imaging study. Neurosurgery 75:614-622; discussion 622, 2014.
62. Matsushige T, Chen B, Ringelstein A, et al: Giant Intracranial Aneurysms at 7T MRI. AJNR Am J Neuroradiol, 2015.
63. Yao B, Li TQ, Gelderen P, et al: Susceptibility contrast in high field MRI of human brain as a function of tissue iron content. Neuroimage 44:1259-1266, 2009.
64. Zwanenburg JJ, Versluis MJ, Luijten PR, et al: Fast high resolution whole brain T2* weighted imaging using echo planar imaging at 7T. Neuroimage 56:1902-1907, 2011.
65. Cho ZH, Choi SH, Chi JG, et al: Classification of the venous architecture of the pineal gland by 7T MRI. J Neuroradiol 38:238-241, 2011.
66. Di Ieva A, Tschabitscher M, Galzio RJ, et al: The veins of the nucleus dentatus: anatomical and radiological findings. Neuroimage 54:74-79, 2011.
67. Dammann P, Wrede KH, Maderwald S, et al: The venous angioarchitecture of sporadic cerebral cavernous malformations: a susceptibility weighted imaging study at 7 T MRI. J Neurol Neurosurg Psychiatry 84:194-200, 2013.
68. Frischer JM, God S, Gruber A, et al: Susceptibility-weighted imaging at 7 T: Improved diagnosis of cerebral cavernous malformations and associated developmental venous anomalies. Neuroimage Clin 1:116-120, 2012.

69. Dammann P, Barth M, Zhu Y, et al: Susceptibility weighted magnetic resonance imaging of cerebral cavernous malformations: prospects, drawbacks, and first experience at ultra-high field strength (7-Tesla) magnetic resonance imaging. Neurosurg Focus 29:E5, 2010.
70. Dal-Bianco A, Hametner S, Grabner G, et al: Veins in plaques of multiple sclerosis patients - a longitudinal magnetic resonance imaging study at 7 Tesla. Eur Radiol 25:2913-2920, 2015.
71. Dixon JE, Simpson A, Mistry N, et al: Optimisation of T(2)*-weighted MRI for the detection of small veins in multiple sclerosis at 3 T and 7 T. Eur J Radiol 82:719-727, 2013.
72. Tallantyre EC, Morgan PS, Dixon JE, et al: A comparison of 3T and 7T in the detection of small parenchymal veins within MS lesions. Invest Radiol 44:491-494, 2009.
73. Tallantyre EC, Dixon JE, Donaldson I, et al: Ultra-high-field imaging distinguishes MS lesions from asymptomatic white matter lesions. Neurology 76:534-539, 2011.
74. Mistry N, Dixon J, Tallantyre E, et al: Central veins in brain lesions visualized with high-field magnetic resonance imaging: a pathologically specific diagnostic biomarker for inflammatory demyelination in the brain. JAMA Neurol 70:623-628, 2013.
75. De Guio F, Vignaud A, Ropele S, et al: Loss of venous integrity in cerebral small vessel disease: a 7-T MRI study in cerebral autosomal-dominant arteriopathy with subcortical infarcts and leukoencephalopathy (CADASIL). Stroke 45:2124-2126, 2014.
76. Sinnecker T, Bozin I, Dorr J, et al: Periventricular venous density in multiple sclerosis is inversely associated with T2 lesion count: a 7 Tesla MRI study. Mult Scler 19:316-325, 2013.
77. Kuijf HJ, Bouvy WH, Zwanenburg JJM, et al: Automated detection of periventricular veins on 7 T brain MRI. Medical Imaging 2015: Image Processing 9413, 2015.
78. Fan AP, Govindarajan ST, Kinkel RP, et al: Quantitative oxygen extraction fraction from 7-Tesla MRI phase: reproducibility and application in multiple sclerosis. J Cereb Blood Flow Metab 35:131-139, 2015.
79. Goodwin JA, Kudo K, Shinohe Y, et al: Susceptibility-Weighted Phase Imaging and Oxygen Extraction Fraction Measurement during Sedation and Sedation Recovery using 7T MRI. J Neuroimaging 25:575-581, 2015.
80. Huber L, Ivanov D, Guidi M, et al: Functional cerebral blood volume mapping with simultaneous multi-slice acquisition. Neuroimage, 2015.
81. Krieger SN, Huber L, Poser BA, et al: Simultaneous acquisition of cerebral blood volume-, blood flow-, and blood oxygenation-weighted MRI signals at ultra-high magnetic field. Magn Reson Med 74:513-517, 2015.

82. Zhang X, Petersen ET, Ghariq E, et al: In vivo blood T(1) measurements at 1.5 T, 3 T, and 7 T. Magn Reson Med 70:1082-1086, 2013.
83. Ghariq E, Teeuwisse WM, Webb AG, et al: Feasibility of pseudocontinuous arterial spin labeling at 7 T with whole-brain coverage. MAGMA 25:83-93, 2012.
84. Gardener AG, Gowland PA, Francis ST: Implementation of quantitative perfusion imaging using pulsed arterial spin labeling at ultra-high field. Magn Reson Med 61:874-882, 2009.
85. Teeuwisse WM, Webb AG, van Osch MJ: Arterial spin labeling at ultra-high field: All that glitters is not gold. Int J Imaging Syst Technol 20:62-70, 2010.
86. Koning W, Petersen ET, Zwanenburg JJ, et al: Full brain and territorial arterial spin labeling with external RF shimmed labeling coil at 7 tesla. Proceedings of the 21st Annual Meeting of ISMRM:Abstract 3042, 2013.
87. Pfeuffer J, Adriany G, Shmuel A, et al: Perfusion-based high-resolution functional imaging in the human brain at 7 Tesla. Magn Reson Med 47:903-911, 2002.
88. Wang Y, Moeller S, Li X, et al: Simultaneous multi-slice Turbo-FLASH imaging with CAIPIRINHA for whole brain distortion-free pseudo-continuous arterial spin labeling at 3 and 7 T. Neuroimage 113:279-288, 2015.
89. Fierstra J, Sobczyk O, Battisti-Charbonney A, et al: Measuring cerebrovascular reactivity: what stimulus to use? J Physiol 591:5809-5821, 2013.
90. van der Zwaag W, Francis S, Head K, et al: fMRI at 1.5, 3 and 7 T: characterising BOLD signal changes. Neuroimage 47:1425-1434, 2009.
91. Siero JC, Hendrikse J, Hoogduin H, et al: Cortical depth dependence of the BOLD initial dip and poststimulus undershoot in human visual cortex at 7 Tesla. Magn Reson Med 73:2283-2295, 2015.
92. De Martino F, Zimmermann J, Muckli L, et al: Cortical depth dependent functional responses in humans at 7T: improved specificity with 3D GRASE. PLoS One 8:e60514, 2013.
93. Koopmans PJ, Barth M, Orzada S, et al: Multi-echo fMRI of the cortical laminae in humans at 7 T. Neuroimage 56:1276-1285, 2011.
94. Siero JC, Petridou N, Hoogduin H, et al: Cortical depth-dependent temporal dynamics of the BOLD response in the human brain. J Cereb Blood Flow Metab 31:1999-2008, 2011.
95. Polimeni JR, Fischl B, Greve DN, et al: Laminar analysis of 7T BOLD using an imposed spatial activation pattern in human V1. Neuroimage 52:1334-1346, 2010.
96. Siero JC, Hermes D, Hoogduin H, et al: BOLD matches neuronal activity at the mm scale: a combined 7T fMRI and ECoG study in human sensorimotor cortex. Neuroimage 101:177-184, 2014.

97. Besle J, Sanchez-Panchuelo RM, Bowtell R, et al: Event-related fMRI at 7T reveals overlapping cortical representations for adjacent fingertips in S1 of individual subjects. Hum Brain Mapp 35:2027-2043, 2014.
98. Siero JC, Hermes D, Hoogduin H, et al: BOLD consistently matches electrophysiology in human sensorimotor cortex at increasing movement rates: a combined 7T fMRI and ECoG study on neurovascular coupling. J Cereb Blood Flow Metab 33:1448-1456, 2013.
99. Stringer EA, Chen LM, Friedman RM, et al: Differentiation of somatosensory cortices by high-resolution fMRI at 7 T. Neuroimage 54:1012-1020, 2011.
100. Stefanescu MR, Thurling M, Maderwald S, et al: A 7T fMRI study of cerebellar activation in sequential finger movement tasks. Exp Brain Res 228:243-254, 2013.
101. Sanchez-Panchuelo RM, Francis S, Bowtell R, et al: Mapping human somatosensory cortex in individual subjects with 7T functional MRI. J Neurophysiol 103:2544-2556, 2010.
102. Schweizer R, Voit D, Frahm J: Finger representations in human primary somatosensory cortex as revealed by high-resolution functional MRI of tactile stimulation. Neuroimage 42:28-35, 2008.
103. Bhogal AA, Siero JC, Fisher JA, et al: Investigating the non-linearity of the BOLD cerebrovascular reactivity response to targeted hypo/hypercapnia at 7T. Neuroimage 98:296-305, 2014.
104. Bhogal AA, Philippens ME, Siero JC, et al: Examining the regional and cerebral depth-dependent BOLD cerebrovascular reactivity response at 7T. Neuroimage 114:239-248, 2015.
105. Conijn MM, Hoogduin JM, van der Graaf Y, et al: Microbleeds, lacunar infarcts, white matter lesions and cerebrovascular reactivity -- a 7 T study. Neuroimage 59:950-956, 2012.
106. Petridou N, Italiaander M, van de Bank BL, et al: Pushing the limits of high-resolution functional MRI using a simple high-density multi-element coil design. NMR Biomed 26:65-73, 2013.
107. Kemper VG, De Martino F, Yacoub E, et al: Variable flip angle 3D-GRASE for high resolution fMRI at 7 tesla. Magn Reson Med, 2015.
108. Hua J, Qin Q, van Zijl PC, et al: Whole-brain three-dimensional T2-weighted BOLD functional magnetic resonance imaging at 7 Tesla. Magn Reson Med 72:1530-1540, 2014.
109. Poser BA, Koopmans PJ, Witzel T, et al: Three dimensional echo-planar imaging at 7 Tesla. Neuroimage 51:261-266, 2010.

110. Boyacioglu R, Schulz J, Koopmans PJ, et al: Improved sensitivity and specificity for resting state and task fMRI with multiband multi-echo EPI compared to multi-echo EPI at 7 T. Neuroimage 119:352-361, 2015.
111. Moeller S, Yacoub E, Olman CA, et al: Multiband multislice GE-EPI at 7 tesla, with 16-fold acceleration using partial parallel imaging with application to high spatial and temporal whole-brain fMRI. Magn Reson Med 63:1144-1153, 2010.
112. Brundel M, Reijmer YD, van Veluw SJ, et al: Cerebral microvascular lesions on high-resolution 7-Tesla MRI in patients with type 2 diabetes. Diabetes 63:3523-3529, 2014.
113. De Reuck JL, Deramecourt V, Auger F, et al: The significance of cortical cerebellar microbleeds and microinfarcts in neurodegenerative and cerebrovascular diseases. A post-mortem 7.0-tesla magnetic resonance study with neuropathological correlates. Cerebrovasc Dis 39:138-143, 2015.
114. Conijn MM, Geerlings MI, Luijten PR, et al: Visualization of cerebral microbleeds with dual-echo T2*-weighted magnetic resonance imaging at 7.0 T. J Magn Reson Imaging 32:52-59, 2010.
115. Conijn MM, Geerlings MI, Biessels GJ, et al: Cerebral microbleeds on MR imaging: comparison between 1.5 and 7T. AJNR Am J Neuroradiol 32:1043-1049, 2011.
116. Theysohn JM, Kraff O, Maderwald S, et al: 7 tesla MRI of microbleeds and white matter lesions as seen in vascular dementia. J Magn Reson Imaging 33:782-791, 2011.
117. Nandigam RN, Viswanathan A, Delgado P, et al: MR imaging detection of cerebral microbleeds: effect of susceptibility-weighted imaging, section thickness, and field strength. AJNR Am J Neuroradiol 30:338-343, 2009.
118. de Bresser J, Brundel M, Conijn MM, et al: Visual cerebral microbleed detection on 7T MR imaging: reliability and effects of image processing. AJNR Am J Neuroradiol 34:E61-64, 2013.
119. Kuijf HJ, de Bresser J, Geerlings MI, et al: Efficient detection of cerebral microbleeds on 7.0 T MR images using the radial symmetry transform. Neuroimage 59:2266-2273, 2012.
120. De Reuck JL, Auger F, Durieux N, et al: Detection of Cortical Microbleeds in Postmortem Brains of Patients with Lewy Body Dementia: A 7.0-Tesla Magnetic Resonance Imaging Study with Neuropathological Correlates. Eur Neurol 74:158-161, 2015.
121. Ni J, Auriel E, Martinez-Ramirez S, et al: Cortical localization of microbleeds in cerebral amyloid angiopathy: an ultra high-field 7T MRI study. J Alzheimers Dis 43:1325-1330, 2015.
122. Verstraete E, Biessels GJ, van Den Heuvel MP, et al: No evidence of microbleeds in ALS patients at 7 Tesla MRI. Amyotroph Lateral Scler 11:555-557, 2010.

123. Smith EE, Schneider JA, Wardlaw JM, et al: Cerebral microinfarcts: the invisible lesions. Lancet Neurol 11:272-282, 2012.
124. van Veluw SJ, Zwanenburg JJ, Engelen-Lee J, et al: In vivo detection of cerebral cortical microinfarcts with high-resolution 7T MRI. J Cereb Blood Flow Metab 33:322-329, 2013.
125. van Veluw SJ, Zwanenburg JJ, Rozemuller AJ, et al: The spectrum of MR detectable cortical microinfarcts: a classification study with 7-tesla postmortem MRI and histopathology. J Cereb Blood Flow Metab 35:676-683, 2015.
126. De Reuck J, Deramecourt V, Auger F, et al: Post-mortem 7.0-tesla magnetic resonance study of cortical microinfarcts in neurodegenerative diseases and vascular dementia with neuropathological correlates. J Neurol Sci 346:85-89, 2014.
127. van Veluw SJ, Jolink WM, Hendrikse J, et al: Cortical microinfarcts on 7T MRI in patients with spontaneous intracerebral hemorrhage. J Cereb Blood Flow Metab 34:1104-1106, 2014.
128. van Veluw SJ, Heringa SM, Kuijf HJ, et al: Cerebral cortical microinfarcts at 7Tesla MRI in patients with early Alzheimer's disease. J Alzheimers Dis 39:163-167, 2014.
129. de Rotte AA, Koning W, den Hartog AG, et al: 7.0 T MRI detection of cerebral microinfarcts in patients with a symptomatic high-grade carotid artery stenosis. J Cereb Blood Flow Metab 34:1715-1719, 2014.
130. van Veluw SJ, Hilal S, Kuijf HJ, et al: Cortical microinfarcts on 3T MRI: Clinical correlates in memory-clinic patients. Alzheimers Dement, 2015.
131. van Dalen JW, Scuric EE, van Veluw SJ, et al: Cortical microinfarcts detected *in vivo* on 3 Tesla MRI: clinical and radiological correlates. Stroke 46:255-257, 2015.
132. Bachmann R, Reilmann R, Schwindt W, et al: FLAIR imaging for multiple sclerosis: a comparative MR study at 1.5 and 3.0 Tesla. Eur Radiol 16:915-921, 2006.
133. Kollia K, Maderwald S, Putzki N, et al: First clinical study on ultra-high-field MR imaging in patients with multiple sclerosis: comparison of 1.5T and 7T. AJNR Am J Neuroradiol 30:699-702, 2009.
134. Kilsdonk ID, Lopez-Soriano A, Kuijer JP, et al: Morphological features of MS lesions on FLAIR* at 7 T and their relation to patient characteristics. J Neurol 261:1356-1364, 2014.
135. Bouvy WH, Biessels GJ, Kuijf HJ, et al: Visualization of perivascular spaces and perforating arteries with 7 T magnetic resonance imaging. Invest Radiol 49:307-313, 2014.
136. Kilsdonk ID, Steenwijk MD, Pouwels PJ, et al: Perivascular spaces in MS patients at 7 Tesla MRI: a marker of neurodegeneration? Mult Scler 21:155-162, 2015.

137. Zong X, Park SH, Shen D, et al: Visualization of perivascular spaces in the human brain at 7T: sequence optimization and morphology characterization. Neuroimage 125:895-902, 2015.
138. Cai K, Tain R, Das S, et al: The feasibility of quantitative MRI of perivascular spaces at 7T. J Neurosci Methods 256:151-156, 2015.
139. Biessels GJ, Zwanenburg JJ, Visser F, et al: Hypertensive cerebral hemorrhage: imaging the leak with 7-T MRI. Neurology 75:572-573, 2010.

Chapter 3

High-resolution postcontrast time-of-flight MR angiography of intracranial perforators at 7.0 tesla

Anita A. Harteveld[1], Laurens J.L. De Cocker[1], Nikki Dieleman[1], Anja G. van der Kolk[1], Jaco J.M. Zwanenburg[1,2], Pierre A. Robe[3], Peter R. Luijten[1], Jeroen Hendrikse[1]

[1]Department of Radiology; [2]Image Sciences Institute; [3]Department of Neurosurgery; University Medical Center Utrecht, Utrecht, the Netherlands

Published in *PLoS One* 2015

Abstract

Objectives

Different studies already demonstrated the benefits of 7T for precontrast TOF-MRA in the visualization of intracranial small vessels. The aim of this study was to assess the performance of high-resolution 7T TOF-MRA after the administration of a gadolinium-based contrast agent in visualizing intracranial perforating arteries.

Materials and Methods

Ten consecutive patients (7 male; mean age, 50.4 ± 9.9 years) who received TOF-MRA at 7T after contrast administration were retrospectively included in this study. Intracranial perforating arteries, branching from the parent arteries of the circle of Willis, were identified on all TOF-MRA images. Provided a TOF-MRA before contrast administration was present, a direct comparison between pre- and postcontrast TOF-MRA was made.

Results

It was possible to visualize intracranial perforating arteries branching off from the entire circle of Willis, and their proximal branches. The posterior cerebral artery (P1 and proximal segment of P2) appeared to have the largest number of visible perforating branches (mean of 5.1 in each patient, with a range of 2-7). The basilar artery and middle cerebral artery (M1 and proximal segment M2) followed with a mean number of 5.0 and 3.5 visible perforating branches (range of 1-9 and 1-8, respectively). Venous contamination in the postcontrast scans sometimes made it difficult to discern the arterial or venous nature of a vessel.

Conclusions

High-resolution postcontrast TOF-MRA at 7T was able to visualize multiple intracranial perforators branching off from various parts of the circle of Willis and proximal intracranial arteries. Although confirmation in a larger study is needed, the administration of a contrast agent for high-resolution TOF-MRA at 7T seems to enable a better visualization of the distal segment of certain intracranial perforators.

Introduction

Intracranial perforating arteries and small branches of the circle of Willis provide blood supply to the brain stem and deep grey and white matter structures of the brain.[1,2] Acute occlusion of these perforating arteries may cause infarctions with profound clinical symptoms, while chronic small vessel disease of the perforating arteries may cause chronic white matter lesions in the pons and the cerebrum.[3-7] Due to the size of these small perforating arteries (<1.1 mm in diameter[1]), a high spatial resolution is required for clear visualization of these vessels and their pathology. With the spatial resolution of magnetic resonance angiography (MRA) at standard field strengths (1.5 or 3.0 tesla (T)), usually only the larger intracranial arteries can be visualized.[8] Therefore, in current clinical practice, intra-arterial digital subtraction angiography (iaDSA) is used to visualize smaller arteries, including the perforating arteries. Disadvantages of iaDSA are its use of ionizing radiation, its invasiveness[8], and its inability to visualize the brain parenchyma.

Visualizing perforating arteries with MRI allows for a combined evaluation of vascular lesions and the consequences of these lesions on the brain parenchymal level (such as infarcts and white matter lesions). Ultrahigh field MRI, like 7T, has the advantage of an increased SNR compared with 1.5T and 3T MRI, enabling a higher spatial resolution within clinically feasible scan times (<10 minutes). Also, the T_1 relaxation time of tissues increases with higher field strengths, yielding a better contrast between suppressed background and flowing blood in time-of-flight MRA (TOF-MRA). Due to the longer T_1, spins in static tissue show decreased relaxation in between the radiofrequency pulses, resulting in lower signal of static tissue.[9] Different studies already demonstrated the benefits of 7T for TOF-MRA in the visualization of intracranial small vessels[8,10-21].

In previous reports, 7T MRI has been shown to be capable of visualizing the lenticulostriate arteries[13,15,17-21], perforating arteries originating from the posterior communicating artery (PCoA)[14], and basilar artery (BA) perforators[16]. These previous studies, in which each individual study focused on the visualization of one type of perforators only, were performed using TOF-MRA techniques without contrast administration.

The lack of contrast administration in TOF-MRA may predispose to signal loss due to saturation effects, particularly in vessels with slow blood flow (like small arteries).[22] Furthermore, more complex flow patterns might be present in patients with vascular lesions leading to changed signal properties.[11] Contrast administration shortens the T_1 relaxation time of blood and thereby might improve the contrast-to-noise ratio between the blood and the surrounding brain parenchyma, giving a clearer depiction of slow-moving blood in distal vessels.[22,23] However, the contrast agent also shortens the T_2^* relaxation time, which could reduce visibility of the blood vessels. Although previous studies have already demonstrated better visualization of the distal segments of large intracranial arteries after the administration of a contrast agent at 1.5T and 3T TOF-MRA[22-24] as well as 7T MPRAGE MRA[25], the value of contrast administration has never been evaluated at 7T TOF-MRA for the smaller intracranial perforating arteries.

The aim of the current study was to assess the visualization of intracranial perforators with high-resolution 7T TOF-MRA after the administration of a gadolinium-based contrast agent.

Materials and Methods

Study population

This retrospective study was approved by the local medical ethics committee of University Medical Center Utrecht. All patients clinically imaged between October 2012 and April 2013 at our institution, who underwent a postcontrast 7T TOF-MRA were included. All included subjects gave written informed consent.

MR imaging protocol

Imaging was performed on a whole-body human 7T MR system (Philips Healthcare, Cleveland, OH, USA) equipped with a 32-channel receive head coil and volume transmit/receive coil for transmission (Nova Medical, Wilmington, MA, USA). A patient-specific clinical imaging protocol was obtained in all patients. Before acquisition of the TOF-MRA sequence, 0.1 mmol/kg of a gadolinium-containing contrast agent (Gadobutrol, Gadovist 1.0 mmol/mL, Bayer Schering Pharma, Newbury, UK) was administered intravenously to the patient. The following imaging parameters were

used for the TOF-MRA sequence: FOV 200x190x50 mm^3 in transverse orientation, acquired voxel size 0.25x0.3x0.4 mm^3, TR 15.3 ms, TE 3.4 ms, flip angle 25 degrees, number of slices 250, acquisition time approximately 9 minutes. A high-resolution Fluid-Attenuated Inversion Recovery (FLAIR) sequence, for anatomical verification, was used with the following imaging parameters: FOV 250x250x190 mm^3, acquired voxel size 0.8x0.8x0.8 mm^3, TR/TE/TI 8000/300/2250 ms, flip angle 100 degrees, number of slices 475, acquisition time approximately 13 minutes.

Processing & image analysis

For analysis of the acquired 3D TOF-MRA data, MPR (multi planar reconstruction; thickness 0.4 mm; no overlap) and MIP (maximum intensity projection; thickness 10 mm; 8 mm overlap) slabs were made in coronal, sagittal and transverse orientations on an offline workstation (Philips). A descriptive, qualitative analysis of the location and number of perforating arteries was performed. Perforating arteries originating directly from the following feeding vessels were evaluated: the anterior, middle and posterior cerebral arteries (A1, M1, P1 and proximal part of A2, M2 and P2); the anterior communicating artery (ACoA); the anterior choroidal artery (AChA); the posterior communicating artery (PCoA); the entire basilar artery (BA); and the distal vertebral artery (VA). Most perforating arteries arise from these vessel segments.[1] The lenticulostriate arteries were divided into a medial group, originating from the anterior cerebral artery, and a lateral group, originating from the middle cerebral artery.[26] Perforators were grouped according to the parent artery they originated from (including left or right) and the direction or target of the perforator. Because of the relatively limited FOV, in some scans the more caudal part of the circle of Willis (distal BA and/or VA) was not included (distal BA and VA: 3 scans; VA: 5 scans). The FLAIR images were used for anatomical assessment of direction or target brain region of the perforators. MPR slabs (thickness 0.8 mm, no overlap) were made in coronal, sagittal and transverse orientation. The perforating arteries were scored by 2 observers (A.H. and L.D.C.).

Comparison with precontrast MRA

In two patients also a TOF-MRA without contrast administration was available, acquired with the same imaging parameters and image orientation. This allowed for an additional comparison between the perforating arteries as visualized on the post- versus precontrast TOF-MRA in the same patient.

Results

Study population

In total 12 consecutive patients were eligible for this study, however, two patients were excluded due to motion artefacts, resulting in a total of 10 patients (7 male; mean age 50.4 ± 9.9 years). The patient population consisted of patients with suspected cerebral vasculitis (n=4), suspected reversible cerebral vasoconstriction syndrome (n=1), pre-operative assessment of the anatomical relation between brain tumor and arterial perforators (n=2), subarachnoid hemorrhage (n=2) and suspected (but undefined) cerebrovascular disease (n=1).

Postcontrast TOF-MRA

Typical images of intracranial perforators from different patients, obtained by postcontrast TOF-MRA at 7T, are shown in **Figure 1**. The high spatial resolution in all three anatomical planes (0.25x0.3x0.4 mm^3) enabled reconstructions without loss of spatial resolution. An overview of the identified perforating arteries branching off from the circle of Willis and proximal intracranial arteries on the postcontrast TOF-MRA scans is given in **Table 1**. A large variety in number and location of the perforating branches between patients could be seen. An overview of the number (mean and range) of perforating branches per parent artery is shown in **Table 2**. The PCA (P1 and proximal segment of P2) appeared to have the largest number of visible perforating branches (mean, 5.1; range, 2-7). The BA and MCA (M1 and proximal segment M2) followed with a mean number of 5.0 and 3.5 visible perforating branches (range, 1-9 and 1-8, respectively).

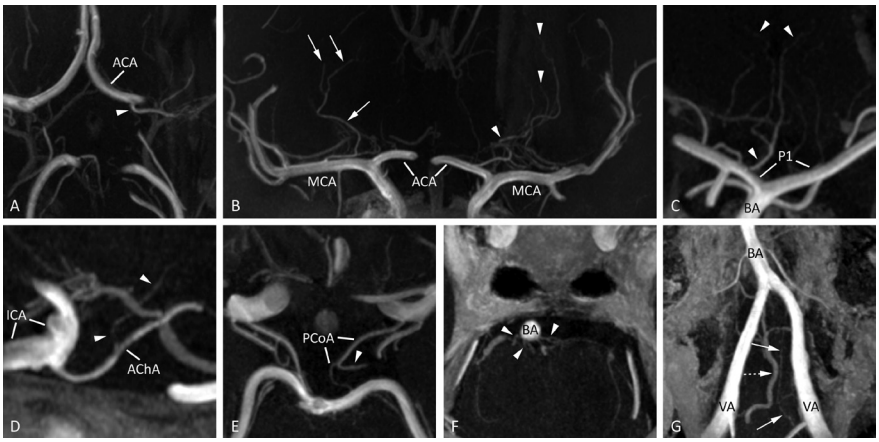

Figure 1 | Typical images of intracranial perforators from different patients, obtained by postcontrast TOF-MRA at 7T. (**A**) A medial lenticulostriate artery (arrowhead), arising from the A1 segment of the ACA (transverse slab MIP, thickness 10 mm), (**B**) lateral lenticulostriate arteries arising from the right MCA (arrows) and medial lenticulostriate arteries arising from the left ACA (arrowheads; coronal slab MIP, thickness 10 mm), (**C**) artery of Percheron (arrowheads), arising from the P1 segment of the PCA (coronal slab MIP, thickness 10 mm), (**D**) perforating branch (arrowheads) arising from the right AChA (sagittal slab MIP, thickness 10 mm), (**E**) thalamoperforating artery (arrowhead), arising from the left PCoA (transverse slab MIP, thickness 6 mm), (**F**) pontine arteries (arrowheads) arising from the BA (transverse slab MIP, thickness 4 mm), and (**G**) the intracranial feeders of the anterior spinal artery (arrows) with an adjacent vein (dashed arrow, transverse slab MIP angulated anterior-posterior in line with the BA, thickness 10 mm).
ACA: anterior cerebral artery; AChA: anterior choroidal artery; BA: basilar artery; ICA: intracranial carotid artery; MCA: middle cerebral artery; MIP: maximum intensity projection; PCA: posterior cerebral artery; PCoA: posterior communicating artery; P1: first segment of the PCA; VA: vertebral artery.

Comparison with precontrast TOF-MRA

No differences were found in the observed number of perforating arteries branching off from the parent arteries of the circle of Willis and proximal intracranial arteries before and after administration of the contrast agent. However, interpretation of the postcontrast images for identifying the perforating arteries was found to be more difficult compared to the precontrast images, especially for the perforators originating from the MCA and BA, because of adjacent venous enhancement in the images after contrast administration. An example of this venous enhancement can be seen in **Figure 2**. On the other hand, the most distal segments of some perforating arteries could be followed over a longer trajectory after the administration of the contrast agent (**Figure 3**).

Table 1 | Overview of the number of perforating arteries branching off from the circle of Willis and proximal

		1		2		3		4	
Parent §artery	Target / direction (name)	# L	# R	# L	# R	# L	# R	# L	# R
ACoA	unknown			1					
ACA	medial lenticulostriate arteries	1 (A1/A2)		1 (A1)	1 (A1)	1 (A2)		1 (A1)	1 (A2)
	unknown								
MCA	lateral lenticulostriate arteries		1 (M1)	1 (M2)	1 (M1)	M1 L absent	1 (M1)	3 (M1)	2 (M1)
	unknown							1 (M1)	2 (M1)
AChA	internal capsule								1
	unknown	1	1	1	3	2	1	1	1
PCoA	various (hypothalamus / optic tract / thalamus)		1				PCoA R absent	PCoA L absent	
	unknown			1	1	1			
PCA	interpeduncular cistern / peduncle	1 (P1)		1 (P1)	1 (P1)	2 (P1)	3 (P1)	1 (P1)	
	midbrain (circumflex arteries)	2 (P2 +P1)	1 (P2)	2 (P1+P2)	1 (P1)	1 (P1)	1 (P1)	1 (P1)	2 (P1)
	both thalami (Percheron)				1 (P1)				
	thalamus							1 (P1)	1 (P1+ BA/P1)
	lentiform nucleus								
	unknown								
BA	pontine	8		(*)		(*)		4 (*)	
	midbrain								
VA	feeder of anterior spinal artery	1	1	(**)		(**)		(**)	

Perforators are grouped based on the parent artery they originate from (including left of right), and their target or direction. Some identified perforating arteries were classified to have 'unknown' target or direction because of incomplete visualization and/or lack of visible anatomical landmarks on the TOF-MRA scan.
(*) only distal segment BA in FOV; (**) VA not in FOV; (***) only distal segment VA L in FOV. A2, M2 and P2:only proximal segment taken into account.

intracranial arteries identified in the individual postcontrast TOF-MRA scans (1-10).

5		6		7		8		9		10	
# L	# R	# L	# R	# L	# R	# L	# R	# L	# R	# L	# R
		1				1				1	
1 (A2)	1 (A1/A2)	2 (A1)	1 (A1)		1 (A1/A2)	2 (A1)	2 (A2)	1 (A1)	1 (A1)	2 (A1 + prox A2)	1 (A1)
	1 (A2)	2 (A1)	1 (A1)								
2 (M1)	1 (M1)	2 (M1)	2 (M1)	3 (M1)	2 (M1)	1 (M1)	2 (M1)	3 (M1)	2 (M1)	2 (M1)	1 (M1)
1		2	2			2	2		1		
1						1	1	PCoA L absent	PCoA R absent	1	1
		1	2	1	1						
2 (P1)						2 (P1)	1 (P1)		1 (P1)	2 (P1)	
1 (P1)	2 (P1)	2 (P1)	2 (P1 + P2)		1 (P1)	1 (P1)	1 (P1)	1 (P1)	2 (P1 + P1/P2)	1 (P1)	2 (P1)
											1 (P1)
			1 (P1)								
										1 (P1)	
					1 (P1)						
4		2		1		7		8 (7x BA, 1x SCA L)		(*)	
									1 (SCA R)		
(**)		(**)		(***)			2	(**)		(**)	

L: left; R: right. A1, M1, P1: first segment of the anterior, middle and posterior cerebral artery; A2, M2, P2: second segment of the anterior, middle, and posterior cerebral artery; ACoA: anterior communicating artery; ACA: anterior cerebral artery; AChA: anterior choroidal artery; BA: basilar artery; MCA: middle cerebral artery; PCA: posterior cerebral artery; PCoA: posterior communicating artery; SCA: superior cerebellar artery; VA: vertebral artery.

Table 2 | Mean number and range of perforating branches per parent artery identified in the 7T postcontrast TOF-MRA images.

Parent artery	Mean (number of perforators/ number of patients)	Range
Anterior communicating artery	0.4 (4/10)	0-1
Anterior cerebral artery	2.5 (25/10)	1-4
Middle cerebral artery	3.5 (35/10)	1-8
Anterior choroidal artery	2.2 (22/10)	0-4
Posterior communicating artery[a]	1.6 (14/9)	1-3
Posterior cerebral artery	5.1 (51/10)	2-7
Basilar artery[b]	5.0 (35/7)	1-9
Vertebral artery[b]	2.0 (4/2)	2

[a]In one patient the posterior communicating artery was absent bilaterally.
[b]Only scans containing this segment within the FOV were taken into account.

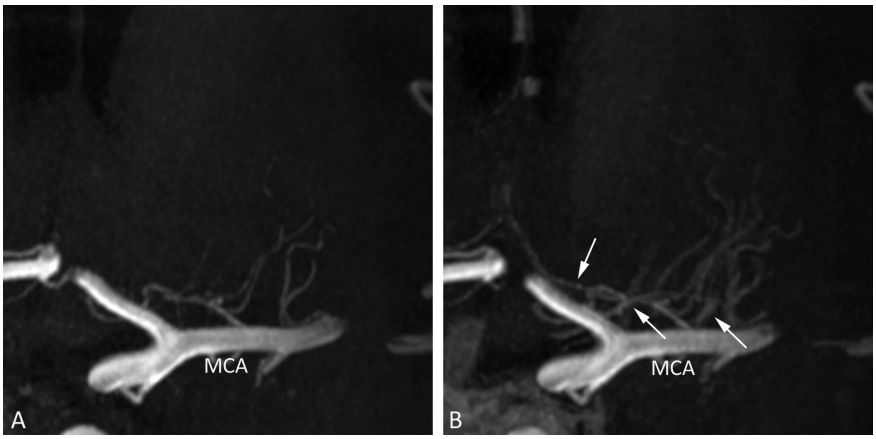

Figure 2 | 7T TOF-MRA, coronal slab MIP images (thickness 10 mm) of the perforating arteries arising from the left MCA before (**A**) and after (**B**) contrast administration. In **B**, the effect of venous enhancement (arrows) can be appreciated, making differentiation between small arteries and veins more difficult.
MCA: middle cerebral artery; MIP: maximum intensity projection.

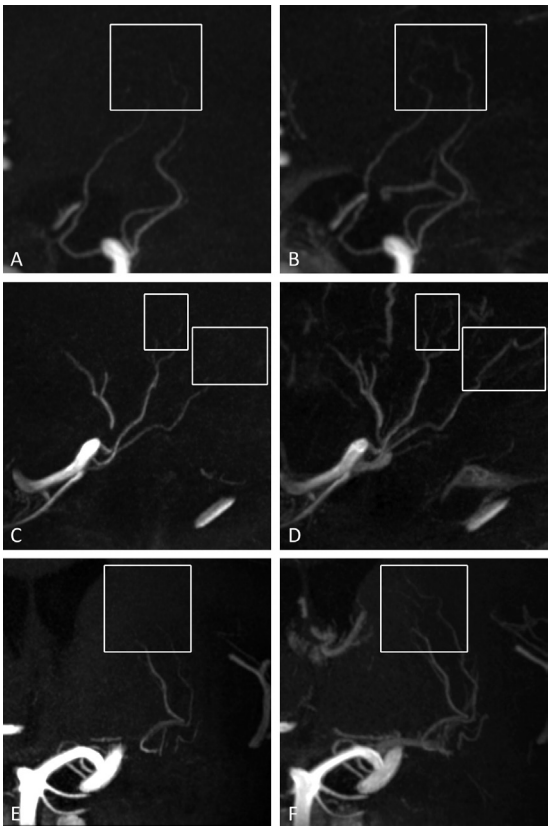

Figure 3 | 7T TOF-MRA MIP images of different intracranial perforating arteries. On the left (**A,C,E**) the precontrast images with the corresponding post-contrast images of the same patient on the right (**B,D,F**). In **B**, **D** and **F**, longer arterial trajectories can be seen after contrast administration as compared to the corresponding unenhanced image in **A, C** and **E** (white boxes). (**A** and **B**) Sagittal slab MIP, thickness 10 mm; (**B** and **C**) sagittal slab MIP, thickness 10 mm; (**E** and **F**) coronal slab MIP, thickness 10 mm.
MIP: maximum intensity projection.

Discussion

The current study shows that high-resolution 7T TOF-MRA combined with a gadolinium-based contrast agent clearly visualizes intracranial perforating arteries branching off from the circle of Willis and proximal intracranial arteries. Unlike foregoing studies[13-21], we did not restrict our study to a particular set of perforators, but aimed to investigate the perforating branches of the entire circle of Willis and the proximal intracranial arteries.

When performing a TOF-MRA scan after contrast administration, veins will enhance in addition to arteries. For some clinical applications, e.g. preoperative assessment of tumor resectability, knowledge of venous anatomy in addition to arterial anatomy may be advantageous.

A previous study[27] proposed a susceptibility-weighted angiography (SWAN) sequence that allowed visualization of both cerebral veins and arteries in one sequence without application of a contrast agent. Nevertheless, SWAN was found to be clearly inferior to TOF-MRA in the depiction of small arteries. Postcontrast TOF-MRA might have the potential to image both the very small arteries as well as the venous vasculature.

Our study revealed several disadvantages of using a contrast agent for TOF imaging. For some perforators the origin from the parent artery was obscured by the close proximity of veins in the postcontrast images. This sometimes made it difficult to discern the arterial or venous nature of a vessel, while the absence of venous enhancement facilitated the detection of intracranial perforators in the scans before contrast administration. Combining both techniques (performing both the pre- and postcontrast scan) may solve this problem[28], given there is sufficient time for this in the scan protocol and the patient is able to lie still.

Although some perforators could be followed over a longer trajectory with postcontrast TOF-MRA compared to precontrast, no differences were found in the number of visualized perforators within the same patient. Our results regarding the visualization of small intracranial arteries over a longer trajectory after contrast administration corresponds to previous study results.[23-25] Özsarlak et al., using 1.5T TOF-MRA with low-dose contrast administration, showed improved visualization and assessment of distal branches of the intracranial arteries, while precontrast MR angiograms were found to be superior to low-dose postcontrast MR angiograms for visualization of the circle of Willis and proximal branches. Yano et al. also showed the usefulness of contrast administration for visualizing the distal arterial branches and venous structures at 1.5T. Umutlu et al. evaluated a pre- versus postcontrast MPRAGE sequence at 7T, and found that contrast administration particularly increased the conspicuity of peripheral vessels as well as the complete posterior circulation. This increased conspicuity of the posterior circulation was not seen in our study, possibly because of our relatively limited FOV which could not always include the entire posterior circulation.

The number of visualized perforators was not increased after contrast administration. However, since these results are based on 2 patients in the

current study, they will need to be confirmed in a larger study. The TOF-MRA sequence before and after contrast administration was performed with the same imaging parameter settings. With optimization (e.g. shorter TR, larger flip angles) of the postcontrast TOF-MRA for the new T_1 relaxation of blood, even better contrast may be obtained with shorter acquisition times, or increased spatial resolution. This may allow for visualization of intracranial perforators which are now below the detection limit of the current sequence, since our sequence only has a spatial resolution of 0.25x0.3x0.4 mm^3, whereas diameters of intracranial perforators have been reported to range from 70 – 1150 μm (post-mortem data)[1].

Clinical opportunities for postcontrast TOF-MRA could include the pre-treatment evaluation of perforators branching from aneurysms, as well as the effects of (flow-diverting) stents which may or may not cause blockage of small perforating arteries in the proximity of aneurysms. In tumor patients, the small vessels that run in close proximity to brain tumors may be identified[29,30]. And in patients with small vessel disease (stenosis or occlusion of small arteries), assessment of these small perforating arteries might show the extent and severity of lipohyalinosis, provided that the size of these arteries or arterioles would be above the detection range. Postcontrast TOF-MRA seems to have the advantage of better visualization of the distal segments of the intracranial (perforating) arteries, possibly beneficial for e.g. tumor resection planning or identification of a distal thrombus. Therefore, in each patient, a compromise has to be made whether better visualization of the distal intracranial (perforating) arteries or the proximal intracranial arteries is more important.

This study has limitations. First, scan time of this sequence is relatively long due to its high spatial resolution, necessitating a relatively small coverage and increasing the likelihood of movement artefacts. The small FOV sometimes made it difficult to include both the entire circle of Willis and the more distal branches. Second, not all perforators of the circle of Willis and proximal intracranial arteries could be visualized, since the number of visualized perforating arteries is still much lower than that found in postmortem studies[1]; for instance, for the MCA a mean of 8.6 with a range of 3-15 perforating branches were found in the postmortem study[1], compared to a mean of 3.5 with a range of 1-8 in our study.

Further, this study describes the results from a small number of (heterogeneous) subjects, in which only 2 subjects had precontrast TOF-MRA available for comparison; as already mentioned before, a prospective study with a large sample size is needed to strengthen the main findings of this study.

Part of the variability in the visibility of the perforating arteries may reflect variability in the mean blood flow velocities in these small arteries. Potential improvements for further use of this method in larger studies would be to divide the 3D FOV in multiple (slightly overlapping) 3D thin slabs[31]. This will improve the visibility of relatively slow flowing blood. Besides, more advanced excitation pulses may be used to reduce the SAR and improve the background suppression.[32] Another potential improvement would be to increase the spatial resolution to image intracranial perforators which are now below the detection limit of the used sequence. However, this comes at the cost of decreased signal-to-noise ratios and an increase in scan time, while the scan time of the currently used sequence is relatively long already. Future developments may lead to receive coils with extremely high numbers of receive coils[33], which provides more flexibility for faster imaging or for increasing the FOV within the same scan time. Faster imaging may facilitate the direct comparison between pre- and postcontrast MRI within the same scan session, while an increased FOV could, in addition to the perforating arteries in the current studies, allow for an assessment of peripheral cortical arteries as well as small arteries within the posterior circulation. In addition, to provide better insight in the number of intracranial perforators currently missed with TOF-MRA, a direct comparison could be made with iaDSA in the same patient.

In conclusion, high-resolution postcontrast TOF-MRA at 7T is able to visualize multiple small intracranial perforators with high image contrast in patients. Although confirmation in a larger study is needed, the administration of a contrast agent for high-resolution TOF-MRA at 7T seems to enable a better visualization of the distal segment of certain intracranial perforators.

References

1. Marinkovic S, Gibo H, Milisavljevic M: The surgical anatomy of the relationships between the perforating and the leptomeningeal arteries. Neurosurgery 39:72-83, 1996.
2. Kumral E, Ozdemirkiran T, Alper Y: Strokes in the subinsular territory: clinical, topographical, and etiological patterns. Neurology 63:2429-2432, 2004.
3. Greenberg SM: Small vessels, big problems. N Engl J Med 354:1451-1453, 2006.
4. Wardlaw JM, Dennis MS, Warlow CP, et al: Imaging appearance of the symptomatic perforating artery in patients with lacunar infarction: occlusion or other vascular pathology? Ann Neurol 50:208-215, 2001.
5. Fisher CM: The arterial lesions underlying lacunes. Acta Neuropathol 12:1-15, 1969.
6. Fisher CM, Caplan LR: Basilar artery branch occlusion: a cause of pontine infarction. Neurology 21:900-905, 1971.
7. Fisher CM: Lacunes: Small, Deep Cerebral Infarcts. Neurology 15:774-784, 1965.
8. Heverhagen JT, Bourekas E, Sammet S, et al: Time-of-flight magnetic resonance angiography at 7 Tesla. Invest Radiol 43:568-573, 2008.
9. van der Kolk AG, Hendrikse J, Zwanenburg JJ, et al: Clinical applications of 7 T MRI in the brain. Eur J Radiol 82:708-718, 2013.
10. von Morze C, Xu D, Purcell DD, et al: Intracranial time-of-flight MR angiography at 7T with comparison to 3T. J Magn Reson Imaging 26:900-904, 2007.
11. Stamm AC, Wright CL, Knopp MV, et al: Phase contrast and time-of-flight magnetic resonance angiography of the intracerebral arteries at 1.5, 3 and 7 T. Magn Reson Imaging 31:545-549, 2013.
12. Nowinski WL, Puspitasaari F, Volkau I, et al: Comparison of magnetic resonance angiography scans on 1.5, 3, and 7 Tesla units: a quantitative study of 3-dimensional cerebrovasculature. J Neuroimaging 23:86-95, 2013.
13. Cho ZH, Kang CK, Han JY, et al: Observation of the lenticulostriate arteries in the human brain *in vivo* using 7.0T MR angiography. Stroke 39:1604-1606, 2008.
14. Conijn MM, Hendrikse J, Zwanenburg JJ, et al: Perforating arteries originating from the posterior communicating artery: a 7.0-Tesla MRI study. Eur Radiol 19:2986-2992, 2009.
15. Hendrikse J, Zwanenburg JJ, Visser F, et al: Noninvasive depiction of the lenticulostriate arteries with time-of-flight MR angiography at 7.0 T. Cerebrovasc Dis 26:624-629, 2008.
16. Kang CK, Park CA, Kim KN, et al: Non-invasive visualization of basilar artery perforators with 7T MR angiography. J Magn Reson Imaging 32:544-550, 2010.

17. Kang CK, Park CA, Lee H, et al: Hypertension correlates with lenticulostriate arteries visualized by 7T magnetic resonance angiography. Hypertension 54:1050-1056, 2009.
18. Kang CK, Park CA, Park CW, et al: Lenticulostriate arteries in chronic stroke patients visualised by 7 T magnetic resonance angiography. Int J Stroke 5:374-380, 2010.
19. Kang CK, Park CW, Han JY, et al: Imaging and analysis of lenticulostriate arteries using 7.0-Tesla magnetic resonance angiography. Magn Reson Med 61:136-144, 2009.
20. Liem MK, van der Grond J, Versluis MJ, et al: Lenticulostriate arterial lumina are normal in cerebral autosomal-dominant arteriopathy with subcortical infarcts and leukoencephalopathy: a high-field *in vivo* MRI study. Stroke 41:2812-2816, 2010.
21. Seo SW, Kang CK, Kim SH, et al: Measurements of lenticulostriate arteries using 7T MRI: new imaging markers for subcortical vascular dementia. J Neurol Sci 322:200-205, 2012.
22. Yang JJ, Hill MD, Morrish WF, et al: Comparison of pre- and postcontrast 3D time-of-flight MR angiography for the evaluation of distal intracranial branch occlusions in acute ischemic stroke. AJNR Am J Neuroradiol 23:557-567, 2002.
23. Yano T, Kodama T, Suzuki Y, et al: Gadolinium-enhanced 3D time-of-flight MR angiography. Experimental and clinical evaluation. Acta Radiol 38:47-54, 1997.
24. Ozsarlak O, Van Goethem JW, Parizel PM: 3D time-of-flight MR angiography of the intracranial vessels: optimization of the technique with water excitation, parallel acquisition, eight-channel phased-array head coil and low-dose contrast administration. Eur Radiol 14:2067-2071, 2004.
25. Umutlu L, Theysohn N, Maderwald S, et al: 7 Tesla MPRAGE imaging of the intracranial arterial vasculature: nonenhanced versus contrast-enhanced. Acad Radiol 20:628-634, 2013.
26. Kang HS, Han MH, Kwon BJ, et al: Evaluation of the lenticulostriate arteries with rotational angiography and 3D reconstruction. AJNR Am J Neuroradiol 26:306-312, 2005.
27. Boeckh-Behrens T, Lutz J, Lummel N, et al: Susceptibility-weighted angiography (SWAN) of cerebral veins and arteries compared to TOF-MRA. Eur J Radiol 81:1238-1245, 2012.
28. Zhou Q, Liu Z, Li C, et al: Preoperative evaluation of neurovascular relationship by using contrast-enhanced and unenhanced 3D time-of-flight MR angiography in patients with trigeminal neuralgia. Acta Radiol 52:894-898, 2011.
29. Moshel YA, Marcus JD, Parker EC, et al: Resection of insular gliomas: the importance of lenticulostriate artery position. J Neurosurg 109:825-834, 2008.
30. Lang FF, Olansen NE, DeMonte F, et al: Surgical resection of intrinsic insular tumors: complication avoidance. J Neurosurg 95:638-650, 2001.

31. Davis WL, Warnock SH, Harnsberger HR, et al: Intracranial MRA: single volume vs. multiple thin slab 3D time-of-flight acquisition. J Comput Assist Tomogr 17:15-21, 1993.
32. Schmitter S, Bock M, Johst S, et al: Contrast enhancement in TOF cerebral angiography at 7 T using saturation and MT pulses under SAR constraints: impact of VERSE and sparse pulses. Magn Reson Med 68:188-197, 2012.
33. Wiggins GC, Polimeni JR, Potthast A, et al: 96-Channel receive-only head coil for 3 Tesla: design optimization and evaluation. Magn Reson Med 62:754-762, 2009.

PART II

In vivo evaluation of intracranial vessel wall MRI

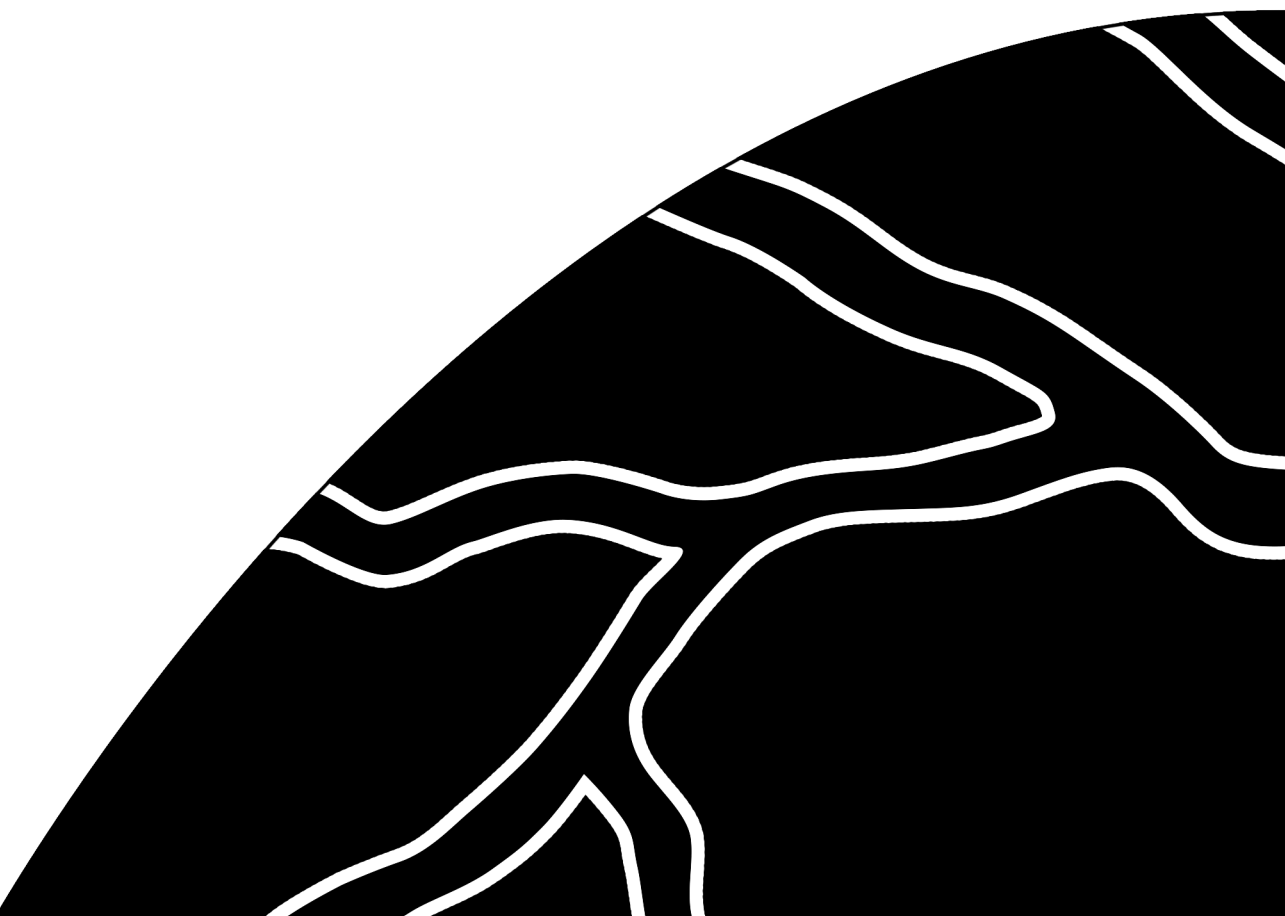

Chapter 4

High-resolution intracranial vessel wall MRI in an elderly asymptomatic population: comparison of 3T and 7T

Anita A. Harteveld[1], Anja G. van der Kolk[1], H. Bart van der Worp[2], Nikki Dieleman[1], Jeroen C.W. Siero[1], Hugo J. Kuijf[3], Catharina J.M. Frijns[2], Peter R. Luijten[1], Jaco J.M. Zwanenburg[1], Jeroen Hendrikse[1]

[1]Department of Radiology;
[2]Department of Neurology and Neurosurgery, Brain Center Rudolf Magnus;
[3]Image Sciences Institute; University Medical Center Utrecht, Utrecht, the Netherlands

Published in *European Radiology* 2017

Abstract

Objectives

Several intracranial vessel wall sequences have been described in recent literature, with either 3T or 7T MRI. In the current study, we compare 3T and 7T MRI in visualizing both the intracranial arterial vessel wall and vessel wall lesions.

Materials and Methods

Twenty-one elderly asymptomatic volunteers were scanned at 3T and 7T MRI with an intracranial vessel wall sequence, both before and after contrast administration. Two raters scored image quality, and presence and characteristics of vessel wall lesions.

Results

Vessel wall visibility was equal or significantly better at 7T for the studied arterial segments, even though there were more artefacts hampering assessment. The better visualization of the vessel wall at 7T was most prominent in the proximal anterior cerebral circulation and the posterior cerebral artery. In the studied elderly asymptomatic population 48 vessel wall lesions were identified at 3T of which 7 showed enhancement. At 7T 79 lesions were identified, of which 29 showed enhancement. 71% of all 3T lesions and 59% of all 7T lesions were also seen at the other field strength.

Conclusions

Despite the large variability in detected lesions at both field strengths, we believe 7T MRI has the highest potential to identify the total burden of intracranial vessel wall lesions.

Introduction

Intracranial atherosclerosis is one of the main causes of ischemic stroke and transient ischemic attack (TIA), and has been associated with a higher risk of recurrent stroke.[1,2] Current standard non-invasive imaging methods, like computed tomography (CT) angiography, visualize the lumen of the intracranial vasculature instead of its vessel wall, thereby risking underestimation of intracranial atherosclerosis in ischemic stroke[3-6] due to compensatory arterial remodeling that maintains lumen diameter[4,7]. Therefore, several MRI sequences have recently been developed for direct evaluation of the intracranial vessel wall and its pathology *in vivo*.[8] Studies have shown that high-resolution MRI is able to identify intracranial vessel wall abnormalities even before causing luminal narrowing.

Intracranial vessel wall imaging has been performed mainly on 3.0 and 7.0 tesla field strengths. At these higher magnetic field strengths the increased signal-to-noise (SNR) and contrast-to-noise ratios (CNR) can be exploited for imaging at a higher spatial resolution within reasonable scan times to clearly show the thin arterial vessel walls, and for improvement of lesion conspicuousness.[7,9] Current challenges at 3T are incomplete cerebrospinal fluid (CSF) suppression, potentially limiting vessel wall assessment, and (often) limited coverage.[8,10,11] 7T MRI offers the advantage of an increased SNR, allowing for complete CSF suppression and whole-brain imaging within clinically feasible scan times[12]; its use, however, is currently hampered by restricted availability and increased transmit field (B_1^+) inhomogeneity causing artefacts that can limit vessel wall assessment.[13] The implications of these differences are unclear, because a direct comparison between intracranial vessel wall MRI at these field strengths has not yet been performed. The purpose of this study was to compare visualization of the intracranial vessel wall and possible vessel wall lesions between 3T and 7T MRI.

Materials and Methods

Study population

This prospective study was approved by the institutional review board of our institution; all subjects provided written informed consent. Between

November 2013 and December 2014, volunteers aged > 50 years, without a history of cerebrovascular or ischemic heart disease or contraindications for MR imaging, were included. These volunteers formed the control group of the ongoing PIVI study (Posterior Intracranial Vessel wall Imaging; NTR5688, www.trialregister.nl).

Imaging

All subjects underwent MRI on both 3T and 7T. For each field strength, an optimized, T_1-weighted intracranial vessel wall imaging sequence was used; a previous *ex vivo* study at 7T[14] showed T_1-weighted imaging to have the most promising image contrast for visualizing and characterizing intracranial arterial vessel wall lesions. In addition, a T_1-weighted sequence enables assessment of vessel wall contrast enhancement. The sequence at 3T had been optimized in volunteers (data not shown) based on a previously published sequence by Qiao *et al*.[10] The 7T-sequence had already been optimized in previous studies[12,15]. At both field strengths, the intracranial vessel wall scan was performed before and after contrast administration; a minimum of 12 hours was taken between both MRI examinations, to make sure the contrast agent had washed out sufficiently, and care was taken that both MRI examinations were planned as close after each other as possible (median 4 days; IQR 3-9 days). The postcontrast vessel wall scan was acquired approximately 5 minutes after intravenous administration of 0.1mL/kg of a gadolinium-containing contrast agent (Gadobutrol, Gadovist 1.0mmol/mL, Bayer Schering Pharma, Newbury, UK). For signal improvement in the cerebellar region at 7T, high permittivity dielectric pads were used (Leiden University Medical Center, Leiden, the Netherlands).[16,17]

3T MRI protocol

Imaging was performed on a 3T whole-body system (Achieva, Philips Healthcare, Best, the Netherlands), with a quadrature body coil for transmission and an eight-channel head coil for reception. The imaging protocol included a 3D T_1-weighted volumetric isotropically reconstructed turbo spin echo acquisition (VIRTA) intracranial vessel wall sequence (adapted from Qiao *et al*.[10] by Dieleman *et al*., submitted for publication). The applied scan parameters are presented in **Table 1**.

Table 1 | Scan parameters of the intracranial vessel wall imaging sequence at 3T and 7T.

Scan parameter	3T VIRTA[a]	7T MPIR-TSE[b]
FOV (mm^3)	200x167x45	250x250x190
Acquisition orientation	Transverse oblique	Sagittal
Acquired spatial resolution (mm^3)	0.6x0.6x1.0	0.8x0.8x0.8
Reconstructed spatial resolution (mm^3)	0.5x0.5x0.5	0.49x0.49x0.49
TR / TE / TI (ms)	1500 / 36 / -	3952 / 37 / 1375
Flip angle (degrees)	90	120
Echo spacing (ms)	4.0	3.3
TSE factor	62 (incl. 6 start-up)	169 (incl. 10 start-up)
Oversampling factor	1.8	1
NSA	1	2
SENSE factor	1.5 (RL)	2 (AP) & 3 (RL)
Acquisition time (min:sec)	6:51	10:40

[a]Sequence was planned so that as much of the circle of Willis as possible was within the FOV. Several parameters were adapted / added to Qiao *et al.*: TR=1500ms and anti-DRIVen Equilibrium (DRIVE) module to increase T_1-weighting and CSF suppression; a low minimum flip angle (25 degrees) in the variable flip angle refocusing pulse train for increased flow suppression[39]; interpolation factor = 2 by zero-padding in the slice direction during reconstruction, slight adjustment of the acquired in-plane resolution, and reducing the TR to reduce scan time further.
[b]In comparison to previous studies[12, 15, 28], sequences were obtained with a dual transmit system that provides a B_1^+ in the brain that matches the nominal flip angle; therefore, all flip angles could be reduced by 20% to obtain the same image contrast.
FOV: field-of-view; MPIR-TSE: magnetization-prepared inversion recovery; NSA: number of signal averages; SENSE: sensitivity encoding; TE: echo time; TI: inversion time; TR: repetition time; TSE: turbo spin echo; VIRTA: volumetric isotropically reconstructed turbo spin echo acquisition.

7T MRI protocol

For 7T MRI, a whole-body system (Philips Healthcare, Cleveland, OH, USA) was used with a 32-channel receive coil and volume transmit/receive coil for transmission (Nova Medical, Wilmington, MA, USA). The imaging protocol included a 3D whole-brain T_1-weighted magnetization-prepared inversion recovery turbo spin echo (MPIR-TSE) intracranial vessel wall sequence[15]. The applied scan parameters are presented in **Table 1**.

Image Assessment

Images were assessed in the same format as they are normally evaluated in clinical practice, which includes the 'standard' image interpolation performed by the scanner software. Multiplanar reconstructions (MPR) were made from the vessel wall scans acquired at 3T (thickness 1.0mm;

no slice gap) and 7T (thickness 0.8 mm; no slice gap), using a standalone workstation (Philips). The used slice thickness was based on the acquired resolution in the slice direction. To obtain the same data sets for further analysis, the 7T vessel wall MPRs were made using the spatial orientation of the 3T images.

3T and 7T MPR images were evaluated in random order by two trained raters (A.K. and A.H.), with 6 and 3 years of experience in assessing intracranial vessel wall images, respectively, who were blinded for each other's assessment and for the findings on the other (3T or 7T) scan. Each scan was analyzed once by each rater; in case of disagreement regarding vessel wall lesions, a consensus reading was performed with a third rater (J.H.; 6 years of experience in assessing intracranial vessel wall images). After consensus, non-corresponding vessel wall lesions at 3T and 7T were assessed in a side-by-side comparison.

The assessed vessel segments included: anterior cerebral artery (ACA; A1-, A2 segment); anterior communicating artery (ACoA); middle cerebral artery (MCA; M1-, M2- and M3 segment); internal carotid artery (ICA; distal intracranial segment; intracranial bifurcation); posterior communicating artery (PCoA); posterior cerebral artery (PCA; P1 segment, bifurcation P1-P2, P2 segment); basilar artery (BA; proximal half, distal half and bifurcation with P1 segment); and vertebral arteries (VA; proximal and distal half).

Image quality

Image quality was evaluated using the method modified from Van der Kolk *et al*.[15], with three qualitative grading scales for overall artefacts (0=artefacts hampering assessment; 1=moderate artefacts, but images assessable; 2=no artefacts), overall visibility of the arterial vessel wall (0=poor; 1=moderate; 2=good), and visibility of all separate arterial vessel walls (0=outside FOV; 1=not visible; 2=poor; 3=moderate; 4=good).

Vessel wall lesions

Vessel wall lesions were scored on the precontrast images according to the methods previously described.[12,18] A vessel wall lesion was defined as either a clear focal or more diffuse thickening of the vessel wall, as compared to the healthy contralateral or neighbouring vessel wall.[19]

For assessment of contrast enhancement, vessel wall images were processed using MeVisLab (version 2.7, MeVis Medical Solutions AG, Bremen, Germany). After coregistering the postcontrast scan to the precontrast scan using elastix[20], the precontrast scan was subtracted from the (coregistered) postcontrast scan. The resulting subtracted images together with the pre- and postcontrast vessel wall images were used for contrast enhancement assessment.[12] In addition to contrast enhancement, specific lesion characteristics (configuration and thickening pattern) were also assessed (see Supplemental Material).

Statistical Analysis

Differences between image quality ratings at 3T and 7T were calculated using a non-parametric Wilcoxon signed-rank test. Interrater agreement of the number and location of vessel wall lesions was evaluated using the Dice's similarity coefficient (DSC)[21] for the 3T and 7T MR images separately. For interrater agreement of contrast enhancement assessment Cohen's kappa was calculated. Statistical analyses were performed using IBM SPSS Statistics (version 21, IBM Corporation, Armonk, NY, USA). A p-value of <0.05 was considered to be statistically significant. Bonferroni correction for multiple comparisons was applied when appropriate.

Results

Study population

Twenty-one healthy volunteers (12 male; age 66 ± 5 years) were included. Baseline characteristics are shown in **Table 2**.

Image quality

Since image quality ratings of both raters were comparable, the mean of both raters was used. 7T images showed significantly more artefacts compared to 3T, both precontrast and postcontrast (**Table 3**). For analysis of vessel wall visibility, subjects scored with artefacts hampering assessment on either 3T or 7T images where the majority of the vessel walls were affected (i.e. due to severe motion artefacts) were excluded (n=6; motion artefacts at 3T (n=2) or 7T (n=4); precontrast n=2 and postcontrast n=4). Overall vessel wall visibility was scored significantly better for the

Table 2 | Baseline characteristics of all 21 subjects.

Characteristic, n(%)		
Gender, male		12 (57.1%)
Age, years (mean ± sd)		65.9 ± 5.0
BMI, kg/m^2 (mean ± sd)		24.8 ± 3.3
Smoking	*current*	1 (4.8%)
	former	10 (47.6%)
	never	10 (47.6%)
Blood pressure, mm Hg (mean ± sd)	*systolic*	141 ± 24
	diastolic	80 ± 9
History of hypertension		8 (38.1%)
Hypercholesterolemia		6 (28.6%)
Diabetes mellitus		1 (4.8%)
History of cardiovascular disease		1 (4.8%)
Family history vascular disease < 60 y		5 (23.8%)

BMI: body mass index

Table 3 | Qualitative scoring of artefacts and overall visibility of the arterial vessel wall on 3T and 7T MRI (pre- and postcontrast).

	Precontrast			**Postcontrast**		
	3T	**7T**	***p-value*[c]**	**3T**	**7T**	***p-value*[c]**
Artefacts[a]						
0	2 (5%)	14 (33%)		6 (14%)	16 (38%)	
1	29 (69%)	28 (67%)		32 (76%)	26 (62%)	
2	11 (26%)	0 (0%)		4 (10%)	0 (0%)	
Proportion of overall agreement (%)	76	62		81	71	
Mean rater 1 (range)	1.24 (0-2)	0.57 (0-1)		0.95 (0-2)	0.57 (0-1)	
Mean rater 2 (range)	1.19 (0-2)	0.76 (0-1)		0.95 (0-2)	0.67 (0-1)	
Mean both raters	1.21	0.67	<0.001	0.95	0.62	0.024
Overall visibility vessel wall[b]						
0	5 (17%)	3 (10%)		5 (17%)	3 (10%)	
1	22 (73%)	11 (37%)		23 (77%)	14 (47%)	
2	3 (10%)	16 (53%)		2 (7%)	13 (43%)	
Proportion of overall agreement (%)	60	80		80	87	
Mean rater 1 (range)	0.87 (0-2)	1.40 (0-2)		0.93 (0-2)	1.33 (0-2)	
Mean rater 2 (range)	1.00 (0-2)	1.47 (0-2)		0.87 (0-2)	1.33 (0-2)	
Mean both raters	0.93	1.43	0.009	0.90	1.33	0.019

Grading scale overall artefacts: 0=artefacts hampering assessment; 1=moderate artefacts, but images assessable; 2=no artefacts. Grading scale overall visibility of the arterial vessel wall: 0=poor; 1=moderate; 2=good. [a]Based on 21 subjects. [b]Based on 15 subjects. [c]Bonferroni corrected significance level $p<0.025$ (corrected for 2 comparisons of rating scales).

Table 4 | Qualitative visibility scoring of all separate arterial vessel wall segments of the circle of Willis and its primary branches on 3T and 7T MRI (precontrast)[a].

Location	3T	7T	*p-value*[b]
Anterior cerebral artery			
A1 segment	2.21 (1-3)	2.79 (2-4)	**0.001**
A2 segment	1.63 (1-3)	2.24 (1-4)	**<0.001**
Anterior communicating artery	1.16 (1-2)	1.32 (1-3)	0.398
Middle cerebral artery			
M1 segment	2.11 (1-3)	2.76 (2-4)	**<0.001**
M2 segment	2.16 (1-3)	2.24 (1-3)	0.802
M3 segment	1.34 (0-3)	1.05 (0-2)	0.052[c]
Internal carotid artery			
Distal intracranial segment	2.82 (2-3)	3.37 (2-4)	**0.002**
Intracranial bifurcation	2.61 (2-4)	3.16 (2-4)	**<0.001**
Posterior communicating artery	1.90 (1-3)	2.50 (1-4)	0.083
Posterior cerebral artery			
P1 segment	2.55 (1-4)	3.13 (2-4)	0.003
Bifurcation	2.26 (1-4)	3.08 (2-4)	0.004
P2 segment	1.79 (1-3)	2.63 (2-3)	**<0.001**
Basilar artery			
Bifurcation	2.74 (1-4)	2.90 (1-4)	0.413
Distal half	2.97 (2-4)	2.90 (1-4)	0.499
Proximal half	3.11 (1-4)	2.97 (1-4)	0.545
Vertebral artery			
Distal half	3.26 (2-4)	2.84 (1-4)	0.168
Proximal half	3.32 (2-4)	2.97 (1-4)	0.214

Scores are given as mean (range) of both raters. Grading scale: 0=outside FOV; 1=not visible; 2=poor; 3=moderate; 4=good.
[a]Based on 19 subjects per location.
[b]Bonferroni corrected significance level $p<0.003$ (corrected for 17 comparisons of arterial segments).
[c]Rating "0" was excluded from statistical analysis (n=3 subjects).

7T images compared to 3T, both precontrast and postcontrast (**Table 3**). On arterial segment level (**Table 4**), the ICA, ACA and proximal MCA (M1 segment) vessel walls were significantly better visible at 7T; this was also the case for the P2 segment.

Vessel wall lesions

For analysis of vessel wall lesions, subjects with poor overall vessel wall visibility scored by both raters on either 3T or 7T precontrast images were excluded (n=5; poor visibility at 3T only (n=1), 7T only (n=2), or both at 3T and 7T (n=2)), resulting in 16 subjects for analysis. For analysis of lesion enhancement, an additional three subjects were excluded based on poor overall visibility of the postcontrast scan (poor visibility at 3T only (n=2) or 7T only (n=1)).

Pre-consensus interrater agreement for number and location of the identified vessel wall lesions was good at both 3T (DSC: 0.68) and 7T (DSC: 0.67). Also, a good to excellent interrater agreement was found for lesion contrast enhancement (kappa 0.85 for 3T, and 0.67 for 7T). On the precontrast scans, 45 (3T) resp. 67 (7T) vessel wall lesions were scored after consensus; an additional 3 (3T) resp. 12 (7T) lesions were identified because of vessel wall enhancement. In total, 48 vessel wall lesions were identified at 3T (mean: 3 per subject, range: 1-7), of which 7 (15%) showed enhancement (**Table 5**). At 7T 79 lesions were identified (mean: 5 per subject, range: 1-10), of which 29 (37%) showed enhancement (**Table 5**).

Side-by-side comparison

Twenty-four vessel wall lesions were identified at both 3T and 7T (**Figure 1**, **Figure 2**). Almost one-third (7/24; 29%) of lesions visible on both 3T and 7T showed enhancement on both field strengths; an additional one-third (9/24; 38%) showed enhancement at 7T only. Most corresponding lesions were present in the vertebral arteries, basilar artery, and internal carotid arteries.

Side-by-side comparison of the non-corresponding vessel wall lesions showed that in retrospect, 10 lesions (21%) scored only at 3T and 23 lesions (29%) scored only at 7T were either visible retrospectively but missed at the other field strength by both raters, or identified but omitted during the consensus reading (**Figure 3**). Fourteen (29%) vessel wall lesions that were identified at 3T could not be retrospectively identified at 7T. At 7T, 32 (41%) vessel wall lesions could not be retrospectively identified at 3T (**Figure 4**). The non-corresponding lesions were mainly located in areas where the vessel wall was less well visible; also, several of these lesions appeared smaller compared to the corresponding lesions. In total, 34

Table 5 | Overview of number, location and enhancement of identified vessel wall lesions on 3T and 7T vessel wall images, as well as lesions that corresponded between 3T and 7T.

Location	3T		7T		Corresponding 3T-7T		
	Lesions	Enhancement[a]	Lesions	Enhancement[b]	Lesions	Enhancement[c]	
						3T	7T
Total anterior circulation	17 (35.4)	1	32 (40.5)	8	7	1	4
Anterior cerebral artery	3 (6.3)	0	3 (3.8)	0	0	0	0
A1 segment	2 (4.2)	0	1 (1.3)	0	0	0	0
A2 segment	1 (2.1)	0	2 (2.5)	0	0	0	0
Anterior communicating artery	0 (0.0)	0	0 (0.0)	0	0	0	0
Middle cerebral artery	6 (12.5)	1	13 (16.5)	2	3	1	2
M1 segment	5 (10.4)	1	9 (11.4)	2	3	1	2
M2 segment	1 (2.1)	0	4 (5.1)	0	0	0	0
M3 segment	0 (0.0)	0	0 (0.0)	0	0	0	0
Internal carotid artery	8 (16.7)	0	16 (20.3)	6	4	0	2
Distal intracranial segment	3 (6.3)	0	6 (7.6)	3	1	0	1
Intracranial bifurcation	5 (10.4)	0	10 (12.7)	3	3	0	1
Total posterior circulation	31 (64.6)	6	47 (59.5)	21	17	6	12
Posterior communicating artery	2 (4.2)	0	2 (2.5)	0	1	0	0
Posterior cerebral artery	4 (8.3)	0	11 (13.9)	1	1	0	0
P1 segment	2 (4.2)	0	0 (0.0)	0	0	0	0
Bifurcation	0 (0.0)	0	4 (5.1)	0	0	0	0
P2 segment	2 (4.2)	0	7 (8.9)	1	1	0	0
Basilar artery	8 (16.7)	0	10 (12.7)	3	4	0	2
Bifurcation	5 (10.4)	0	5 (6.3)	1	2	0	1
Distal half	3 (6.3)	0	2 (2.5)	1	2	0	1
Proximal half	0 (0.0)	0	3 (3.8)	1	0	0	0
Vertebral artery	17 (35.4)	6	24 (30.4)	17	11	6	10
Distal half	3 (6.3)	0	6 (7.6)	3	1	0	1
Proximal half	14 (29.2)	6	18 (22.8)	14	10	6	9
Total	**48**	**7**	**79**	**29**	**24**	**7**	**16**

Number of lesions per location (% from total).
[a]n=7 lesions not assessable on postcontrast scans. [b]n=13 lesions not assessable on postcontrast scans. [c]n=3 lesions not assessable on postcontrast scans.

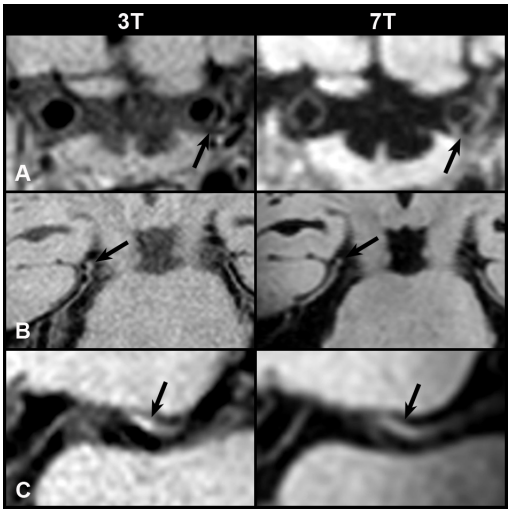

Figure 1 | 3T-7T corresponding vessel wall lesions (arrows) on the precontrast images: located at the left distal intracranial segment of the ICA (**A**), right P2 segment of the PCA (**B**), and left M1 segment of the MCA (**C**). *ICA: intracranial internal carotid artery; MCA: middle cerebral artery; PCA: posterior cerebral artery.*

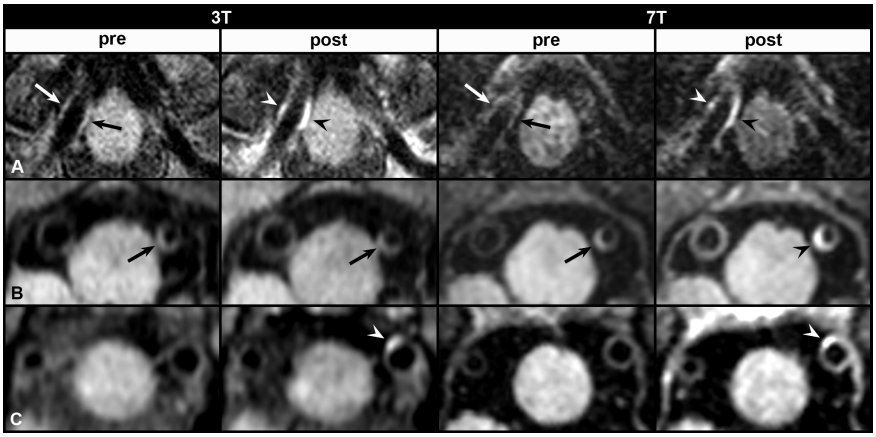

Figure 2 | Vessel wall enhancement after contrast administration. (**A**, **B**) Vessel wall lesions identified on the precontrast 3T and 7T vessel wall images (arrows), with enhancement (arrowheads) on the postcontrast images at 3T and 7T (**A**; right proximal VA), and 7T only (**B**; left proximal VA). (**C**) Vessel wall lesion identified based on enhancement of the vessel wall on the postcontrast 3T and 7T vessel wall images (**C**; left proximal VA). *VA: vertebral artery.*

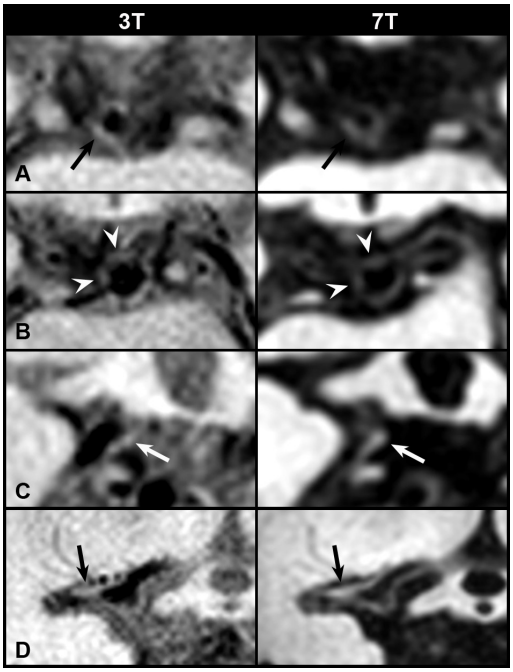

Figure 3 | Non-corresponding intracranial vessel wall lesions (arrow(head)s) identified on either the 3T (**A**, **B**) or 7T (**C**, **D**) vessel wall images that were identified retrospectively on the other scan: located at the right P1 segment of the PCA (**A**), bifurcation BA-P1 (**B**), right bifurcation P1-P2 segment of the PCA (**C**), and right M1 segment of the MCA (**D**). *BA: basilar artery; MCA: middle cerebral artery; PCA: posterior cerebral artery.*

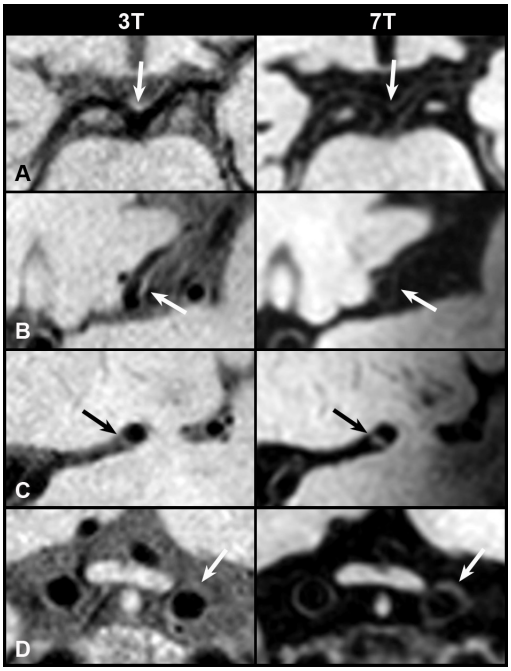

Figure 4 | Non-corresponding intracranial vessel wall lesions (arrows) identified on either the 3T (**A**, **B**) or 7T (**C**, **D**) vessel wall images that could also not be identified on the other field strength retrospectively: located at the bifurcation BA-P1 (**A**; visible at 3T), left M2 segment of the MCA (**B**; visible at 3T), left M1 segment of the MCA (**C**; visible at 7T), and left distal intracranial segment of the ICA (**D**; visible at 7T). *BA: basilar artery; ICA: internal carotid artery; MCA: middle cerebral artery.*

(71%) of all lesions identified at 3T (24 after consensus + 10 in retrospect) and 47 (59%) at 7T (24 after consensus + 23 in retrospect) were also seen on the other field strength.

Discussion

In the current study, vessel wall visibility was equal or significantly better at 7T compared to 3T for the studied arterial segments, even though there were more artefacts hampering assessment at 7T. Furthermore, more vessel wall lesions were scored on 7T images. However, surprisingly, only 71% of all 3T lesions were seen at 7T.

Better visualization of the vessel wall at 7T was most prominent in the proximal anterior cerebral circulation and the P2 segment of the PCA; the basilar artery and vertebral arteries were visualized equally good at both field strengths. The latter could be explained by better CSF suppression in this region compared to other brain regions at 3T, probably because of higher local CSF flow pulsation. Artefacts at 7T were mainly caused by motion artefacts or signal loss and B_1^+ inhomogeneities in the areas of the temporal lobes and cerebellum. Although motion artefacts were also present at 3T, they occurred more frequently at 7T. This might be related to the longer acquisition time of the 7T-sequence compared to 3T, increasing the possibility of subject motion during scanning.[22] B_1^+ inhomogeneities at 7T result in a spatially varying SNR and contrast that is most pronounced at the temporal lobes and cerebellum.[13,16] In this study, dielectric bags were placed in the upper neck region of the subjects to improve imaging of the cerebellar region, which improved part of the signal loss, but did not reduce signal loss in all subjects.

Most vessel wall lesions were found using 7T, which was expected since CSF suppression is better at 7T than at 3T in most brain regions. At 3T, no explicit CSF suppression can be performed; therefore, suppression depends on the amount of CSF flow during the spin echo train which is spatially dependent, resulting in varying quality of CSF suppression in different brain regions. The 7T-sequence contains a non-selective adiabatic inversion pulse for global CSF suppression. Most corresponding lesions between 3T and 7T were present in the vertebral arteries, basilar

artery, and internal carotid arteries: all larger arterial segments of the circle of Willis around which considerable CSF flow pulsation is present. These segments scored relatively good for vessel wall visibility at both 3T and 7T.

Close to one-half of 7T lesions (41%) could not be identified at 3T MRI. On the other hand, a striking one-third (29%) of all lesions identified at 3T were not visible at 7T. The latter might be explained by the higher acquired in-plane spatial resolution of the 3T-sequence (0.6x0.6 mm^2) compared with the 7T-sequence (0.8x0.8 mm^2), so that very small lesions seen at 3T might have been missed at 7T. The first could be explained by the increased SNR and CNR as well as better CSF suppression at 7T. Another possible explanation, applicable to both findings, could be that for smaller lesions we are currently at the edge of what can be visualized with the used vessel wall imaging sequences. For these small lesions, scan parameter differences between both field strengths (e.g. slice thickness, voxel sizes) as well as field inhomogeneities may become more important.[23] Consequently, both SNR and CNR may become too low to reliably differentiate lesions from noise, resulting in more subjective assessment. Also, there might be a higher risk of misinterpreting vessel wall irregularities caused by other phenomena like slow flow directly alongside the artery mimicking a lesion, or incomplete CSF suppression.[11,24,25] In addition, we can contemplate whether these wall thickenings might actually reflect normal thickness variation throughout the intracranial arterial vasculature. Although two recent postmortem studies have shown that ultrahigh-resolution 7T MRI can identify atherosclerotic plaques in intracranial arteries[14,26], validation of *in vivo* MRI results with histology has not yet been performed. Therefore, we do not really know to what extent all identified vessel wall lesions in this study are true atherosclerotic lesions, especially when these lesions are seen on one field strength only. This makes it difficult to determine which field strength shows vessel wall lesions best.

One striking secondary result is that in the elderly asymptomatic population included in this study, a substantial amount of intracranial vessel wall lesions have been found. Most studies have attempted to target symptomatic intracranial atherosclerosis; until now, only transcranial Doppler has been used to assess the presence of

intracranial atherosclerosis in an asymptomatic population[27] but this technique solely provides information about the presence of stenotic i.e. advanced atherosclerotic lesions. Previous studies in a symptomatic patient population with ischemic stroke/TIA imaged with the same 7T MRI sequence found 84% of patients had on average 3 vessel wall lesions in the circle of Willis arteries, and 100% of patients had on average 4 lesions if the vertebral arteries were also (mostly) taken into account.[19,28] These results show a striking similarity with our current results of 100% of subjects with on average 5 vessel wall lesions at 7T; however, our study population consists of asymptomatic healthy elderly volunteers instead of patients with symptomatic cerebrovascular disease.

Another striking result is that in our elderly asymptomatic population, many of the intracranial vessel wall lesions showed enhancement after contrast administration, predominantly at 7T. Shortening of the T_1 relaxation time caused by the injected contrast agent is suggested to be reduced at higher field strengths.[29] However, the increased SNR at 7T may theoretically make the sequence more sensitive for smaller amounts of contrast agent, e.g. when present in a vessel wall lesion. Also, the 7T-sequence used in this study might be stronger T_1-weighted than the 3T-sequence, making the 7T-sequence more sensitive for visualizing enhancement. Another possible explanation might be that the time between contrast administration and acquisition of the postcontrast vessel wall scan was not exactly identical during both MRI examinations[8] (approximately 4 minutes shorter at 3T). Contrast enhancement of intracranial atherosclerotic plaques has been associated with acute ischemic stroke[30-32] and could be a marker of plaque inflammation or neovascularization[33], and even potentially of intracranial plaque instability and stroke risk.[32] Our results, however, show that enhancing lesions are not always associated with (acute) ischemic stroke or plaque inflammation.

The results from this study shed new light on the clinical application of intracranial vessel wall imaging, and raise important issues that need to be considered. Currently, differentiation between atherosclerotic lesions and normal vessel wall thickness variations resp. (CSF) flow artefacts alongside the artery walls is difficult. Although much is known already about *in vivo* vessel wall (intima-media) thickness of extracranial arteries[34],

limited information is available on (normal) vessel wall thickness variations of the arteries of the circle of Willis. The current study shows vessel wall lesion burden of the asymptomatic population was comparable to that of symptomatic patients in previous studies. Apart from being vessel wall lesions, these wall thickenings could also be a reflection of 'normal' variation in vessel wall thickening throughout the intracranial arterial vasculature. Therefore, the clinical relevance of these vessel wall lesions might be limited. This may especially be true for enhancing lesions that, based on our current study, are apparently not always associated with ischemic stroke or plaque inflammation, as has thus far been assumed. Therefore, future studies comparing both symptomatic and asymptomatic patients should be performed, to gain more insight in differences of vessel wall lesion burden / thickness variations as well as contrast enhancement of the vessel wall.

The current study uses a 7T vessel wall sequence with a relatively low spatial resolution compared to most published (and our own) 3T-sequence(s). A disadvantage of using an inversion recovery pulse (for optimal CSF suppression) is that it increases acquisition time. Therefore, the spatial resolution of the 7T-sequence used in our study is currently restricted to 0.8x0.8x0.8 mm^3. As a consequence, some of the scored vessel wall lesions will be smaller than the true voxel size of this 7T-sequence (although this is also true for most used 3T-sequences), since the intracranial vessel wall is typically very thin. However, a previous study by Kleinloog *et al*.[35], in which the same 7T vessel wall sequence was used as in the current study, showed that signal intensity variation of the vessel wall reflects thickness variation. Therefore, it is possible to infer thickness variations from the 7T vessel wall images even for vessel walls that are thinner than the acquired voxel size. Also, the advantage of high image contrast between vessel wall (lesions) and surrounding tissue at 7T, due to the applied inversion recovery pulse, could compensate for, or be even more important than, spatial resolution for visualizing vessel wall lesions. Although other research groups have reported vessel wall sequences with higher resolutions, they achieved less optimal CSF suppression.[10,11,36,37] Future work should be done to evaluate the relative importance of resolution versus contrast and CSF suppression.

This study has several limitations. First, the MRI sequences used at both field strengths were not exactly the same: the main differences were the higher in-plane spatial resolution of the 3T-sequence and higher through-plane (slice thickness) spatial resolution of the 7T-sequence, and the lack of an inversion pulse for CSF suppression at 3T. However, to achieve a fair comparison between both field strengths, we found using optimized imaging sequences for each field strength the best option. Second, the receive coils used in this study were different (eight-channel head coil at 3T versus 32-channel head coil at 7T). Third, in this study all minor vessel wall thickness variations were scored as vessel wall lesions. As discussed earlier, especially for small vessel wall lesions, we cannot be certain that these are all actual vessel wall lesions; for translation of the vessel wall imaging findings to clinical practice, as well as usability in future studies, validation with a gold standard (histology) is a prerequisite. Fourth, blinding the raters for field strength was not possible due to the inherent slightly different image contrast between 3T and 7T; this might have induced a bias in image rating. Fifth, the sample size of this study was relatively small. However, this is the first study to provide a comparison of 3T and 7T intracranial vessel wall imaging, as well as vessel wall imaging in an asymptomatic elderly population with the administration of a contrast agent to assess enhancement of the vessel wall. Lastly, although 7T MRI is still less available compared to the lower field strength MR systems, the number of installed 7T MR systems has increased over the last years.[38] Together with the tremendous growth of technical developments at 7T MRI over the last decade to overcome difficulties of imaging at higher field strength, its use may become more broadly available in the near future.

In summary, in this comparative study of a dedicated 3T VIRTA and 7T MPIR-TSE intracranial vessel wall sequence in asymptomatic individuals, 7T vessel wall imaging appears to have the highest potential to identify the total burden of vessel wall lesions in the arteries of the circle of Willis and its branches. However, a direct comparison between symptomatic and asymptomatic patients is warranted to elucidate the potential for clinical application of intracranial vessel wall imaging.

References

1. Arenillas JF: Intracranial atherosclerosis: current concepts. Stroke 42:S20-23, 2011.
2. Qureshi AI, Caplan LR: Intracranial atherosclerosis. Lancet 383:984-998, 2014.
3. Mazighi M, Labreuche J, Gongora-Rivera F, et al: Autopsy prevalence of intracranial atherosclerosis in patients with fatal stroke. Stroke 39:1142-1147, 2008.
4. Glagov S, Weisenberg E, Zarins CK, et al: Compensatory enlargement of human atherosclerotic coronary arteries. N Engl J Med 316:1371-1375, 1987.
5. Ward MR, Pasterkamp G, Yeung AC, et al: Arterial remodeling. Mechanisms and clinical implications. Circulation 102:1186-1191, 2000.
6. Leng X, Wong KS, Liebeskind DS: Evaluating intracranial atherosclerosis rather than intracranial stenosis. Stroke 45:645-651, 2014.
7. Bodle JD, Feldmann E, Swartz RH, et al: High-resolution magnetic resonance imaging: an emerging tool for evaluating intracranial arterial disease. Stroke 44:287-292, 2013.
8. Dieleman N, van der Kolk AG, Zwanenburg JJ, et al: Imaging intracranial vessel wall pathology with magnetic resonance imaging: current prospects and future directions. Circulation 130:192-201, 2014.
9. Koops A, Ittrich H, Petri S, et al: Multicontrast-weighted magnetic resonance imaging of atherosclerotic plaques at 3.0 and 1.5 Tesla: ex-vivo comparison with histopathologic correlation. Eur Radiol 17:279-286, 2007.
10. Qiao Y, Steinman DA, Qin Q, et al: Intracranial arterial wall imaging using three-dimensional high isotropic resolution black blood MRI at 3.0 Tesla. J Magn Reson Imaging 34:22-30, 2011.
11. Wang J, Helle M, Zhou Z, et al: Joint blood and cerebrospinal fluid suppression for intracranial vessel wall MRI. Magn Reson Med 75:831-838, 2016.
12. van der Kolk AG, Zwanenburg JJ, Brundel M, et al: Intracranial vessel wall imaging at 7.0-T MRI. Stroke 42:2478-2484, 2011.
13. van der Kolk AG, Hendrikse J, Zwanenburg JJ, et al: Clinical applications of 7 T MRI in the brain. Eur J Radiol 82:708-718, 2013.
14. Harteveld AA, Denswil NP, Siero JC, et al: Quantitative Intracranial Atherosclerotic Plaque Characterization at 7T MRI: An Ex Vivo Study with Histologic Validation. AJNR Am J Neuroradiol, 2015.
15. van der Kolk AG, Hendrikse J, Brundel M, et al: Multi-sequence whole-brain intracranial vessel wall imaging at 7.0 tesla. Eur Radiol 23:2996-3004, 2013.

16. Vaughan JT, Garwood M, Collins CM, et al: 7T vs. 4T: RF power, homogeneity, and signal-to-noise comparison in head images. Magn Reson Med 46:24-30, 2001.
17. Teeuwisse WM, Brink WM, Webb AG: Quantitative assessment of the effects of high-permittivity pads in 7 Tesla MRI of the brain. Magn Reson Med 67:1285-1293, 2012.
18. Swartz RH, Bhuta SS, Farb RI, et al: Intracranial arterial wall imaging using high-resolution 3-tesla contrast-enhanced MRI. Neurology 72:627-634, 2009.
19. Dieleman N, van der Kolk AG, Zwanenburg JJ, et al: Relations between location and type of intracranial atherosclerosis and parenchymal damage. J Cereb Blood Flow Metab, 2015.
20. Klein S, Staring M, Murphy K, et al: elastix: a toolbox for intensity-based medical image registration. IEEE Trans Med Imaging 29:196-205, 2010.
21. Kuijf HJ, van Veluw SJ, Viergever MA, et al: How to assess the reliability of cerebral microbleed rating? Front Aging Neurosci 5:57, 2013.
22. Versluis MJ, Peeters JM, van Rooden S, et al: Origin and reduction of motion and f0 artifacts in high resolution T2*-weighted magnetic resonance imaging: application in Alzheimer's disease patients. Neuroimage 51:1082-1088, 2010.
23. van der Kolk AG, Hendrikse J, Luijten PR: Ultrahigh-field magnetic resonance imaging: the clinical potential for anatomy, pathogenesis, diagnosis, and treatment planning in brain disease. Neuroimaging Clin N Am 22:343-362, xii, 2012.
24. Xie Y, Yang Q, Xie G, et al: Improved black-blood imaging using DANTE-SPACE for simultaneous carotid and intracranial vessel wall evaluation. Magn Reson Med, 2015.
25. Ryoo S, Cha J, Kim SJ, et al: High-resolution magnetic resonance wall imaging findings of Moyamoya disease. Stroke 45:2457-2460, 2014.
26. van der Kolk AG, Zwanenburg JJ, Denswil NP, et al: Imaging the intracranial atherosclerotic vessel wall using 7T MRI: initial comparison with histopathology. AJNR Am J Neuroradiol 36:694-701, 2015.
27. Lopez-Cancio E, Dorado L, Millan M, et al: The Barcelona-Asymptomatic Intracranial Atherosclerosis (AsIA) study: prevalence and risk factors. Atherosclerosis 221:221-225, 2012.
28. van der Kolk AG, Zwanenburg JJ, Brundel M, et al: Distribution and natural course of intracranial vessel wall lesions in patients with ischemic stroke or TIA at 7.0 Tesla MRI. Eur Radiol 25:1692-1700, 2015.
29. Shen Y, Goerner FL, Snyder C, et al: T1 relaxivities of gadolinium-based magnetic resonance contrast agents in human whole blood at 1.5, 3, and 7 T. Invest Radiol 50:330-338, 2015.

30. Skarpathiotakis M, Mandell DM, Swartz RH, et al: Intracranial atherosclerotic plaque enhancement in patients with ischemic stroke. AJNR Am J Neuroradiol 34:299-304, 2013.
31. Vakil P, Vranic J, Hurley MC, et al: T1 gadolinium enhancement of intracranial atherosclerotic plaques associated with symptomatic ischemic presentations. AJNR Am J Neuroradiol 34:2252-2258, 2013.
32. Qiao Y, Zeiler SR, Mirbagheri S, et al: Intracranial plaque enhancement in patients with cerebrovascular events on high-spatial-resolution MR images. Radiology 271:534-542, 2014.
33. Portanova A, Hakakian N, Mikulis DJ, et al: Intracranial vasa vasorum: insights and implications for imaging. Radiology 267:667-679, 2013.
34. Lorenz MW, Markus HS, Bots ML, et al: Prediction of clinical cardiovascular events with carotid intima-media thickness: a systematic review and meta-analysis. Circulation 115:459-467, 2007.
35. Kleinloog R, Korkmaz E, Zwanenburg JJ, et al: Visualization of the aneurysm wall: a 7.0-tesla magnetic resonance imaging study. Neurosurgery 75:614-622; discussion 622, 2014.
36. Viessmann O, Li L, Benjamin P, et al: T2-Weighted intracranial vessel wall imaging at 7 Tesla using a DANTE-prepared variable flip angle turbo spin echo readout (DANTE-SPACE). Magn Reson Med, 2016.
37. Zhu C, Haraldsson H, Tian B, et al: High resolution imaging of the intracranial vessel wall at 3 and 7 T using 3D fast spin echo MRI. MAGMA, 2016.
38. Madai VI, von Samson-Himmelstjerna FC, Sandow N, et al: Ultrahigh-field MPRAGE Magnetic Resonance Angiography at 7.0T in patients with cerebrovascular disease. Eur J Radiol 84:2613-2617, 2015.
39. Busse RF, Brau AC, Vu A, et al: Effects of refocusing flip angle modulation and view ordering in 3D fast spin echo. Magn Reson Med 60:640-649, 2008.
40. Dieleman N, van der Kolk AG, van Veluw SJ, et al: Patterns of intracranial vessel wall changes in relation to ischemic infarcts. Neurology 83:1316-1320, 2014.

Supplemental material

Supplementary – Vessel wall lesion characteristics

In addition to contrast enhancement, intracranial vessel wall lesions were also assessed for specific lesion characteristics, according to the methods previously described.[12,18,40] Vessel wall lesion characteristics included: (1) configuration: eccentric (thickening clearly limited to one side of the vessel wall or if the thickest part was more than twice the thinnest part) or concentric (uniform and circumferential thickening); and (2) thickening pattern: focal or diffuse (thickening extending over a longer distance). The characteristics of vessel wall lesions were scored on the precontrast vessel wall images. Interrater agreement of vessel wall lesion characteristic (configuration and thickening pattern) assessment was calculated using Cohen's kappa, and showed a good to excellent interrater agreement for assessment of configuration (kappa 0.81 for 3T, and 0.82 for 7T) and thickening pattern (kappa 0.73 for 3T, and 0.78 for 7T) of each vessel wall lesion scored by both raters. However, in the side-by-side comparison, a poor agreement was found between 3T and 7T for assessment of configuration (kappa 0.06) and thickening pattern (kappa 0.04) of the corresponding vessel wall lesions. Therefore, any possible correlation between lesion characteristics and field strength could not be assessed. This might be explained by the same reason previously mentioned in the Discussion section. For the small lesions identified in this study we are currently working at the edge of what can be visualized with these intracranial vessel wall sequences. Therefore, for these lesions both the SNR and CNR may become too low to reliably differentiate them from noise in the image, resulting in more subjective identification of lesions as well as their characteristics.

Chapter 5

Detecting intracranial vessel wall lesions with 7T MRI: patients with posterior circulation ischemia versus healthy controls

Anita A. Harteveld[1], Anja G. van der Kolk[1], H. Bart van der Worp[2], Nikki Dieleman[1], Jaco J.M. Zwanenburg[1], Peter R. Luijten[1], Jeroen Hendrikse[1]

[1]Department of Radiology; [2]Department of Neurology and Neurosurgery, Brain Center Rudolf Magnus; University Medical Center Utrecht, Utrecht, the Netherlands

Submitted

Abstract

Objectives

Vessel wall MRI sequences have been developed to directly visualize the intracranial vessel wall, enabling detection of vessel wall changes, including those that have not yet caused luminal narrowing. In this study, vessel wall lesion burden was assessed in patients with recent posterior circulation ischemia using 7T MRI and compared with matched healthy controls.

Materials and Methods

Fifty subjects (25 patients, and 25 age- and sex-matched healthy controls) underwent 7T MRI with an intracranial vessel wall sequence, before and after contrast administration. Two raters scored the presence and contrast enhancement of arterial wall lesions in individual segments of the circle of Willis and its primary branches.

Results

Overall, vessel wall lesion burden and distribution were comparable between patients and controls. Regarding individual arterial segments, only vessel wall lesions in the posterior cerebral artery were more frequently observed in patients (18.0%) than in controls (5.4%; p=0.003). Many of these lesions showed enhancement, both in patients (48.9%) and controls (43.5%; p=0.41). In patients the proportion of enhancing lesions was higher in the posterior circulation (53.3%) than in the anterior circulation (20.6%; p=0.008).

Conclusions

Although overall intracranial vessel wall lesion burden and contrast enhancement were comparable between patients with recent posterior circulation ischemia and healthy controls, this study also revealed significant differences between the two groups, suggesting an association between posterior circulation lesion burden/enhancement and ischemic events. Future studies are essential for identifying different vessel wall lesion subtypes to distinguish pathological from normal vessel wall thickening and contrast enhancement.

Introduction

Ischemic stroke and transient ischemic attack (TIA) in the territory of the posterior circulation account for approximately 20-30% of all cerebral ischemic events. Approximately one-third of ischemic events is caused by large artery atherosclerosis (both intracranial and extracranial).[1,2] Patients with a vertebrobasilar stenosis have a high risk of early recurrent ischemic events.[3,4]

Understanding the role of intracranial atherosclerosis in the development of cerebral ischemic events necessitates non-invasive visualization of the intracranial arteries. For *in vivo* detection and assessment of intracranial atherosclerosis, several imaging techniques are available.[5,6] Conventional imaging techniques (e.g. computed tomography angiography (CTA) or magnetic resonance angiography (MRA)) are based on visualizing the lumen of the intracranial vasculature, thereby giving indirect information about underlying vessel wall pathology. Due to compensatory arterial remodeling, in which the luminal diameter remains equal despite the presence of an underlying atheroma[7], these conventional techniques may result in underestimation of the extent of intracranial atherosclerosis[6,8]. In recent years, *in vivo* high-field (3T and 7T) MRI sequences have been developed for direct visualization of the intracranial vessel wall.[9] These techniques enable detection of (small) vessel wall changes, including those that have not yet caused luminal narrowing.[5,10]

Thus far, several studies have been performed using intracranial vessel wall MRI in patients with posterior circulation ischemia for assessment of atherosclerosis. However, these studies all focused on the assessment of one specific artery of the posterior circulation, i.e. the basilar[11,12] or vertebral artery[13], often with a known stenosis on conventional angiography. With the improvement of vessel wall imaging techniques at 3T and 7T, more recent studies were able to include all major arteries of the circle of Willis and its primary branches to assess total vessel wall lesion burden in each individual patient. These recent studies, however, have included either patients with anterior circulation ischemia[14-16], or an elderly general/asymptomatic population[17,18]. Assessment of vessel wall

lesion burden in patients with posterior circulation ischemia, as well as a direct comparison between patients and asymptomatic healthy controls to further understand the pathogenesis and natural history of intracranial atherosclerosis, is still lacking.

Therefore, the aim of the current study was to assess the presence of vessel wall lesions within the intracranial arteries of patients with recent posterior cerebral circulation ischemia, using intracranial vessel wall MRI at 7T, and compare findings with age- and sex-matched asymptomatic volunteers.

Materials and Methods

Study population

Between November 2013 and August 2016, consecutive patients presenting in our institution with ischemic stroke or TIA in the posterior cerebral circulation, as well as age- and sex-matched volunteers without a history of cerebrovascular disease, were screened for inclusion in the ongoing PIVI study (Posterior Intracranial Vessel wall Imaging; NTR5688, www.trialregister.nl). Subjects with a contraindication for MR imaging (e.g. claustrophobia, specific metal objects in or on the body, pregnancy, known allergy to gadolinium-containing contrast agent, or severely impaired renal function) were excluded. Additionally, patients with a TIA or ischemic stroke secondary to a surgical or interventional procedure, previous vertebrobasilar surgery or endovascular therapy, or patients who were unable to endure an MRI examination, were also excluded. Baseline characteristics of all patients and healthy controls (including sex, age, vascular risk factors) were collected at inclusion. This prospective study was approved by the institutional review board of our institution; all subjects provided written informed consent.

Imaging

Subjects were scanned on a 7T whole-body system (Philips Healthcare, Best, The Netherlands) with a 32-channel receive coil and volume transmit/receive coil for transmission (Nova Medical, Wilmington, MA, USA). Two previous studies showed that 7T provided significantly better image quality

of the vessel wall and improved diagnostic confidence compared with 3T.[18,19] High permittivity dielectric pads were used for signal improvement in the cerebellar region (LUMC, Leiden, the Netherlands), and placed at the back of the head and neck.[20] For patients, the MRI examination was performed within three months after onset of ischemic symptoms.

Scan protocol

The imaging protocol included a high-resolution 3D T_1-weighted magnetization-prepared inversion recovery turbo spin echo (MPIR-TSE) intracranial vessel wall sequence[21] before and after contrast administration. Postcontrast vessel wall images were obtained to visualize potential vessel wall / lesion enhancement, and were acquired with a delay of approximately 5 minutes after intravenous administration of a gadolinium-containing contrast agent (dose 0.1 mL/kg; Gadobutrol, Gadovist 1.0 mmol/mL, Bayer Schering Pharma, Newbury, UK). The following scan parameters were used[18,21]: field-of-view 250x250x190 mm^3 in sagittal orientation, acquired resolution 0.8x0.8x0.8 mm^3, flip angle 120 degrees, TR/TI/TE 3952/1375/37 ms, TSE factor 169 (including 10 start-up echoes), echo train length 560 ms, magnetization preparation mixing time 50 ms, number of signal averages 2, 2D sensitivity encoding (SENSE) factor 6 (2 in AP direction, 3 in RL direction), and acquisition time 10:40 minutes.

Image assessment

For assessment, multiplanar reconstructions (MPRs) were made from the vessel wall scans (thickness 0.8 mm; no slice gap) using a standalone workstation (Philips). Scans of both patients and controls were arranged randomly for independent evaluation by two trained raters (A.K. and A.H.; 7 and 4 years of experience in assessing intracranial vessel wall images, respectively), who were blinded for each other's assessment and the clinical history of subjects. In case of disagreement between the two raters, a consensus reading was performed with a third rater (J.H.; 7 years of experience).

Vessel wall lesions (number and location) were scored on the precontrast vessel wall images according to methods previously described[10,22].

A lesion was defined as either a clear focal or more diffuse thickening of the vessel wall, compared with the healthy contralateral or neighboring vessel wall.[14] Additionally, vessel wall enhancement (present or absent) was scored[10] on subtraction images obtained from the pre- and postcontrast images using MeVisLab (version 2.7, MeVis Medical Solutions AG, Bremen, Germany).[18] The assessed arteries included all individual segments and proximal branches of the circle of Willis.[15,18]

Statistical analysis

Interrater agreement on the number and location of scored vessel wall lesions was evaluated using the Dice's similarity coefficient (DSC)[23], and for interrater agreement on contrast enhancement assessment Cohen's kappa was calculated. Differences between groups were analyzed with Pearson's chi-squared, Fisher's exact, or Mann-Whitney U test; for differences within groups the Wilcoxon signed-rank test was used. Final results of vessel wall lesions and enhancement after consensus were used. Statistical analyses were performed using IBM SPSS Statistics (version 21 for Windows, IBM Corporation, Armonk, NY, USA). Statistical significance was set at $p<0.05$. Bonferroni correction for multiple comparisons was applied when appropriate.

Results

Study population

Twenty-five patients and 25 controls were included in this study. Imaging was successful in 46 subjects; four subjects with poor overall image quality on both pre- and postcontrast images (e.g. due to motion artefacts or low signal-to-noise ratio) were excluded from analysis (3 patients, 1 control). This resulted in a total of 22 patients (17 with stroke and 5 with TIA) and 24 asymptomatic controls that were included for analysis. For analysis of lesion enhancement one additional control subject was excluded based on poor overall image quality of the postcontrast images only. Demographic and clinical data of subjects are summarized in **Table 1**.

Table 1 | Baseline characteristics of study population.

Characteristic	Patients (n=22)	Controls (n=24)	*P-value*
Gender, male	19 (86.4)	20 (83.3)	1.000
Age, years (mean ± sd)	61.5 ± 10.3	59.6 ± 12.4	0.715
BMI, kg/m^2 (mean ± sd)	24.9 ± 3.0	25.5 ± 3.5	0.620
Vascular risk factors			
Smoking: current or past	13 (59.1)	14 (58.3)	0.958
Blood pressure, mm Hg (mean ± sd)			
systolic	138 ± 27	136 ± 20	0.875
diastolic	79 ± 11	81 ± 9	0.422
History of hypertension	10 (45.5)	6 (25.0)	0.146
Hyperlipidemia	10 (45.5)	3 (12.5)	0.013
Diabetes mellitus	3 (13.6)	0 (0.0)	0.101
History of cardiovascular disease	3 (13.6)	1 (4.2)	0.336
Family history vascular disease < 60y	6 (27.3)	4 (16.7)	0.484
Thrombolysis	6 (27.3)	N/A	
Symptomatic ischemic event anterior circulation	2 (9.1)	N/A	
Subtype ischemic stroke / TIA mechanism[a]			
Large-artery atherosclerosis	8 (36.4)	N/A	
Cardioembolism	1 (4.5)	N/A	
Small-artery occlusion	1 (4.5)	N/A	
Stroke of other determined etiology	2 (9.1)	N/A	
Stroke of undetermined etiology	10 (45.5)	N/A	
Time between ischemic event and MRI examination, days (median; IQR)	36; 29-50	N/A	

Number (% from total).
[a]According to the Stop Stroke Study Trial of Org 10172 in Acute Stroke Treatment (SSS-TOAST) classification criteria.[38]
BMI: body mass index; IQR: interquartile range

Vessel wall lesions

Interrater agreement on number and location of vessel wall lesions was good in both the patient (DSC: 0.72) and healthy control group (DSC: 0.69). A good interrater agreement was also found for the scored vessel wall contrast enhancement (kappa: 0.61 patients; 0.67 controls).

Prevalence and distribution

Vessel wall lesion burden for each individual subject and for individual arterial segments are presented in **Figure 1** and **Table 2**, respectively. Apart from three patients who had a relatively high number of vessel wall lesions (**Figures 1** and **2**), the distribution of vessel wall lesion burden between patient group and control group was comparable (**Figure 1**).

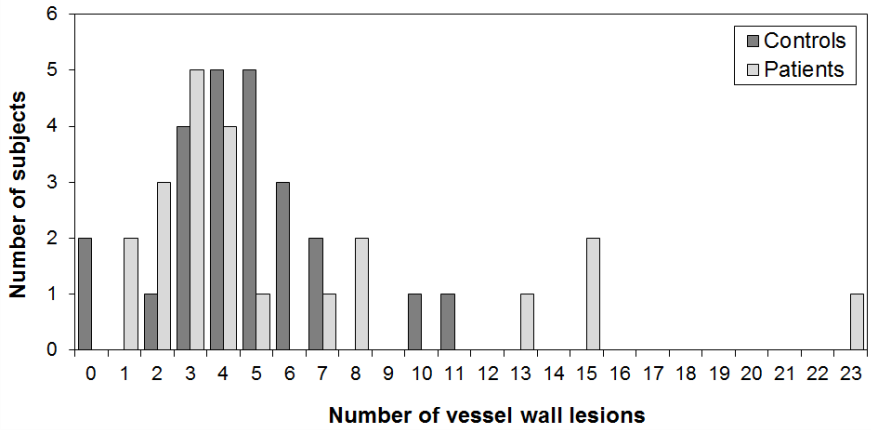

Figure 1 | Number of vessel wall lesions identified in each subject for the patient group (n=22) and asymptomatic control group (n=24). In three subjects in the patient group, only arterial segments of the anterior circulation (n=2) or posterior circulation (n=1) could be used; the other segments were not assessable.

Table 2 | Number of scored vessel wall lesions and enhancement on 7T vessel wall images for all included intracranial arterial segments in the patient and healthy control group (after consensus).

	Vessel wall lesions							Enhancement		
	Patients (n=22)			Controls (n=24)				Patients (n=22)	Controls (n=23)[d]	
Location	Right	Left	Total	Right	Left	Total	*p-value*[c]			*p-value*[c]
Total anterior circulation[a]	21	25	47 (35.3)	19	24	45 (40.2)		13 (20.0)	16 (34.0)	
Anterior cerebral artery	3	5	8 (6.0)	5	4	9 (8.0)	0.535	0 (0.0)	1 (2.1)	1.000
A1 segment	3	4	7 (5.3)	2	3	5 (4.5)		0 (0.0)	1 (2.1)	
A2 segment	0	1	1 (0.8)	3	1	4 (3.6)		0 (0.0)	0 (0.0)	
Anterior communicating artery			1 (0.8)			2 (1.8)	0.594	0 (0.0)	0 (0.0)	N/A
Middle cerebral artery	6	7	13 (9.8)	4	3	7 (6.3)	0.316	3 (4.6)	3 (6.4)	0.613
M1 segment	4	4	8 (6.0)	3	3	6 (5.4)		1 (1.5)	2 (4.3)	
M2 segment	2	3	5 (3.8)	0	0	0 (0.0)		2 (3.1)	0 (0.0)	
M3 segment	0	0	0 (0.0)	1	0	1 (0.9)		0 (0.0)	1 (2.1)	
Internal carotid artery	12	13	25 (18.8)	10	17	27 (24.1)	0.311	10 (15.4)	12 (25.5)	0.746
Distal intracranial segment	8	7	15 (11.3)	6	7	13 (11.6)		7 (10.8)	7 (14.9)	
Intracranial bifurcation	4	6	10 (7.5)	4	10	14 (12.5)		3 (4.6)	5 (10.6)	
Total posterior circulation[b]	36	32	86 (64.7)	21	24	67 (59.8)		52 (80.0)	31 (66.0)	
Posterior communicating artery	4	0	4 (3.0)	1	1	2 (1.8)	0.691	1 (1.5)	0 (0.0)	1.000
Posterior cerebral artery	15	9	24 (18.0)	2	4	6 (5.4)	0.003*	10 (15.4)	0 (0.0)	0.074
P1 segment	3	3	6 (4.5)	1	1	2 (1.8)		3 (4.6)	0 (0.0)	
Bifurcation	2	0	2 (1.5)	0	1	1 (0.9)		1 (1.5)	0 (0.0)	
P2 segment	10	6	16 (12.0)	1	2	3 (2.7)		6 (9.2)	0 (0.0)	
Basilar artery			18 (13.5)			22 (19.6)	0.197	10 (15.4)	6 (12.8)	0.088
Bifurcation			5 (3.8)			6 (5.4)		1 (1.5)	1 (2.1)	
Distal half			6 (4.5)			8 (7.1)		4 (6.2)	3 (6.4)	
Proximal half			7 (5.3)			8 (7.1)		5 (7.7)	2 (4.3)	
Vertebral artery	17	23	40 (30.1)	18	19	37 (33.0)	0.619	31 (47.7)	25 (53.2)	0.692
Distal half	7	8	15 (11.3)	6	5	11 (9.8)		9 (13.8)	7 (14.9)	
Proximal half	10	15	25 (18.8)	12	14	26 (23.2)		22 (33.8)	18 (38.3)	
Total	**57**	**57**	**133**	**40**	**48**	**112**		**65**	**47**	**0.407**

Number of lesions per location (% from total).
[a]Based on 20 patients; anterior circulation was not assessable in two patients. [b]Based on 21 patients; posterior circulation was not assessable in one patient. [c]Bonferroni corrected significance level p<0.006* (corrected for 8 comparisons of arterial segments). [d]n=4 lesions not assessable on postcontrast vessel wall scan.

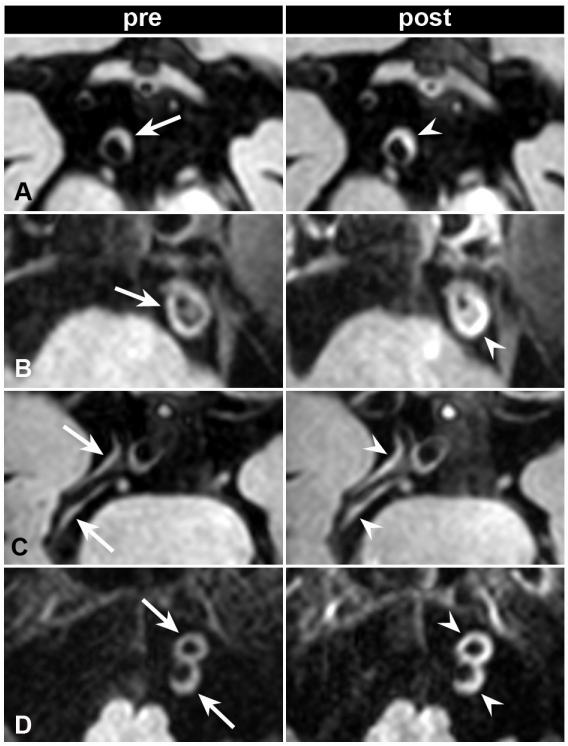

Figure 2 | A 73-year-old male patient presented with recent ischemic stroke in the vertebrobasilar territory as a result of a basilar occlusion, and had a relatively high number of vessel wall lesions. (**A-D**) Vessel wall lesions identified on the precontrast 7T transverse vessel wall images (arrows), showing enhancement on the postcontrast images (arrowheads), located in the distal basilar artery (**A**), proximal basilar artery (**B**), P2 segment of the right posterior cerebral artery (**C**), and left and right distal vertebral artery (**D**).

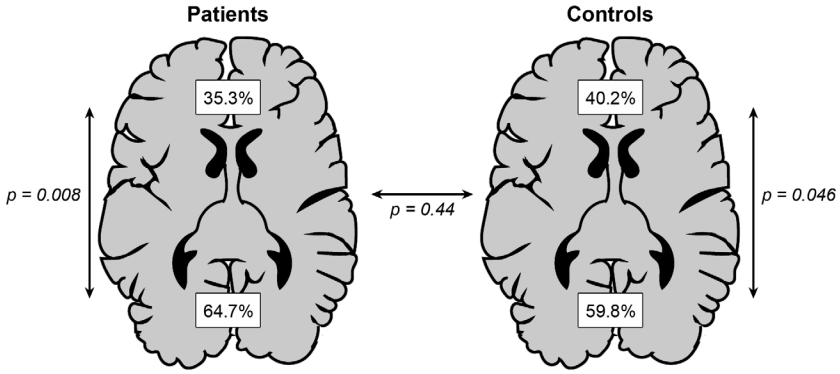

Figure 3 | Distribution of vessel wall lesions over arterial segments of the anterior and posterior circulation in patients and healthy controls. In patients, 35.3% (47/133) of vessel wall lesions were identified in the anterior circulation versus 64.7% (86/133) posterior, in controls this was 40.2% (45/112) versus 59.8% (67/112), respectively. Statistical analysis showed there was no significant difference between both groups in lesion distribution over the circulation territories (p = 0.44). Within each subject more vessel wall lesions were present in the posterior circulation than in the anterior circulation in both groups (p=0.008 for patients, p=0.046 for controls).

The median number of vessel wall lesions per subject was 4 (range: 1-23) in the patient group, and 4.5 (range: 0-11) in the control group (U = 250, p = 0.76). Within both groups, lesions occurred more often in the posterior circulation (median number per subject: 3, in both groups) than in the anterior circulation (median number per subject: 2, in both groups) (Z = -2.657, p = 0.008 and Z = -1.996, p = 0.046 for resp. patients and controls), while there was no significant difference in lesion burden between left and right side of the circle of Willis (Z = -0.351, p = 0.73 and Z = -1.546, p = 0.12 for patients and controls, respectively). Between groups, there was no significant difference in lesion distribution over both circulation areas (35.3% vs. 40.2% in the anterior circulation, and 64.7% vs. 59.8% in the posterior circulation, for respectively patients vs. controls; $\chi^2(1)$ = 0.607, p = 0.44). These results are illustrated in **Figure 3**. Regarding individual arterial segments, only vessel wall lesions in the posterior cerebral artery (PCA) were more frequently observed in patients (24/133, 18.0%) than in controls (6/112, 5.4%; $\chi^2(1)$ = 9.109, p = 0.003).

Contrast enhancement

Overall, there was no statistically significant difference in the proportion of vessel wall lesions showing contrast enhancement between patients (65/133, 48.9%) and controls (47/108, 43.5%; $\chi^2(1) = 0.687$, $p = 0.41$). In both groups, the proportion of vessel wall lesions showing enhancement was higher in the posterior circulation (mean proportion per subject: 53.3% in patients and 40.3% in controls) compared with the anterior circulation (mean proportion per subject: 20.6% in patients and 27.8% in controls). This difference was significant in the patient group (Z = -2.673, p = 0.008), but not in the control group (Z = -1.470, p = 0.142). For the individual arterial segments, there were no statistically significant differences in contrast enhancement between both groups (**Table 2**). Examples of vessel wall lesions showing enhancement after contrast administration in a patient and healthy control are shown in **Figures 4** and **Figure 5**.

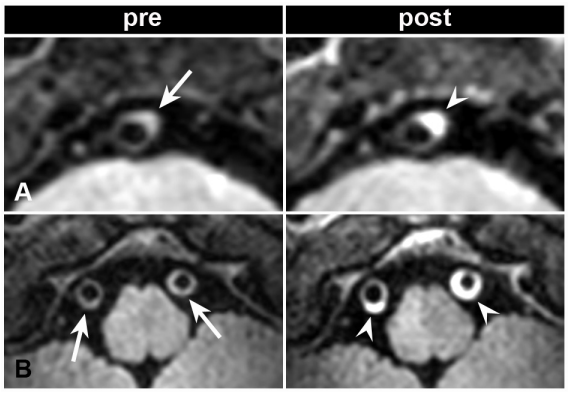

Figure 4 | A 72-year-old male patient with a history of ischemic stroke of the left cerebellum presented with a recent TIA in the vertebrobasilar territory. (**A**, **B**) Vessel wall lesions identified on the transverse precontrast 7T vessel wall images (arrows) showing enhancement on the postcontrast images (arrowheads), located at the proximal basilar artery (**A**) and left and right proximal vertebral artery (**B**).

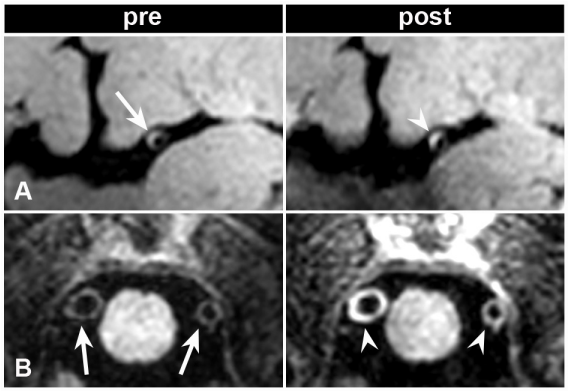

Figure 5 | A 71-year-old male control subject without a history of cerebrovascular disease. (**A**, **B**) Vessel wall lesions identified on the precontrast 7T vessel wall images (arrows) showing enhancement on the postcontrast images (arrowheads), located at the left middle cerebral artery (**A**; sagittal slice) and left and right proximal vertebral artery (**B**; transverse slice).

Discussion

In the current study, overall vessel wall lesion burden and distribution were comparable between patients with recent posterior circulation ischemia and an age- and sex-matched controls without a history of cerebrovascular disease. Only in the PCA vessel wall lesions were more frequently observed in patients. Furthermore, a large proportion of vessel wall lesions showed contrast enhancement in both groups. Patients more often had contrast enhancement in posterior vessel wall lesions than in anterior lesions.

Thus far, a direct comparison between recently symptomatic patients and asymptomatic healthy controls had not been performed. The results of the current study show that based on overall vessel wall lesion burden there are no significant differences between both groups. This result is striking, since one would expect patients to have a higher burden of vessel wall lesions than healthy persons. In the literature a wide prevalence range of intracranial atherosclerosis has been reported for patients with ischemic stroke, as well as for the asymptomatic population (6-80%).[8,24-26] Characteristics of intracranial arteries and atherosclerosis have rarely been studied systematically[27], and results are influenced by different factors, like race, arteries assessed, patient population studied, or used imaging techniques (in case of *in vivo* assessment).[8,26,28]

Interestingly, on the arterial segment level, patients showed a significantly higher burden of vessel wall lesions in the PCA. This finding might suggest an association between PCA lesion burden and ischemic events. In the current patient group it is difficult to identify the exact role of this higher lesion burden found in the PCA in relation to posterior circulation ischemia, as well as why this was not found for other segments of the posterior circulation. During image assessment, all locations with clear focal or more diffuse thickening of the vessel wall were identified as vessel wall lesions. However, with the current vessel wall imaging techniques it is difficult to differentiate between pathological thickening and normal intracranial vessel wall thickness variation, especially in the case of relatively small vessel wall lesions which were often present in this study population. Therefore, next to assessing the prevalence of vessel wall lesions, the addition of quantitative measurements of vessel wall thickening might reveal more pronounced differences between patients and controls. In extracranial arteries these measurements have revealed a significantly larger wall thickness of the carotid arteries and thoracic aorta in patients with prior major cardiovascular and cerebrovascular events compared with patients without such events.[29]

A large proportion of vessel wall lesions showed contrast enhancement in both groups. In patients this proportion was higher for the posterior circulation compared with the anterior circulation. A recent systematic review and meta-analysis, including multiple studies evaluating the

association of plaque enhancement on vessel wall MRI with recent ischemic stroke, concluded that MRI-detected intracranial plaque enhancement is strongly associated with ipsilateral acute ischemic stroke.[30] However, in the current study, asymptomatic controls also showed a large amount of enhancing vessel wall lesions. For the carotid arteries it has been shown that histological composition of enhancing areas varies depending on the location, highlighting different mechanisms of contrast uptake.[31] Plaques that contain extensive microvessels (neovasculature) showed strongest contrast enhancement.[32] Intracranially, vasa vasorum are known to develop with advancing age and with the development of vascular disease.[33] It has been hypothesized that all vessel walls may have a critical thickness beyond which vasa vasorum must exist to supplement luminal diffusion to adequately nourish thicker walls.[33] Therefore, apart from the association of contrast enhancement with (acute) ischemic stroke, vessel wall enhancement could also represent vasa vasorum neovascularization that may have developed as a result of normal vessel wall thickening during ageing.[33,34]

This study has limitations. First, because of strict MRI contraindications, patients with e.g. a pacemaker or vascular stents could not be included. Since these patients often have a more severe history of cardiovascular diseases, there may have been a selection bias towards stable patients with relatively mild impairments. Second, validation of the MRI results with a gold standard (histology) was not possible, due to the inaccessibility of the intracranial arteries. For usability and translation of the vessel wall imaging findings to clinical practice, this validation step, although difficult, is essential, because this will shed light on whether identified vessel wall lesions are due to pathological thickening or normal vessel wall thickness variations (including pathophysiology of enhancement). Third, only one contrast weighting (T_1-weighting) was used. Additional sequences with other contrast weightings might identify other lesion properties[35], and may help identify different lesions subtypes. However, as we already acquired pre- and postcontrast T_1-weighted images, there will be limited room for acquiring multiple contrasts that will be able to include all major intracranial arteries with the required spatial resolution and sufficient image contrast. Furthermore, a previous study at 7T with

ex vivo circle of Willis specimens[36] showed T_1-weighted imaging to have the most promising image contrast for visualizing intracranial arterial vessel wall lesions. An additional benefit of using a T_1-weighted sequence is the possibility of contrast enhancement assessment. Finally, patients were scanned within three months after symptom onset. Theoretically, vessel wall lesions might have changed within this time period. However, previous studies showed lesions do not significantly change between one week and one month (mean: 53 days; range: 23-205 days) after onset of symptoms[15], and also contrast enhancement does not become less until a few months after the acute event[37].

In conclusion, patients with recent posterior circulation ischemia showed comparable overall intracranial vessel wall lesion burden with age- and sex-matched healthy volunteers. Also, in both groups a large amount of vessel wall lesions showed enhancement. A significantly higher vessel wall lesion burden was found in the PCA of the patient group, suggesting an association with posterior circulation ischemia. Patients also showed relatively more often contrast enhancement in posterior vessel wall lesions compared with anterior lesions, where the controls did not. Future studies should be directed towards stratifying pathological from normal vessel wall thickening and assessing the pathological substrate of contrast enhancement.

Acknowledgements

The authors would like to thank Theo D. Witkamp (neuroradiologist at the Department of Radiology, University Medical Center Utrecht, the Netherlands) for his help with image assessment, and Hugo J. Kuijf (post-doctoral researcher at the Image Sciences Institute, University Medical Center Utrecht, the Netherlands) for his help with image processing.

References

1. Caplan LR, Wityk RJ, Glass TA, et al: New England Medical Center Posterior Circulation registry. Ann Neurol 56:389-398, 2004.
2. Savitz SI, Caplan LR: Vertebrobasilar disease. N Engl J Med 352:2618-2626, 2005.
3. Marquardt L, Kuker W, Chandratheva A, et al: Incidence and prognosis of > or = 50% symptomatic vertebral or basilar artery stenosis: prospective population-based study. Brain 132:982-988, 2009.
4. Gulli G, Khan S, Markus HS: Vertebrobasilar stenosis predicts high early recurrent stroke risk in posterior circulation stroke and TIA. Stroke 40:2732-2737, 2009.
5. Bodle JD, Feldmann E, Swartz RH, et al: High-resolution magnetic resonance imaging: an emerging tool for evaluating intracranial arterial disease. Stroke 44:287-292, 2013.
6. Leng X, Wong KS, Liebeskind DS: Evaluating intracranial atherosclerosis rather than intracranial stenosis. Stroke 45:645-651, 2014.
7. Glagov S, Weisenberg E, Zarins CK, et al: Compensatory enlargement of human atherosclerotic coronary arteries. N Engl J Med 316:1371-1375, 1987.
8. Mazighi M, Labreuche J, Gongora-Rivera F, et al: Autopsy prevalence of intracranial atherosclerosis in patients with fatal stroke. Stroke 39:1142-1147, 2008.
9. Dieleman N, van der Kolk AG, Zwanenburg JJ, et al: Imaging intracranial vessel wall pathology with magnetic resonance imaging: current prospects and future directions. Circulation 130:192-201, 2014.
10. van der Kolk AG, Zwanenburg JJ, Brundel M, et al: Intracranial vessel wall imaging at 7.0-T MRI. Stroke 42:2478-2484, 2011.
11. Huang B, Yang WQ, Liu XT, et al: Basilar artery atherosclerotic plaques distribution in symptomatic patients: a 3.0T high-resolution MRI study. Eur J Radiol 82:e199-203, 2013.
12. Kim YS, Lim SH, Oh KW, et al: The advantage of high-resolution MRI in evaluating basilar plaques: a comparison study with MRA. Atherosclerosis 224:411-416, 2012.
13. Chung JW, Kim BJ, Choi BS, et al: High-resolution magnetic resonance imaging reveals hidden etiologies of symptomatic vertebral arterial lesions. J Stroke Cerebrovasc Dis 23:293-302, 2014.
14. Dieleman N, van der Kolk AG, Zwanenburg JJ, et al: Relations between location and type of intracranial atherosclerosis and parenchymal damage. J Cereb Blood Flow Metab 36:1271-1280, 2016.
15. van der Kolk AG, Zwanenburg JJ, Brundel M, et al: Distribution and natural course of intracranial vessel wall lesions in patients with ischemic stroke or TIA at 7.0 Tesla MRI. Eur Radiol 25:1692-1700, 2015.

16. Dieleman N, Yang W, Abrigo JM, et al: Magnetic Resonance Imaging of Plaque Morphology, Burden, and Distribution in Patients With Symptomatic Middle Cerebral Artery Stenosis. Stroke 47:1797-1802, 2016.
17. Qiao Y, Guallar E, Suri FK, et al: MR Imaging Measures of Intracranial Atherosclerosis in a Population-based Study. Radiology 280:860-868, 2016.
18. Harteveld AA, van der Kolk AG, van der Worp HB, et al: High-resolution intracranial vessel wall MRI in an elderly asymptomatic population: comparison of 3T and 7T. Eur Radiol, 2016.
19. Zhu C, Haraldsson H, Tian B, et al: High resolution imaging of the intracranial vessel wall at 3 and 7 T using 3D fast spin echo MRI. MAGMA, 2016.
20. Teeuwisse WM, Brink WM, Webb AG: Quantitative assessment of the effects of high-permittivity pads in 7 Tesla MRI of the brain. Magn Reson Med 67:1285-1293, 2012.
21. van der Kolk AG, Hendrikse J, Brundel M, et al: Multi-sequence whole-brain intracranial vessel wall imaging at 7.0 tesla. Eur Radiol 23:2996-3004, 2013.
22. Swartz RH, Bhuta SS, Farb RI, et al: Intracranial arterial wall imaging using high-resolution 3-tesla contrast-enhanced MRI. Neurology 72:627-634, 2009.
23. Kuijf HJ, van Veluw SJ, Viergever MA, et al: How to assess the reliability of cerebral microbleed rating? Front Aging Neurosci 5:57, 2013.
24. Bos D, van der Rijk MJ, Geeraedts TE, et al: Intracranial carotid artery atherosclerosis: prevalence and risk factors in the general population. Stroke 43:1878-1884, 2012.
25. Lopez-Cancio E, Dorado L, Millan M, et al: The Barcelona-Asymptomatic Intracranial Atherosclerosis (AsIA) study: prevalence and risk factors. Atherosclerosis 221:221-225, 2012.
26. Arenillas JF: Intracranial atherosclerosis: current concepts. Stroke 42:S20-23, 2011.
27. Denswil NP, van der Wal AC, Ritz K, et al: Atherosclerosis in the circle of Willis: Spatial differences in composition and in distribution of plaques. Atherosclerosis 251:78-84, 2016.
28. Caplan LR, Gorelick PB, Hier DB: Race, sex and occlusive cerebrovascular disease: a review. Stroke 17:648-655, 1986.
29. Mani V, Muntner P, Gidding SS, et al: Cardiovascular magnetic resonance parameters of atherosclerotic plaque burden improve discrimination of prior major adverse cardiovascular events. J Cardiovasc Magn Reson 11:10, 2009.
30. Gupta A, Baradaran H, Al-Dasuqi K, et al: Gadolinium Enhancement in Intracranial Atherosclerotic Plaque and Ischemic Stroke: A Systematic Review and Meta-Analysis. J Am Heart Assoc 5, 2016.
31. Millon A, Boussel L, Brevet M, et al: Clinical and histological significance of gadolinium enhancement in carotid atherosclerotic plaque. Stroke 43:3023-3028, 2012.

32. Yuan C, Kerwin WS, Ferguson MS, et al: Contrast-enhanced high resolution MRI for atherosclerotic carotid artery tissue characterization. J Magn Reson Imaging 15:62-67, 2002.
33. Portanova A, Hakakian N, Mikulis DJ, et al: Intracranial vasa vasorum: insights and implications for imaging. Radiology 267:667-679, 2013.
34. Aoki S, Shirouzu I, Sasaki Y, et al: Enhancement of the intracranial arterial wall at MR imaging: relationship to cerebral atherosclerosis. Radiology 194:477-481, 1995.
35. Cai JM, Hatsukami TS, Ferguson MS, et al: Classification of human carotid atherosclerotic lesions with *in vivo* multicontrast magnetic resonance imaging. Circulation 106:1368-1373, 2002.
36. Harteveld AA, Denswil NP, Siero JC, et al: Quantitative Intracranial Atherosclerotic Plaque Characterization at 7T MRI: An Ex Vivo Study with Histologic Validation. AJNR Am J Neuroradiol 37:802-810, 2016.
37. Mandell DM, Mossa-Basha M, Qiao Y, et al: Intracranial Vessel Wall MRI: Principles and Expert Consensus Recommendations of the American Society of Neuroradiology. AJNR Am J Neuroradiol, 2016.
38. Adams HP, Jr., Bendixen BH, Kappelle LJ, et al: Classification of subtype of acute ischemic stroke. Definitions for use in a multicenter clinical trial. TOAST. Trial of Org 10172 in Acute Stroke Treatment. Stroke 24:35-41, 1993.

PART III

Ex vivo validation of intracranial vessel wall MRI

Chapter 6

Quantitative intracranial atherosclerotic plaque characterization at 7.0 tesla MRI: an *ex vivo* study with histological validation

Anita A. Harteveld[1], Nerissa P. Denswil[6], Jeroen C.W. Siero[1], Jaco J.M. Zwanenburg[1,2], Aryan Vink[3], Behdad Pouran[4,5,7], Wim G.M. Spliet[3], Dennis W.J. Klomp[1], Peter R. Luijten[1], Mat J. Daemen[6], Jeroen Hendrikse[1], Anja G. van der Kolk[1]

[1]Department of Radiology; [2]Image Sciences Institute; [3]Department of Pathology; [4]Department of Orthopedics; [5]Department of Rheumatology; University Medical Center Utrecht, Utrecht, the Netherlands; [6]Department of Pathology, Academic Medical Center, Amsterdam, the Netherlands; [7]Department of Biomedical Engineering, Faculty of Mechanical, Maritime, and Materials Engineering, Delft University of Technology, Delft, the Netherlands

Published in *American Journal of Neuroradiology* 2016

Abstract

Objectives

In recent years, several high-resolution vessel wall MRI techniques have emerged for the characterization of intracranial atherosclerotic vessel wall lesions *in vivo*. However, a thorough validation of MRI results of intracranial plaques with histopathology is still lacking. The aim of this study was to characterize atherosclerotic plaque components in a quantitative manner by obtaining the MR signal characteristics (T_1, T_2, T_2^* and PD) at 7T in *ex vivo* circle of Willis specimens, using histopathology for validation.

Materials and Methods

A multi-parametric ultrahigh-resolution quantitative MRI protocol was performed at 7T to identify the MR signal characteristics of different intracranial atherosclerotic plaque components, using histopathology for validation. In total 38 advanced plaques were matched between MRI and histology, and ROI analysis was performed on the identified tissue components.

Results

Mean T_1, T_2, T_2^* relaxation times and PD values were significantly different between different tissue components. The quantitative T_1 map showed most differences between individual tissue components of intracranial plaques with significant differences in T_1 values between lipid accumulation (T_1= 838 ± 167 ms), fibrous tissue (T_1= 583 ± 161 ms), fibrous cap (T_1= 481 ± 98 ms), calcifications (T_1= 314 ± 39 ms) and the intracranial arterial vessel wall (T_1= 436 ± 122 ms).

Conclusions

Different tissue components of advanced intracranial plaques have distinguishable imaging characteristics with ultrahigh-resolution quantitative MR imaging at 7T. Based on this study, the most promising method for distinguishing intracranial plaque components is T_1-weighted imaging.

Introduction

Ischemic stroke is one of the major diseases in the Western world, associated with a high morbidity and mortality.[1,2] Identifying the cause of ischemic stroke is of great clinical importance, not only for deciding which treatment options are best for the individual patient, but also with regard to possible prevention of future ischemic events, both recurrent and new.

Intracranial atherosclerosis is one of the main causes of ischemic stroke and TIA worldwide, accounting for approximately 9-33% of all ischemic strokes and TIAs (depending on race-ethnicity), and is the major cause of cerebral ischemic events in the Asian population. Additionally, the risk of recurrent ischemic stroke is increased in patients with underlying intracranial atherosclerosis.[3-8] Similar to extracranial atherosclerosis, for intracranial atherosclerosis the degree of luminal stenosis is currently the main factor determining if an atherosclerotic plaque is symptomatic, and/or if treatment is necessary. In the last decade, plaque composition has become an additional important feature in extracranial atherosclerosis management, enabling identification of specific culprit lesions requiring treatment, even when not causing significant stenosis.[9-12] However, for intracranial atherosclerosis this is not yet common practice, even though literature suggests that also intracranially, stenosis grade is not always associated with a risk of ischemic events: in patients with a high-grade stenosis, only one in every [5-10] patients will have a recurrent ischemic stroke [5,6,13,14] This implies that – like in extracranial atherosclerosis – luminal information is not the only important marker for future cerebrovascular events.

In recent years, several high-resolution intracranial vessel wall imaging techniques using 3.0 and 7.0 tesla MRI have emerged for the evaluation and characterization of atherosclerotic vessel wall lesions *in vivo*.[15] However, these *in vivo* techniques so far have not been validated with histopathology, due to poor accessibility of the intracranial arteries. Therefore, the question arises if these techniques are truly able – i.e. have enough image contrast – to distinguish different atherosclerotic plaque components. In the last two years, two *ex vivo* correlation studies have been performed at 7T MRI to assess its ability in visualizing different

intracranial atherosclerotic plaque components.[16,17] These *ex vivo* studies showed that 7T MRI is capable of identifying focal thickening of the intracranial arterial vessel wall, as well as distinguishing different plaque components within advanced intracranial atherosclerotic plaques with different image contrast weightings. Recently, a first case report was published demonstrating the correlation between certain intracranial atherosclerotic plaque components visualized *in vivo* at 3.0T and histological validation of the plaque post-mortem.[18] Those studies used qualitative MR sequences to score the atherosclerotic plaque signal heterogeneities. As a next step towards validation, quantitative assessment of MR signal characteristics of specific plaque components might enable more firm conclusions regarding the ability of T_1-, T_2-, T_2^*- and PD-weighted sequences in characterizing intracranial atherosclerotic plaques. Once it is known which plaque components can be identified with *ex vivo* MRI sequences, a translation may be made to *in vivo* intracranial vessel wall MR imaging, by developing sequences based on the NMR tissue properties of the identified atherosclerotic plaque components.

In the current study, a multi-parametric ultrahigh-resolution quantitative MRI protocol was performed to identify the MR signal characteristics of different intracranial atherosclerotic plaque components, using histopathology for validation.

Materials and Methods

Specimens

Human circle of Willis (CoW) specimens with macroscopic presence of a high atherosclerotic plaque burden were selected by an experienced pathologist (AV) from >100 autopsy cases that were performed in our institution. Material was handled in a coded manner that met the criteria of the Code of conduct used in the Netherlands for the responsible use of human tissue in medical research (www.federa.org/codes-conduct), and institutional review board approval for this retrospective study was obtained.

Specimen preparation

All specimens had been stored in buffered formalin (4%). Preparation of the specimens for MR imaging and histological sampling was performed according to the method previously described by Van der Kolk *et al.*[16] Cactus spines were used as fiducials and placed at 15 locations in the agarose gel adjacent to an artery for histological sampling, to enable spatial correlation with histology. The 15 locations were chosen to sample all major vessels of the CoW including their branches (e.g. A2 segment of the anterior cerebral artery), and were placed at the location of a visible vessel wall abnormality (if present). The locations included: the anterior cerebral (A1 and A2 segments), middle cerebral (M1 segment), intracranial internal carotid (C7 segment), posterior cerebral (P2 segment), basilar (upper, middle and lower part) and vertebral arteries (left and right if applicable).

Imaging

The embedded specimens were scanned in a 7T whole body system (Philips Healthcare, Cleveland, OH, USA). A custom-made high density receive coil (16-channels per 70 cm^2; MR Coils BV, Drunen, the Netherlands) was used for signal reception[19], and a volume transmit/receive coil for transmission (Nova Medical, Wilmington, MA, USA). Each embedded specimen was imaged individually. The petri dish containing the embedded specimen was placed in the middle of the transmit coil on top of the receive coil; plastic filling was used to stabilize and secure the petri dish.

Protocol

Imaging was performed at room temperature. The scan protocol contained three sequences with different contrast weightings to image the specimens, from which quantitative MR parameter maps were calculated. For T_1, T_2 and PD mapping the Driven Equilibrium Single Pulse Observation of T_1 (DESPOT1) and T_2 (DESPOT2) sequences were used.[20] Repetition time was chosen as short as possible allowed by the desired spatial resolution and field of view. Optimal flip angle pairs for the DESPOT1 and DESPOT2 scans were calculated assuming a range of T_1 and T_2 values of 150-650 ms and 10-30 ms, respectively. T_2^* maps were obtained using a dual-echo 3D

T_2^*-weighted scan. The applied scan parameters are presented in **Table 1**. A 3D B_1 map was acquired using the actual flip angle method to correct for B_1 inhomogeneity during post-processing of the MR images.[21] Total scan time was approximately 19h and 30min per specimen. All MR images were acquired with an isotropic resolution. This allowed reconstructions along arbitrary planes, which enabled accurate matching of the MR images to the sectioning plane of the histological sections.

Table 1 | Scan parameters of the 7T MRI protocol.

Pulse sequence	DESPOT1	DESPOT2	T_2^* map
TR/TE1/TE2 (ms)	16/4.3/-	36/18/-	53/6/26
Flip angle (˚)	11/44	12/62	29
No. of slices	153	153	153
FOV (mm)	150x150x20	150x150x20	150x150x20
Acquisition matrix	1152x1154	1152x1152	1152x1154
Acquired voxel size (mm)	0.13x0.13x0.13	0.13x0.13x0.13	0.13x0.13x0.13
Bandwidth (Hz/pixel)	165	41	101
TFE-factor	1154	1152	1154
Repeated scans	4	3	1
Acquisition time (hh:mm:ss)	06:21:28	11:07:34	02:00:53

MR image processing

The MR images were processed using Matlab version R2014b (Mathworks, Natick, Massachusetts, USA). First, the DESPOT1 and DESPOT2 dynamic scans were co-registered to correct for small shifts between the matching images. Next, the parametric images (T_1, T_2, T_2^* relaxation times and PD values) were calculated from the original MRI data sets according to the method previously described by Deoni *et al.*[20] B_1 correction was performed during calculation of the parametric T_1 and T_2 maps, to correct for B_1 inhomogeneity within the specimen.

Histopathology

After MR imaging, 0.5 mm thick tissue samples were taken from the 15 marked locations of each CoW specimen for histologic processing. Histologic processing was performed using an in-house developed protocol, as previously described.[16] Classification of the histological sections was performed according to the modified American Heart Association classification by Virmani *et al*.[22], a well-established method that is based on atherosclerotic characteristics as follows: 1) no anomaly; 2) early lesion, including intimal thickening (<50% smooth-muscle cells, no lipids, inflammatory cells), fatty streak, and pathological intimal thickening (>50% smooth muscle cells, rich in proteoglycans, foamy macrophages); and 3) advanced lesion, including fibrolipid plaque (>40% lipid), thin cap atheroma (<65μm thickness), fibrous plaque (<40% lipid), fibrocalcified plaque (>40% calcified) and calcified nodule (calcified element protruding the intima). When applicable, plaque complications – rupture, hemorrhage or erosion – were also assessed. The histological classification was performed blinded for the MRI results by one experienced observer (N.D.).

Matching of MR and histology images

Image reconstructions were made perpendicular to the relevant arteries (slice thickness: 0.13 mm) at the locations of the fiducials seen on the MR images, using the software program VesselMASS (Leiden University Medical Center, Leiden, the Netherlands). The MR images and the histological sections were manually matched by one observer (A.H.) using the marked locations with the fiducials in the MR images, the ink markings in the histological sections, and gross morphologic features. Samples were excluded when no match was found, or when air bubbles were present in the MR images.

Plaque component analysis

To analyze different plaque components, only plaques histologically scored as advanced – therefore including several components – were used, since a previous study showed no heterogeneity in qualitative signal intensity in early lesions.[16] The identified plaque components included fibrous tissue, fibrous cap, lipid accumulation (increasing mass

of lipids (lipid retention) within the intimal area, which is defined as the plaque), intraplaque hemorrhage (IPH) and calcifications (deposition of extracellular calcium within the plaque). Based on the identified plaque components in a histological section, ROIs were drawn manually within the corresponding regions on T_1-weighted MR images (DESPOT1 acquired with flip angle of 44 degrees, used for calculation of the quantitative maps) by one observer (A.H.). The ROIs were used to calculate the mean T_1, T_2, T_2^* relaxation times and PD values for those regions in the MR parameter maps, using the dedicated vessel wall analysis software VesselMASS.

Statistical analysis

All statistical analyses were performed using IBM SPSS Statistics (version: 20.0, IBM Corp., Armonk, NY, USA). Since the data was normally distributed, but the assumption of homogeneity of variance was not met, Welch's test was conducted to compare the mean ROI values of the different tissue components. Games-Howell's post hoc tests were performed for pairwise comparisons. A p-value of <0.05 was considered to be statistically significant.

Results

Fifteen CoW specimens were selected for this study (9 male; mean age 68.7 ± 13.3 years). In total 213 samples of CoW arteries were obtained (in 8 specimens, one (or more) vessel segments were absent (n=12 vessel segments)); 8 of the 213 samples (3.8%) were excluded because they were not assessable for histological classification (the samples could not be sliced properly), resulting in 205 samples available for histological classification.

Histological classification

Six samples (2.9%) were scored as non-diseased, 143 samples (69.8%) showed early lesions (intimal thickening (n=97), pathological intimal thickening (n=19), and fatty streak (n=27)), and 56 samples (27.3%) showed advanced plaques (fibrous plaque (n=28), fibrolipid plaque (n=25), and fibrocalcified plaque (n=3)). No calcified nodules or thin cap atheromas were seen. Of the 56 advanced plaques, 18 plaques (32%) were excluded

due to lack of match (n=3), or air bubble present in MR images (n=15), resulting in 38 MR-matched advanced atherosclerotic plaques (20 fibrous plaques, 16 fibrolipid plaques and 2 fibrocalcified plaques) that could be used for the ROI analysis. ROIs were drawn in the matched MR images of the advanced atherosclerotic plaques within the corresponding regions of the tissue components identified in the histological sections: lipid accumulation n=17, fibrous tissue n=24, fibrous cap n=12, calcifications n=5, and vessel wall n=37.

Quantitative MR parameter maps

Figures 1-3 show examples of histological sections with the matched MR parameter maps (T_1, T_2, T_2^*, and PD) of advanced plaques from the CoW specimens. **Figure 4** and **Table 2** show the results of the ROI analysis. For each quantitative MR parameter map a significant difference was found between certain identified tissue components. In **Figure 3B** the single sample containing intraplaque hemorrhage is shown. The hemorrhage can be distinguished from the surrounding fibrous tissue in the T_1 and PD maps. This sample was not included in the statistical analysis, since only one sample contained an intraplaque hemorrhage in this study.

Post hoc analysis

Table 3 gives an overview of the post hoc tests performed for pairwise comparisons of mean ROI values of the identified tissue components, with the resulting p-values.

Figure 1 | Histological sections (EvG stain) of two different samples from the CoW specimens classified as fibrolipid plaques: (**A**) left vertebral artery; and (**B**) left middle cerebral artery (arrow: lipid accumulation; arrowhead: fibrous cap). The corresponding T_1-weighted image (T_1w; DESPOT1 acquired with flip angle of 44 degrees) and the calculated parametric maps (T_1, T_2, T_2^* and PD) are shown. Regions of interest (ROIs) were drawn at the location of tissue components identified in the histological section (yellow ROI: lipid accumulation; blue ROI: fibrous cap; green+red ROI: vessel wall) to calculate the mean T_1-, T_2-, T_2^*-, and PD-values for those regions. Lipid accumulation can be distinguished from the fibrous cap and the vessel wall in the T_1, PD and T_2 maps. In (**A**) the lipid accumulation area is already developed into the beginning of a lipid core.

Figure 2 | Histological sections (EvG stain) of two different samples from the CoW specimens classified as fibrous plaques: (**A**) right middle cerebral artery; and (**B**) left intracranial internal carotid artery (arrowhead: fibrous tissue). The corresponding T_1-weighted image (T_1w; DESPOT1 acquired with flip angle of 44 degrees) and the calculated parametric maps (T_1, T_2, T_2^* and PD) are shown. Regions of interest (ROIs) were drawn at the location of tissue components identified in the histological section (blue ROI: fibrous tissue; green+red ROI: vessel wall) to calculate the mean T_1-, T_2-, T_2^*-, and PD-values for those regions. Here, fibrous tissue can be distinguished from the vessel wall in the T_1 and T_2 map (partly), and to a lesser extent in the T_2^* map.

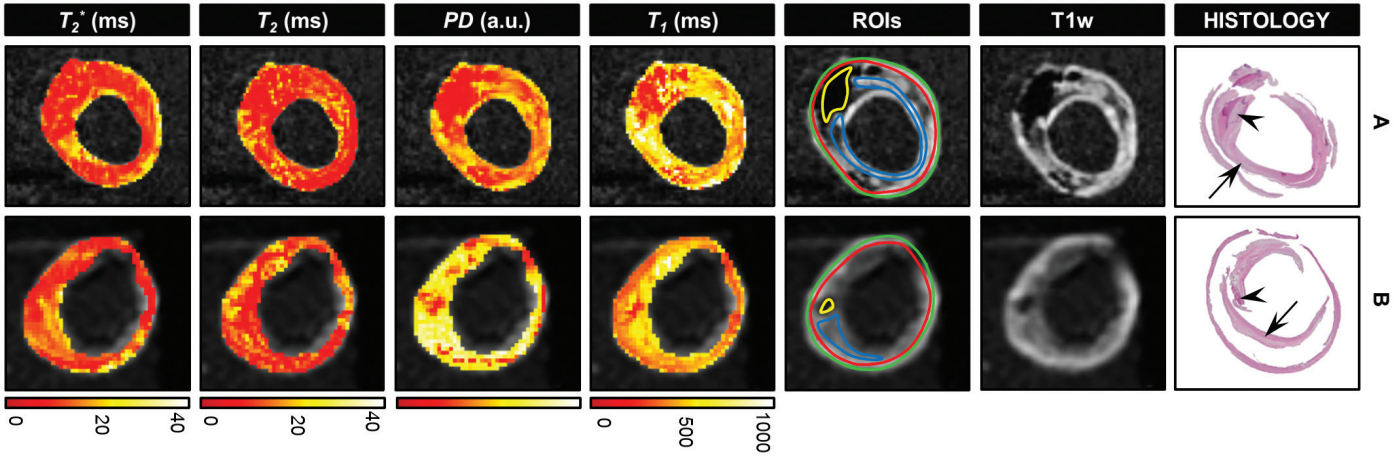

Figure 3 | Histological sections (H&E stain) of two different samples from the CoW specimens containing calcifications (**A**) and an intraplaque hemorrhage (**B**): (**A**) right intracranial internal carotid artery, classified as fibrocalcified plaque; and (**B**) middle part of the basilar artery, classified as fibrous plaque with an old hemorrhage (arrow: fibrous tissue; arrowhead: calcification (**A**), and hemorrhage (**B**)). The corresponding T_1-weighted image (T_1w; DESPOT1 acquired with flip angle of 44 degrees) and the calculated parametric maps (T_1, T_2, T_2^* and PD) are shown. Regions of interest (ROIs) were drawn at the location of tissue components identified in the histological section (yellow ROI: calcification (**A**), or intraplaque hemorrhage (**B**); blue ROI: fibrous tissue; green+red ROI: vessel wall) to calculate the mean T_1-, T_2-, T_2^*-, and PD-values for those regions. Here, the tissue area containing calcifications can be distinguished well in both the PD and T_1 maps, and to a lesser extent in the T_2 and T_2^* maps. The intraplaque hemorrhage can be distinguished from the surrounding fibrous tissue in the T_1 and PD maps.

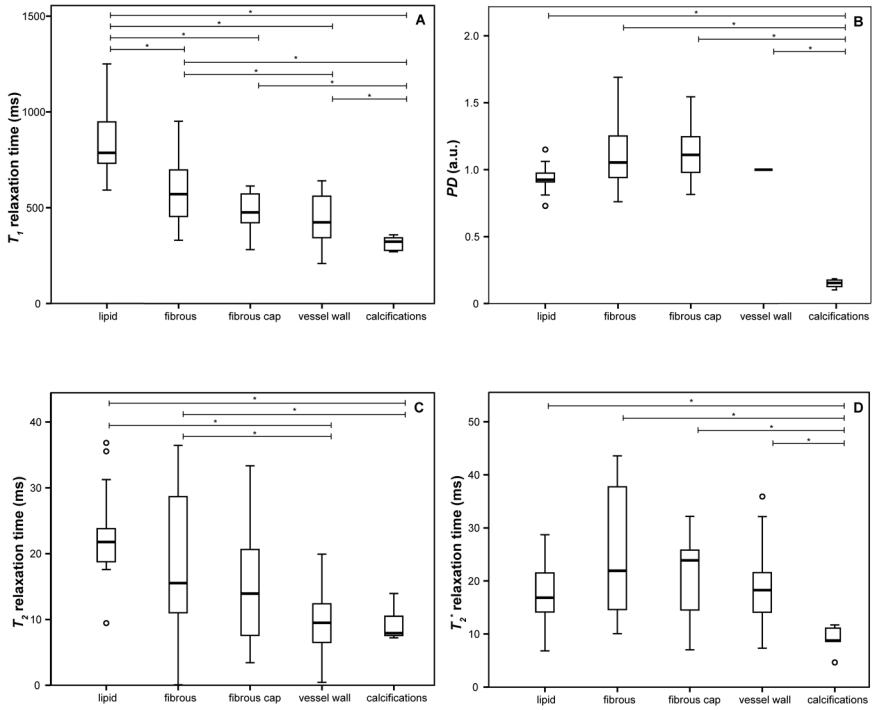

Figure 4 | Boxplots showing the distribution of the mean ROI values of each identified tissue component determined in the quantitative (**A**) T_1, (**B**) PD, (**C**) T_2, and (**D**) T_2^* maps of each advanced plaque sample. *Post hoc pairwise comparison $p<0.05$.

6

Table 2 | NMR characteristics of different intracranial plaque tissue components (mean±SD) [a]

	Lipid accumulation (n=17)	Fibrous tissue (n=24)	Fibrous cap (n=12)	Calcifications (n=5)	Vessel wall (n=37)
T_1 (ms)	838 ± 167	583 ± 161	481 ± 98	314 ± 39	436 ± 122
PD[b]	0.94 ± 0.10	1.10 ± 0.26	1.13 ± 0.21	0.15 ± 0.03	1.0 ± 0
T_2 (ms)	22 ± 6.8	18 ± 10	15 ± 9.2	9.4 ± 2.8	10 ± 4.4
T_2^* (ms)	18 ± 6.2	25 ± 11	21 ± 8.4	8.9 ± 3.0	18 ± 6.5

For each identified plaque component the mean ± SD of the mean ROI values for all parameters (T_1, PD, T_2, T_2^*) are given.
[a]Group differences between tissue components were tested with Welch's test; all maps showed a significant difference ($p<.001$) between tissue components.
[b]Normalized to vessel wall.

Table 3 | Post hoc pairwise comparisons[a] of the identified tissue components.

T_1 relaxation time	Lipid accumulation	Fibrous tissue	Fibrous cap	Calcifications
Fibrous tissue	<.001[b]	-	-	-
Fibrous cap	<.001[b]	0.155	-	-
Calcifications	<.001[b]	<.001[b]	0.001[b]	-
Vessel wall	<.001[b]	0.004[b]	0.691	0.002[b]
PD-value	**Lipid accumulation**	**Fibrous tissue**	**Fibrous cap**	**Calcifications**
Fibrous tissue	0.052	-	-	-
Fibrous cap	0.068	0.998	-	-
Calcifications	<.001[b]	<.001[b]	<.001[b]	-
Vessel wall	0.108	0.323	0.288	<.001[b]
T_2 relaxation time	Lipid accumulation	Fibrous tissue	Fibrous cap	Calcifications
Fibrous tissue	0.522	-	-	-
Fibrous cap	0.164	0.878	-	-
Calcifications	<.001[b]	0.014[b]	0.375	-
Vessel wall	<.001[b]	0.011[b]	0.446	0.986
T_2^* relaxation time	Lipid accumulation	Fibrous tissue	Fibrous cap	Calcifications
Fibrous tissue	0.065	-	-	-
Fibrous cap	0.793	0.688	-	-
Calcifications	0.003[b]	<.001[b]	0.005[b]	-
Vessel wall	0.994	0.079	0.884	0.001[b]

[a]Games-Howell's post hoc tests were performed for pairwise comparisons.
[b]$p<0.05$

Discussion

The current study focused on obtaining *ex vivo* quantitative T_1, T_2, T_2^* relaxation times and PD values for different intracranial atherosclerotic plaque components. Its goal was to provide detailed insight into the ability of MR imaging to characterize intracranial atherosclerotic plaque components. Our main results show that primarily T_1 relaxation times were significantly different between different plaque components, the other quantitative maps (PD, T_2 and T_2^*) showed mostly non-significant differences between the individual tissue components present in the advanced intracranial plaques.

Thus far, atherosclerotic plaques have been extensively studied in extracranial carotid arteries with both *in vivo* [23-25] and *ex vivo* [26-29] MRI. These studies showed good correlation between MRI plaque characteristics and histologic findings. The advantage of extracranial carotid artery plaques is that *in vivo* MR imaging can be performed prior to a carotid endarterectomy procedure allowing for direct correlation with histopathology. However, extrapolation of MR signal characteristics of extracranial plaques to intracranial plaques may not be directly applicable because intracranial arteries are smaller, and have some unique histological features.[18,30-32] Even so, several studies have recently reported visualization of different intracranial plaque components *in vivo* using MRI, such as lipids[33], fibrous cap[33-35], and intraplaque hemorrhage[34,36-38]. These *in vivo* techniques, however, have not been validated thoroughly with histopathology, due to the poor accessibility of the intracranial arteries. Recently, Turan *et al.*[18] published a first case report demonstrating the correlation between certain intracranial atherosclerotic plaque components visualized *in vivo* at 3.0T with histological validation of the plaque post-mortem. However, further correlations are needed to define additional plaque components, as well as to increase the number of cases. As a first step towards MR validation, two *ex vivo* correlation studies[16,17] assessed the ability of 7T MRI to image plaque components. These qualitative studies showed 7T to have sufficient image contrast to distinguish different plaque components within advanced plaques. As a second step towards validation, the current study quantitatively assessed intracranial atherosclerotic plaques, to enable more firm conclusions regarding the ability of T_1-, T_2-, T_2^*- and PD-weighted sequences in characterizing intracranial atherosclerotic plaques.

Our results showed the T_1 relaxation times gave most differences between individual tissue components of advanced intracranial plaques. Tissue components identified in the histological sections as lipid accumulation, fibrous tissue, fibrous cap, calcifications and vessel wall showed significant differences in T_1 relaxation times, indicating they can be distinguished from each other in a T_1-weighted sequence. Lipid accumulation showed the longest mean T_1 relaxation time, indicating this may appear as a hypo-isointense region in a T_1-weighted sequence. Van

der Kolk *et al.*[16] also showed the lipid-rich core to be hypointense on T_1-weighted imaging of *ex vivo* CoW specimens at 7T MRI, while Turan *et al.*[18] *in vivo* demonstrated lipid and loose matrix to have an isointense signal intensity compared to the surrounding tissue on a T_1-weighted image at 3.0T MRI. However, both studies were based on a limited number of observations. Previous studies on carotid atherosclerotic plaques[11,27,39] have shown the lipid-rich core to be hyperintense on T_1-weighted imaging. An explanation for this difference could be that the stage of development of the lipid-rich core in the current study might be earlier compared with the extracranial carotid artery studies. In the current study only one sample was identified showing the beginning of a lipid core (see **Figure 1A**), all other samples that were classified as a fibrolipid plaque were still at the stage of lipid accumulation. Intracranial arteries show more stable lesions, and develop mainly as fibrous plaques[30]. Another explanation could be that lipids in an atherosclerotic plaque undergo a partially irreversible phase transition when cooled[40], however, it is not clear if this transition affects the MRI properties of the lipids[27].

The other quantitative maps (PD, T_2 and T_2^*) showed less significant differences between the mean ROI values of the individual tissue components present in the advanced intracranial plaques. The fibrous cap and fibrous tissue showed a larger mean PD value compared to lipid accumulation, however, these differences did not reach statistical significance. Chung *et al.*[34] also found the fibrous cap to be hyperintense in PD-weighted imaging of intracranial plaques *in vivo*. Based on the T_2 relaxation time a distinction can be made between lipids/fibrous tissue on the one hand, and vessel wall/calcifications on the other hand. However, for each analyzed tissue component the T_2 relaxation times showed a large relative standard deviation. Also the T_2 relaxation times were not consistently larger than the T_2^*, this in contrast to what is known from NMR theory. The DESPOT2 method for estimating the T_2 relaxation times might be more sensitive to noise than the DESPOT1 and, might thus have suffered from the limited SNR that is a result of the high resolution used in the current study. Future studies specifically focused on plaque T_2 relaxation times may show more significant results. For carotid plaque characterization it has been shown that reviewing multiple contrast-

weighted images provided the most comprehensive evaluation for certain plaque components (e.g. IPH and lipid-rich necrotic core).[27,41]

Only at a few locations intracranial calcified plaques were detected. This is in agreement with the low prevalence of intracranial calcified plaques beyond the proximal segments of the ICA and VA.[30,42] The calcifications that were detected showed low values in all quantitative maps. The PD map showed the largest differences between calcifications and other plaque components and intracranial vessel wall. It would be expected that this large difference would also be present on the T_2^* maps, due to the increased susceptibility effects; however, this was not seen in our small sample. This could be due to the relatively lower SNR for the T_2^* maps (only one signal average was used for the T_2^*-weighted sequence). Also, the T_2^* of calcifications is known to be very short relative to the shortest echo-time of the current T_2^*-weighted sequence. [43] These factors can potentially impede accurate fitting of the T_2^* relaxation times. To overcome this, a sequence can be used that measures at even shorter echo times, however this would come at a price of attainable spatial resolution.

Plaque complications were very rare in this study: only one sample with an intraplaque hemorrhage was found. Previous studies have shown a lower prevalence of intraplaque hemorrhage in intracranial compared with extracranial atherosclerosis, and the prevalence of intraplaque hemorrhage is higher in plaques of symptomatic patients (who experienced a cerebral infarct) compared to asymptomatic patients.[30,31,38] In the current study, the CoW specimens were selected based on the macroscopic presence of a high atherosclerotic plaque burden, without knowledge of the clinical background of the patients. Also, samples were taken at 15 marked locations per CoW specimen only. Increasing the number of samples per specimen and selecting specimens from symptomatic patients might increase the number of plaque complications found.

This study has several limitations. First, fixation effects of formalin have been shown to change relaxation parameters over time.[44,45] Compared to relaxation times *in vivo* for the vessel wall of the extracranial carotid arteries [46], the relaxation times in the current *ex vivo* study are considerably shorter. Similar shortening was found in a previous post-

mortem study, where the relaxation times for grey and white matter were measured in formalin-fixed human brains.[47] With an understanding of the effects of sample preparation, the MR data can be correctly related to *in vivo* data.[44] Second, the MRI experiments were performed at room temperature instead of body temperature, which will have influenced the quantitative measurements in the post-mortem specimens.[44] The 7T MR platform does not provide the possibility to perform temperature controlled imaging. For now, this is the first study trying to identify specific intracranial plaque components in a quantitative manner to measure whether individual tissue components can be distinguished from each other based on their NMR tissue properties. This might already give a suggestion which contrast weighting(s) need further consideration to offer the greatest potential to really discriminate different plaque components *in vivo*. A next step for future studies would be to validate the current findings in a new set of intracranial plaques with optimized MRI sequences – preferably of patients with cerebrovascular disease – by characterizing the plaque components based on the MR images alone (with histologic validation afterwards), where also the reliability of the measurements can be assessed.

This study was performed to investigate which MR relaxation times discriminate best between the different plaque components; and thereby, in essence, to predict which image contrast weighting would work best *in vivo* in characterizing atherosclerotic plaques. Based on this study, the T_1 relaxation time seems to be the most promising parameter. For now, a direct translation of the quantitative sequences used in the current *ex vivo* setting to *in vivo* will be difficult due to the long scan times necessary to achieve the ultrahigh-resolution to be able to identify different plaque components. However, this study shows T_1-weighted imaging is probably the best method for distinguishing intracranial plaque components *ex vivo*, and therefore might also be most promising for *in vivo* application. Now it is known which plaque components can be identified with *ex vivo* MRI sequences, a translation may be made to *in vivo* intracranial vessel wall MR imaging by fine-tuning the current *in vivo* sequences based on the NMR tissue properties of the identified atherosclerotic plaque components to obtain optimal image contrast between the different

tissue components. Also, future developments in receive coil technology (increasing the number of receive elements) may provide significant improvement in SNR to make quantitative assessment of the intracranial arterial vessel wall possible *in vivo*. Furthermore, *in vivo* we expect that quantitative assessment will first become feasible for the thicker arterial vessel wall of the more proximal intracranial arteries including the distal carotid artery and the vertebrobasilar arterial vessel walls.

In conclusion, we showed that different tissue components of advanced intracranial plaques have distinguishable imaging characteristics using ultrahigh-resolution quantitative MR imaging at 7T MRI. Now it is known which plaque components can be identified with *ex vivo* MRI sequences, a translation may be made to *in vivo* intracranial vessel wall MR imaging to obtain optimal image contrast between the different plaque components. Based on this study, the most promising method for distinguishing these plaque components is T_1-weighted imaging.

References

1. Go AS, Mozaffarian D, Roger VL, et al: Heart disease and stroke statistics--2014 update: a report from the American Heart Association. Circulation 129:e28-e292, 2014.
2. Lozano R, Naghavi M, Foreman K, et al: Global and regional mortality from 235 causes of death for 20 age groups in 1990 and 2010: a systematic analysis for the Global Burden of Disease Study 2010. Lancet 380:2095-2128, 2012.
3. Arenillas JF: Intracranial atherosclerosis: current concepts. Stroke 42:S20-23, 2011.
4. Bos D, Portegies ML, van der Lugt A, et al: Intracranial carotid artery atherosclerosis and the risk of stroke in whites: the Rotterdam Study. JAMA Neurol 71:405-411, 2014.
5. Chimowitz MI, Lynn MJ, Derdeyn CP, et al: Stenting versus aggressive medical therapy for intracranial arterial stenosis. N Engl J Med 365:993-1003, 2011.
6. Chimowitz MI, Lynn MJ, Howlett-Smith H, et al: Comparison of warfarin and aspirin for symptomatic intracranial arterial stenosis. N Engl J Med 352:1305-1316, 2005.
7. Gorelick PB, Wong KS, Bae HJ, et al: Large artery intracranial occlusive disease: a large worldwide burden but a relatively neglected frontier. Stroke 39:2396-2399, 2008.
8. Qureshi AI, Caplan LR: Intracranial atherosclerosis. Lancet 383:984-998, 2014.
9. Hellings WE, Peeters W, Moll FL, et al: Composition of carotid atherosclerotic plaque is associated with cardiovascular outcome: a prognostic study. Circulation 121:1941-1950, 2010.
10. Saam T, Hatsukami TS, Takaya N, et al: The vulnerable, or high-risk, atherosclerotic plaque: noninvasive MR imaging for characterization and assessment. Radiology 244:64-77, 2007.
11. Saba L, Anzidei M, Sanfilippo R, et al: Imaging of the carotid artery. Atherosclerosis 220:294-309, 2012.
12. Takaya N, Yuan C, Chu B, et al: Association between carotid plaque characteristics and subsequent ischemic cerebrovascular events: a prospective assessment with MRI--initial results. Stroke 37:818-823, 2006.
13. Kasner SE, Chimowitz MI, Lynn MJ, et al: Predictors of ischemic stroke in the territory of a symptomatic intracranial arterial stenosis. Circulation 113:555-563, 2006.
14. Leng X, Wong KS, Liebeskind DS: Evaluating intracranial atherosclerosis rather than intracranial stenosis. Stroke 45:645-651, 2014.
15. Dieleman N, van der Kolk AG, Zwanenburg JJ, et al: Imaging intracranial vessel wall pathology with magnetic resonance imaging: current prospects and future directions. Circulation 130:192-201, 2014.

16. van der Kolk AG, Zwanenburg JJ, Denswil NP, et al: Imaging the Intracranial Atherosclerotic Vessel Wall Using 7T MRI: Initial Comparison with Histopathology. AJNR Am J Neuroradiol, 2014.
17. Majidi S, Sein J, Watanabe M, et al: Intracranial-derived atherosclerosis assessment: an in vitro comparison between virtual histology by intravascular ultrasonography, 7T MRI, and histopathologic findings. AJNR Am J Neuroradiol 34:2259-2264, 2013.
18. Turan TN, Rumboldt Z, Granholm AC, et al: Intracranial atherosclerosis: correlation between in-vivo 3T high resolution MRI and pathology. Atherosclerosis 237:460-463, 2014.
19. Petridou N, Italiaander M, van de Bank BL, et al: Pushing the limits of high-resolution functional MRI using a simple high-density multi-element coil design. NMR Biomed 26:65-73, 2013.
20. Deoni SC, Rutt BK, Peters TM: Rapid combined T1 and T2 mapping using gradient recalled acquisition in the steady state. Magn Reson Med 49:515-526, 2003.
21. Yarnykh VL: Actual flip-angle imaging in the pulsed steady state: a method for rapid three-dimensional mapping of the transmitted radiofrequency field. Magn Reson Med 57:192-200, 2007.
22. Virmani R, Kolodgie FD, Burke AP, et al: Lessons from sudden coronary death: a comprehensive morphological classification scheme for atherosclerotic lesions. Arterioscler Thromb Vasc Biol 20:1262-1275, 2000.
23. Cai JM, Hatsukami TS, Ferguson MS, et al: Classification of human carotid atherosclerotic lesions with *in vivo* multicontrast magnetic resonance imaging. Circulation 106:1368-1373, 2002.
24. Cai J, Hatsukami TS, Ferguson MS, et al: In vivo quantitative measurement of intact fibrous cap and lipid-rich necrotic core size in atherosclerotic carotid plaque: comparison of high-resolution, contrast-enhanced magnetic resonance imaging and histology. Circulation 112:3437-3444, 2005.
25. Hofman JM, Branderhorst WJ, ten Eikelder HM, et al: Quantification of atherosclerotic plaque components using *in vivo* MRI and supervised classifiers. Magn Reson Med 55:790-799, 2006.
26. Coombs BD, Rapp JH, Ursell PC, et al: Structure of plaque at carotid bifurcation: high-resolution MRI with histological correlation. Stroke 32:2516-2521, 2001.
27. Shinnar M, Fallon JT, Wehrli S, et al: The diagnostic accuracy of ex vivo MRI for human atherosclerotic plaque characterization. Arterioscler Thromb Vasc Biol 19:2756-2761, 1999.

28. Serfaty JM, Chaabane L, Tabib A, et al: Atherosclerotic plaques: classification and characterization with T2-weighted high-spatial-resolution MR imaging-- an in vitro study. Radiology 219:403-410, 2001.
29. Clarke SE, Hammond RR, Mitchell JR, et al: Quantitative assessment of carotid plaque composition using multicontrast MRI and registered histology. Magn Reson Med 50:1199-1208, 2003.
30. Ritz K, Denswil NP, Stam OC, et al: Cause and mechanisms of intracranial atherosclerosis. Circulation 130:1407-1414, 2014.
31. Chen XY, Wong KS, Lam WW, et al: Middle cerebral artery atherosclerosis: histological comparison between plaques associated with and not associated with infarct in a postmortem study. Cerebrovasc Dis 25:74-80, 2008.
32. Portanova A, Hakakian N, Mikulis DJ, et al: Intracranial vasa vasorum: insights and implications for imaging. Radiology 267:667-679, 2013.
33. Turan TN, Rumboldt Z, Brown TR: High-resolution MRI of basilar atherosclerosis: three-dimensional acquisition and FLAIR sequences. Brain Behav 3:1-3, 2013.
34. Chung JW, Kim BJ, Choi BS, et al: High-resolution magnetic resonance imaging reveals hidden etiologies of symptomatic vertebral arterial lesions. J Stroke Cerebrovasc Dis 23:293-302, 2014.
35. Yang WQ, Huang B, Liu XT, et al: Reproducibility of high-resolution MRI for the middle cerebral artery plaque at 3T. Eur J Radiol 83:e49-55, 2014.
36. Turan TN, Bonilha L, Morgan PS, et al: Intraplaque hemorrhage in symptomatic intracranial atherosclerotic disease. J Neuroimaging 21:e159-161, 2011.
37. Park JK, Kim SH, Kim BS, et al: Imaging of intracranial plaques with black-blood double inversion recovery MR imaging and CT. J Neuroimaging 21:e64-68, 2011.
38. Xu WH, Li ML, Gao S, et al: Middle cerebral artery intraplaque hemorrhage: prevalence and clinical relevance. Ann Neurol 71:195-198, 2012.
39. Yuan C, Mitsumori LM, Beach KW, et al: Carotid atherosclerotic plaque: noninvasive MR characterization and identification of vulnerable lesions. Radiology 221:285-299, 2001.
40. Lundberg B: Chemical composition and physical state of lipid deposits in atherosclerosis. Atherosclerosis 56:93-110, 1985.
41. Yuan C, Mitsumori LM, Ferguson MS, et al: In vivo accuracy of multispectral magnetic resonance imaging for identifying lipid-rich necrotic cores and intraplaque hemorrhage in advanced human carotid plaques. Circulation 104:2051-2056, 2001.

42. Homburg PJ, Plas GJ, Rozie S, et al: Prevalence and calcification of intracranial arterial stenotic lesions as assessed with multidetector computed tomography angiography. Stroke 42:1244-1250, 2011.
43. Sharma S, Boujraf S, Bornstedt A, et al: Quantification of calcifications in endarterectomy samples by means of high-resolution ultra-short echo time imaging. Invest Radiol 45:109-113, 2010.
44. Thelwall PE, Shepherd TM, Stanisz GJ, et al: Effects of temperature and aldehyde fixation on tissue water diffusion properties, studied in an erythrocyte ghost tissue model. Magn Reson Med 56:282-289, 2006.
45. Thickman DI, Kundel HL, Wolf G: Nuclear magnetic resonance characteristics of fresh and fixed tissue: the effect of elapsed time. Radiology 148:183-185, 1983.
46. Koning W, de Rotte AA, Bluemink JJ, et al: MRI of the carotid artery at 7 Tesla: quantitative comparison with 3 Tesla. J Magn Reson Imaging 41:773-780, 2015.
47. Pfefferbaum A, Sullivan EV, Adalsteinsson E, et al: Postmortem MR imaging of formalin-fixed human brain. Neuroimage 21:1585-1595, 2004.

Chapter 7

Vessel wall thickness measurements of the circle of Willis using 7T MRI

Anita A. Harteveld[1], Nerissa P. Denswil[4], Wim Van Hecke[2], Hugo J. Kuijf[3], Aryan Vink[2], Wim G.M. Spliet[2], Mat J. Daemen[4], Peter R. Luijten[1], Jaco J.M. Zwanenburg[1], Jeroen Hendrikse[1], Anja G. van der Kolk[1]

[1]Department of Radiology; [2]Department of Pathology; [3]Image Sciences Institute; University Medical Center Utrecht, Utrecht, the Netherlands
[4]Department of Pathology, Academic Medical Center, Amsterdam, the Netherlands

Submitted

Abstract

Objectives

MRI can detect intracranial vessel wall thickening before any luminal stenosis is present. Apart from representing a vessel wall lesion, wall thickening could also reflect normal (age-related) variation in vessel wall thickness present throughout the intracranial arterial vasculature. The aim of this study was to perform vessel wall thickness measurements of the major intracranial arteries in *ex vivo* circle of Willis (CoW) specimens using 7T MRI, to obtain more detailed information about wall thickness variations of the intracranial arteries.

Materials and Methods

Fifteen human CoW specimens were scanned at 7T MRI with an ultrahigh-resolution T_1-weighted sequence. Five specimens were used for validation of MRI measurements with histology and evaluation of interrater reliability and agreement. The other 10 specimens from patients with (n=5) and without (n=5) cerebrovascular disease were used for vessel wall thickness measurements over the entire length of the major arterial segments of the CoW using MRI only.

Results

MRI measurements showed excellent agreement with histology. Mean wall thickness varied from 0.44-0.71 mm, minimum wall thickness from 0.30-0.46 mm, maximum wall thickness from 0.49-0.96 mm, and normalized wall index from 0.59-0.80. On average vessel walls were thicker for the symptomatic patients compared to the asymptomatic patients.

Conclusions

High-resolution MRI enables accurate measurement of vessel wall thickness in *ex vivo* CoW specimens. Vessel wall thickness measurements over the entire length of segments showed considerable variation both within and between arterial segments of patients. Symptomatic patients generally had thicker walls than asymptomatic patients.

Introduction

In the last decade, several MRI sequences have been developed for direct visualization of the intracranial vessel wall.[1] Their advantage, compared with conventional imaging techniques for visualization of the intracranial arteries (e.g. MRA or CTA), is the ability to detect vessel wall lesions before any luminal stenosis is present.[2] A vessel wall lesion is generally defined as a focal or more diffuse but restricted area of vessel wall thickening. However, apart from representing a vessel wall lesion, wall thickening could also reflect normal (age-related) variation in vessel wall thickness present throughout the intracranial arterial vasculature.

Currently, differentiation between pathological thickening and normal (age-related) vessel wall thickness variation is difficult. Autopsy studies have described the spatial distribution and severity of atherosclerosis in the intracranial arteries.[3-5] However, in contrast to vessel wall (intima-media) thickness of extracranial arteries, which have been studied more extensively thus far, limited information is available on the quantitative assessment of vessel wall thickness and thickness variation over entire arterial segments of the arteries of the circle of Willis (CoW).[6-9] This is mainly because the intracranial arteries are small and have a tortuous orientation, which demands high quality (both with respect to contrast-to-noise and spatial resolution) of the used imaging techniques to properly visualize the vessel wall *in vivo*. Also, the arteries are difficult to access, hampering correlation of *in vivo* imaging results with histology.[10] Next to differentiating normal thickness variation from vessel wall lesions, information regarding wall thickness would also shed new light on the minimum spatial resolution required for dedicated *in vivo* vessel wall imaging. MR imaging of *ex vivo* specimens enables visualization of these small and tortuous intracranial arteries with ultrahigh spatial resolution from which thickness measurements over the entire length of arterial segments can be derived, combined with histologic validation to distinguish between pathological thickening and normal vessel wall thickness.

In the current study, vessel wall thickness measurements of the major intracranial arteries were performed in *ex vivo* specimens of the CoW using 7T MRI, to obtain more detailed information about wall thickness variations of the intracranial arteries. Histology was used for validation

of the MRI measurements. Thickness measurements were performed in patients with and without cerebrovascular disease, to compare vessel wall thickness between both groups.

Materials and Methods

Specimens

For this study human CoW specimens were selected from > 100 autopsy cases that were performed in our institution. For validation with histology, specimens were used that had been selected for a previous study on plaque characteristics[11]. For the other specimens used in this study, both specimens from patients with and without a clinical history of cerebrovascular disease were selected, to enable comparison of vessel wall thickness in both populations. All specimens were stored in buffered formalin (4%). Institutional review board approval was obtained for this retrospective study. The material was handled in a coded manner that met the criteria of the Code of conduct used in the Netherlands for responsible use of human tissue in medical research (www.federa.org/codes-conduct).

Specimen preparation

Before scanning, all specimens were cleaned from clotted blood products and embedded in a petri dish containing 2% agarose solution, as previously described.[12] , To enable spatial correlation between MR images and histological slides for validation of MRI measurements, fiducials (cactus spines) were placed in the agarose gel at 15 locations adjacent to an arterial segment. The locations were chosen to sample all major arterial segments of the CoW including their branches (**Figure 1A**).[11]

MR imaging

Imaging was performed at room temperature on a 7T whole body system (Philips Healthcare, Best, the Netherlands), with a custom-made high-density receive coil (16 channels per 70 cm^2; MR Coils BV, Zaltbommel, the Netherlands)[13], and a volume transmit/receive coil for transmission (Nova Medical, Wilmington, MA, USA). The embedded specimens used for validation were imaged individually; the petri dish containing the specimen was placed in the middle of the transmit/receive coil on top of the high-

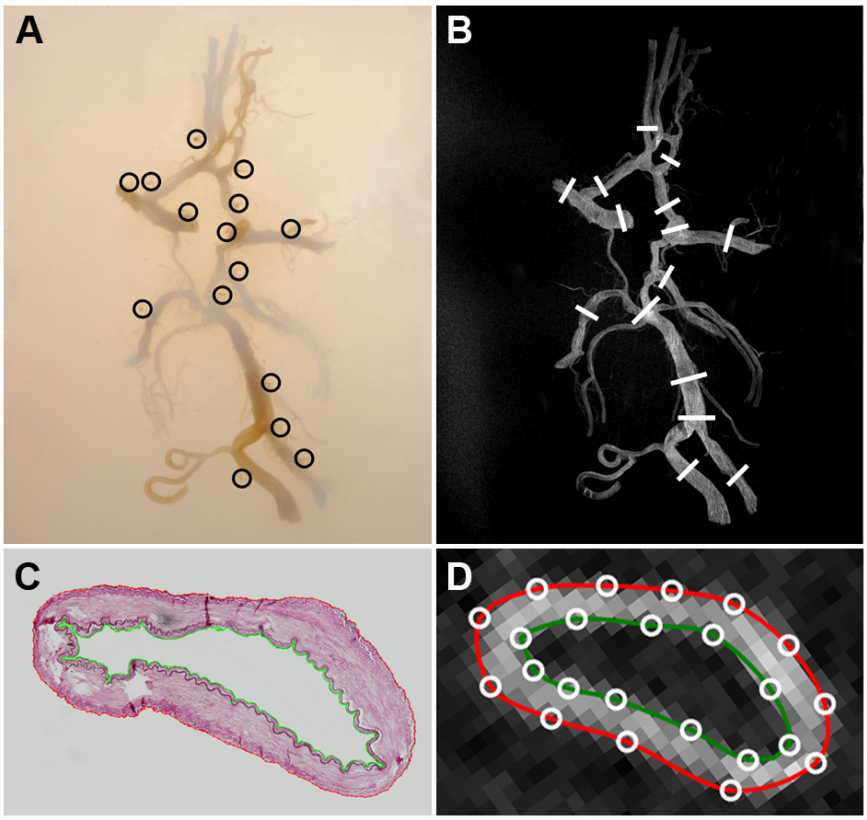

Figure 1 | (**A**) Photograph and (**B**) T_1-weighted image (MIP, thickness 20 mm) of an embedded CoW specimen used for validation of the vessel wall thickness measurements. The black circles in (**A**) indicate fiducials (cactus spines) placed for spatial correlation at 15 locations along the major arterial segments of the CoW. The white markings in (**B**) show the locations used for histological sampling and making the MPRs of the MR images. (**C**) Histological section of a sample from the CoW specimen (right vertebral artery) with the corresponding T_1-weighted image (**D**), showing the manually drawn vessel wall boundaries of the outer wall (red) and lumen (green) from which the vessel wall thickness parameters were calculated.

density receive coil. The other specimens (without histopathological validation) were imaged two at a time, with two high-density receive coils placed above and below the two petri dishes containing the specimens.

Protocol

All specimens were scanned with an ultrahigh resolution T_1-weighted sequence. In a previous *ex vivo* study at 7T[11], T_1-weighted imaging was

shown to have the most promising image contrast for visualizing the intracranial arterial vessel wall. The specimens used for validation were scanned with the following scan parameters: FOV 150x150x20 mm^3, acquired resolution 0.13x0.13x0.13 mm^3, TR/TE 16/4.3 ms, flip angle 44 degrees, bandwidth 165 Hz/pixel, 1154 ky-lines per shot, acquisition time approximately 1h35min per specimen.[11] For the other specimens a sequence with an even higher spatial resolution was used[12], optimized for the vessel wall T_1 relaxation times found previously at 7T[11]: FOV 95x130x35 mm^3, acquired resolution 0.11x0.11x0.11 mm^3, TR/TE 55/6.1 ms, flip angle 28 degrees, bandwidth 184 Hz/pixel, 1182 ky-lines per shot, acquisition time approximately 5h46min for two specimens. To mitigate potential artefacts caused by scanner frequency drift, the scanner resonance frequency was measured and adjusted between each shot during scanning. The isotropic resolution of the acquired MR images allowed for reconstructions along arbitrary planes.

Validation of MRI measurements with histology

After scanning, samples were taken from the 15 marked locations of each CoW specimen that was used for validation. Each sample was marked with ink for spatial orientation after histological processing. Histological processing was performed using an in-house developed protocol, as previously described.[12] From the MR images MPRs were made (interslice distance: 0.5 mm) perpendicular to the centerline of the artery (drawn manually) at the fiducial locations, using dedicated vascular analysis software (Cardiovascular Angiographic Analysis System (CAAS) MRA; Pie Medical Imaging, Maastricht, the Netherlands). Next, the MR and histological images were matched manually by one rater (A.H.) using the ink markings in the histological sections, the locations marked with the fiducials in the MR images, and the gross morphological features. Samples were excluded from validation when no match was found, when air bubbles were present in the MR images, or when the histological section was too fragmented.

After matching the histological sections with the corresponding MR images, vessel wall boundaries (outer wall and lumen contours) were drawn in the histological sections by one rater (A.H.) blinded to the MRI

data, and vice versa (**Figure 1**). Total vessel and lumen area derived from the drawn vessel wall contours were used for comparison of MRI measurements with histology.

Vessel wall thickness analysis

For the histological sections, vessel wall boundaries were drawn manually using MeVisLab (version 2.7; MeVis Medical Solutions, Bremen, Germany; **Figure 1C**). For the MRI slices, vessel wall boundaries were drawn on the reconstructed images using the software program CAAS MRA, with dedicated add-on software MRTool (**Figure 1D**). Based on the manually traced vessel boundary contours, vessel wall parameters were calculated by the software programs for each analyzed slice (for MRI and histology separately). These parameters included: lumen area (LA), total vessel area (TVA), wall area (WA; TVA-LA), wall thickness (mean, minimum, and maximum), and normalized wall index (WA/TVA). The mean vessel wall thickness was calculated based on the vessel areas[14]. In this method mean vessel wall thickness for each slice is calculated as the difference in the radii of the total vessel and lumen area (**Supplemental Figure I**). Minimum and maximum wall thickness were calculated as the minimal and maximal distance measured between outer wall and luminal boundary. Distance between outer wall and luminal boundary were automatically determined at multiple locations (≥100) by the used software programs.

Interrater reliability and agreement of the calculated vessel wall parameters were assessed using vessel wall boundaries drawn by a second rater (A.K.) in a subset of the histological sections and their matching MRI slices.

MRI measurements of arterial segments

Vessel wall thickness measurements were performed over the entire length of the major arterial segments of the CoW, using the CAAS MRA software, blinded to the clinical history of the patients. First, MPRs were made perpendicular to the centerline of each arterial segment (interslice distance: 1.0 mm). Next, vessel wall boundaries (outer wall and lumen) were drawn in each reconstructed slice by one rater (A.H.). Based on the drawn vessel wall boundaries, vessel wall thickness parameters were calculated (**Figure 2**). All segments were analyzed from proximal to distal,

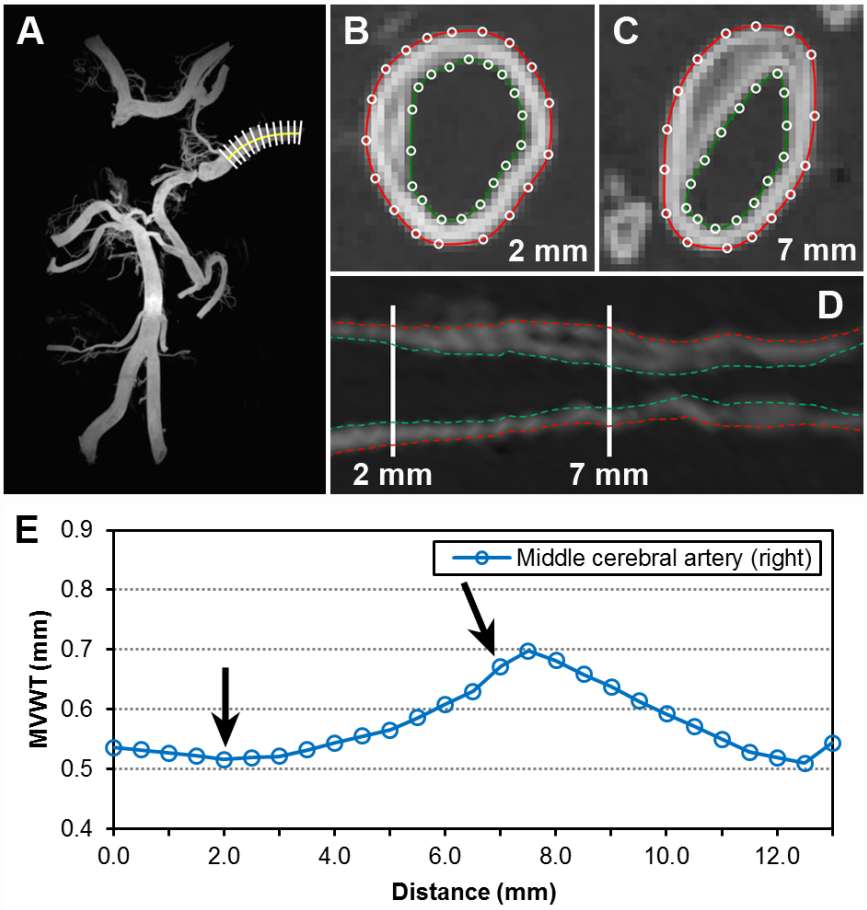

Figure 2 | (**A**) T_1-weighted image (MIP, thickness 14 mm) of an embedded CoW specimen used for the MRI-based vessel wall thickness assessment over the entire length of different vessel segments. The white markings demonstrate the MPRs that were made perpendicular to the centerline (yellow line) for the right middle cerebral artery. (**B, C**) Examples of MPR images at 2 mm (**B**) and 7 mm (**C**) showing the vessel wall boundaries delineated for the outer wall (red) and lumen (green). Based on the drawn vessel wall boundaries in each reconstructed slice, vessel wall thickness parameters were calculated for the entire arterial segment (**D, E**).

and over a fixed length for all specimens (longest length possible to still include the majority of subjects). The analyzed vessel segments included: anterior cerebral artery (A1 segment, length: 10 mm; A2 segment, length: 5 mm), intracranial internal carotid artery (C7 segment, length: 4 mm), middle cerebral artery (M1 segment, length: 7 mm), basilar artery (proximal part, length: 9 mm; distal part, length: 9 mm), posterior cerebral artery (P1 and P2 segments, length: 8 mm), and vertebral artery (length: 12 mm). Slices containing side branches originating from the artery of interest (possibly resulting in overestimation of thickness measurements) or slices where the vessel wall contours were not well visible (e.g. due to air present in the arterial lumen or collapsed vessel) were excluded from thickness calculations. Linear interpolation of calculated vessel wall thickness parameters was performed for the vessel walls located in between the reconstructed slices, as well as for the excluded slices.

Statistical analysis

MRI measurements of vessel wall parameters were compared with the histological measurements by linear regression analysis. Interrater reliability and agreement of the derived vessel wall parameters were evaluated using the intraclass correlation coefficient and Bland-Altman analysis. Mean and standard deviation values for the vessel wall parameters were calculated for each slice of the included segments (with fixed length) over all specimens (grouped for asymptomatic and symptomatic patients). The Mann-Whitney U test was conducted to compare segment averages of the vessel wall thickness parameters between asymptomatic and symptomatic patients. A p-value of <0.05 was considered statistically significant.

Results

Specimens

Fifteen CoW specimens were included in this study. Five specimens were used for validation with histology (3 male; mean age 66.2 years; range 42-92 years). The other 10 specimens were used for vessel wall thickness measurements over entire arterial segments using MRI only: n=5 specimens from symptomatic patients with a history of TIA

or ischemic stroke (2 males; mean age 77.4 years; range 75-80 years), and n=5 specimens from asymptomatic patients without a history of cerebrovascular or ischemic heart disease (2 males; mean age 74.4 years; range 66-84 years).

Validation of MRI measurements with histology

In total 70 samples were obtained from the different arterial segments of the five CoW specimens used for validation (n=5 arterial segments were absent). Of these samples, 25 were excluded due to lack of match between the MR image and histological section (n=8), fragmentation of the histological section (n=16), or the presence of air on MRI (n=1), leaving 45 samples for validation analysis.

Scatterplots and Bland-Altman plots of lumen and total vessel area measurements on the histological sections and corresponding MR images are shown in **Figure 3**. The total vessel and lumen areas measured on

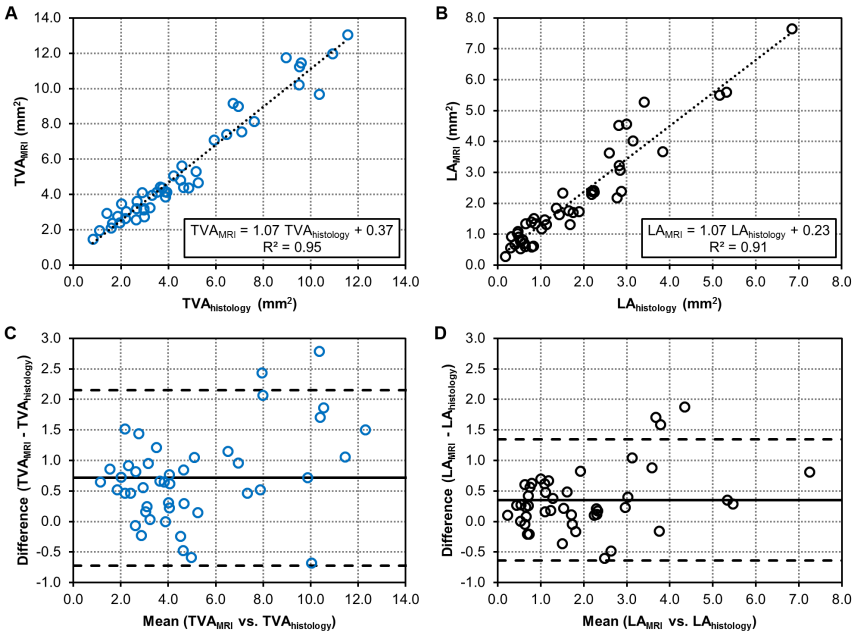

Figure 3 | Scatterplots (**A, B**) and Bland-Altman plots (**C, D**) of the lumen (LA) and total vessel area (TVA) measured on the histological sections and the corresponding MR images, derived from the drawn vessel wall contours for the outer wall (**A, C**) and lumen (**B, D**).

MRI both had a high goodness-of-fit with histology, (R^2=0.95 and R^2=0.91, respectively), with a root-mean-square-error of 1.02 mm^2 and 0.62 mm^2, respectively. Furthermore, Bland-Altman plots (**Figure 3C, D**) showed a positive bias for MRI measurement relative to histology measurement for both total vessel and lumen area (0.71 mm^2 and 0.35 mm^2, respectively).

Interrater reliability of parameters derived from the delineated vessel wall boundaries in a subset of 10 samples (22%) was excellent for both MRI and histology; all intraclass correlation coefficients were above 0.85 (**Table 1**).

Table 1 | Interrater reliability and agreement of the derived vessel wall parameters.

	ICC[a] (95% CI)	mean difference (95% LoA)
Histology		
Total vessel area (mm^2)	1.000 (1.000 − 1.000)	0.02 (-0.01 − 0.06)
Lumen area (mm^2)	1.000 (0.999 − 1.000)	0.01 (-0.09 − 0.11)
Wall area (mm^2)	1.000 (0.999 − 1.000)	0.06 (-0.06 − 0.17)
Vessel wall thickness (mm)		
mean	0.999 (0.996 − 1.000)	0.01 (-0.01 − 0.04)
minimum	0.996 (0.984 − 0.999)	0.01 (-0.01 − 0.03)
maximum	0.996 (0.982 − 0.999)	0.06 (-0.06 − 0.18)
Normalized wall index	1.000 (0.999 − 1.000)	0.01 (-0.01 − 0.02)
MRI		
Total vessel area (mm^2)	0.993 (0.861 − 0.999)	-0.46 (-1.17 − 0.24)
Lumen area (mm^2)	0.999 (0.992 − 1.000)	-0.10 (-0.32 − 0.12)
Wall area (mm^2)	0.985 (0.814 − 0.997)	-0.36 (-1.01 − 0.29)
Vessel wall thickness (mm)		
mean	0.989 (0.929 − 0.998)	-0.03 (-0.11 − 0.04)
minimum	0.849 (0.434 − 0.962)	-0.02 (-0.09 − 0.06)
maximum	0.992 (0.970 − 0.998)	-0.04 (-0.20 − 0.13)
Normalized wall index	0.995 (0.964 − 0.999)	-0.02 (-0.05 − 0.02)

[a]Two-way mixed model with absolute agreement.
CI: confidence interval; ICC: intraclass correlation coefficient; LoA: limits of agreement

MRI measurements of arterial segments

In the ten specimens selected for MRI-based vessel wall thickness assessment, 123 segments were present (n=7 segments were absent; n=4 asymptomatic, n=3 symptomatic). Of these 123 segments, 21

Table 2 | MRI measurements of vessel wall thickness parameters for different arterial segments of the

	Lumen area (mm²)			Total vessel area (mm²)			Wall area (mm²)		
	asymp.	symp.	*p*	asymp.	symp.	p	asymp.	symp.	*p*
ACA									
A1	1.03 (0.39)	0.57 (0.44)	**0.0496***	3.18 (0.89)	2.52 (0.95)	0.388	2.16 (0.57)	1.95 (0.54)	0.689
A2	0.79 (0.29)	0.72 (0.51)	0.068	2.93 (0.70)	2.96 (1.00)	1.000	2.14 (0.51)	2.25 (0.60)	0.573
ICA	3.77 (1.41)	3.12 (2.17)	0.535	8.94 (1.66)	8.86 (3.79)	0.456	5.18 (0.96)	5.73 (1.79)	0.710
MCA	2.24 (0.91)	1.47 (0.96)	0.074	5.90 (1.40)	5.30 (1.79)	0.423	3.66 (0.79)	3.83 (0.98)	0.743
PCA	1.23 (0.52)	0.95 (0.39)	0.282	3.82 (1.14)	3.61 (0.97)	0.852	2.59 (0.73)	2.66 (0.67)	0.573
BA									
proximal	2.73 (1.00)	1.86 (0.76)	0.393	6.71 (1.52)	6.91 (1.10)	1.000	3.98 (0.98)	5.05 (1.00)	0.393
distal	1.93 (0.70)	1.95 (1.27)	0.556	4.79 (1.30)	6.11 (2.24)	0.413	2.86 (0.77)	4.15 (1.13)	0.111
VA	1.43 (0.67)	1.64 (1.16)	1.000	4.20 (1.48)	5.21 (2.15)	0.397	2.77 (1.04)	3.58 (1.11)	0.189

Values are given as mean (standard deviation). For each vessel segment the measurements were averaged over the fixed length, and left and right were taken together (if applicable).
[a]Group differences between asymptomatic and symptomatic patients were tested with Mann-Whitney U test; **bold*** indicates $p<0.05$ (two-tailed).

were excluded for different reasons: the segment was too short (n=10; 5 asymptomatic, 5 symptomatic), the segment was hypoplastic (n=5; 3 asymptomatic, 2 symptomatic), the vessel had collapsed (n=4; 1 aymptomatic, 3 symptomatic), or the presence of air in the lumen (n=2; 2 symptomatic). This resulted in a total of 102 vessel segments that were included for analysis (52 asymptomatic; 50 symptomatic).

Segment averages of thickness measurements for the asymptomatic and symptomatic patients are presented in **Table 2**. Comparing the segment averages between the symptomatic and asymptomatic groups, a significant difference ($p<0.05$; **Table 2**) was found for the mean vessel wall thickness of the A1 segment, middle cerebral artery, distal basilar artery, and the vertebral artery.

CoW from asymptomatic and symptomatic patients.[a]

Vessel wall thickness (mm)											
Mean			Minimum			Maximum			Normalized wall index		
asymp.	symp.	*p*	asymp.	symp.	*p*	asymp.	symp.	*p*	asymp.	symp.	*p*
0.44 (0.06)	0.48 (0.04)	**0.036***	0.30 (0.03)	0.33 (0.04)	0.145	0.49 (0.09)	0.55 (0.08)	**0.0496***	0.68 (0.06)	0.80 (0.08)	**0.003***
0.46 (0.07)	0.50 (0.08)	0.203	0.30 (0.05)	0.34 (0.05)	0.195	0.49 (0.09)	0.58 (0.14)	0.068	0.73 (0.06)	0.77 (0.08)	0.068
0.61 (0.13)	0.71 (0.09)	0.097	0.39 (0.08)	0.46 (0.09)	0.259	0.77 (0.18)	0.94 (0.20)	0.128	0.59 (0.11)	0.69 (0.11)	0.097
0.54 (0.10)	0.64 (0.09)	**0.027***	0.34 (0.05)	0.37 (0.08)	0.423	0.73 (0.23)	0.84 (0.18)	0.236	0.63 (0.10)	0.75 (0.11)	**0.036***
0.48 (0.07)	0.52 (0.07)	0.345	0.31 (0.05)	0.36 (0.07)	0.103	0.61 (0.13)	0.61 (0.11)	0.950	0.69 (0.08)	0.74 (0.06)	0.228
0.54 (0.13)	0.73 (0.15)	0.143	0.34 (0.03)	0.44 (0.15)	0.250	0.58 (0.14)	0.96 (0.23)	0.071	0.60 (0.09)	0.73 (0.09)	0.143
0.45 (0.08)	0.62 (0.10)	**0.032***	0.31 (0.04)	0.40 (0.09)	0.190	0.50 (0.11)	0.75 (0.20)	0.063	0.60 (0.07)	0.70 (0.10)	0.190
0.48 (0.13)	0.58 (0.08)	**0.040***	0.31 (0.06)	0.39 (0.05)	**0.004***	0.51 (0.16)	0.66 (0.15)	**0.021***	0.66 (0.08)	0.72 (0.10)	0.189

ACA: anterior cerebral artery; BA: basilar artery; ICA: internal carotid artery; MCA: middle cerebral artery; PCA: posterior cerebral artery; VA: vertebral artery

Thickness measurements over the entire length of each analyzed vessel segment are shown in **Figure 4** (mean wall thickness) and **Figure 5** (minimum and maximum wall thickness). Although there was quite some variation between individual patients (both asymptomatic and symptomatic) for each segment (**Supplemental Figure II**), on average the vessel wall was thicker for the symptomatic patients compared to the asymptomatic patients for all analyzed segments (**Figure 4**). Overall, a bigger difference was observed for the maximum wall thickness between the symptomatic and asymptomatic groups compared with the minimum wall thickness (**Figure 5**).

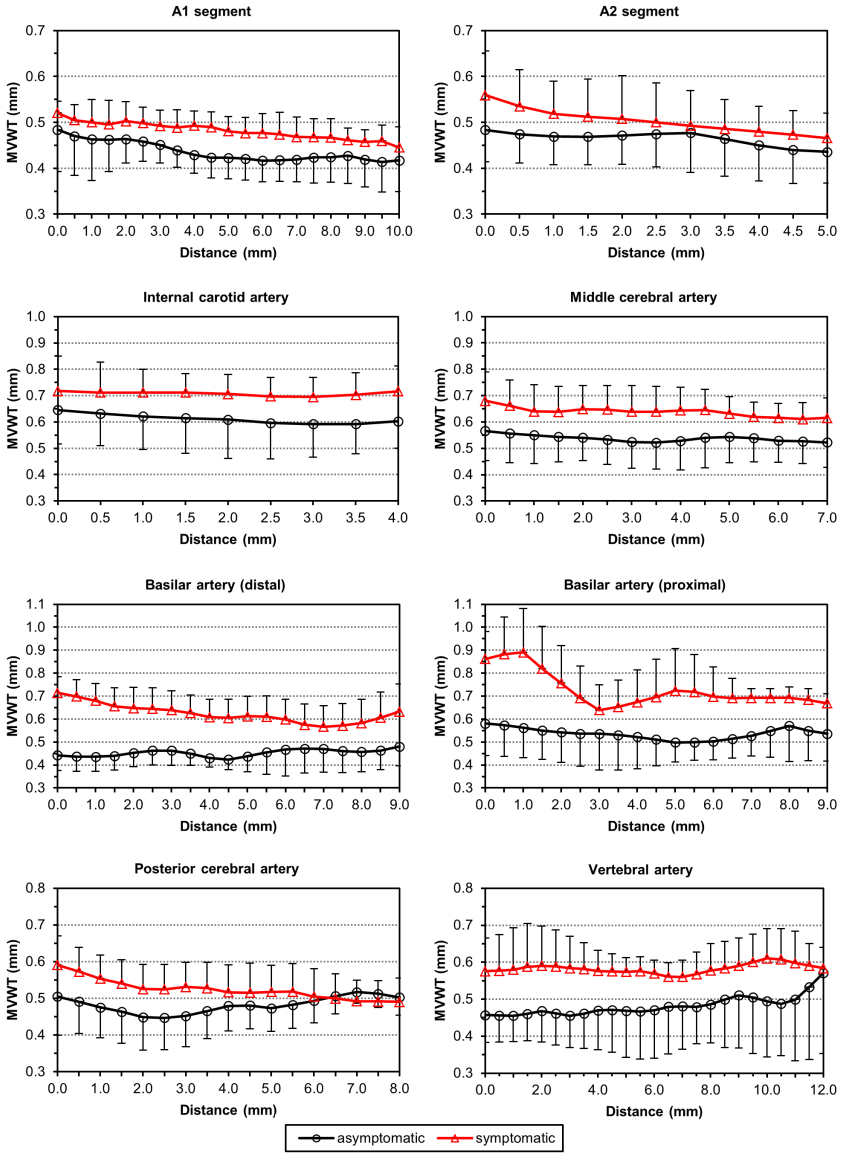

Figure 4 | Mean vessel wall thickness (MVWT) MRI measurements over the fixed length of each analyzed vessel segment. For set locations along the length of the arterial segments (sample distance: 0.5 mm) mean and standard deviation were calculated for the symptomatic (red) and asymptomatic (black) specimens separately. One-sided error bars are shown for clarity. The distance represents the locations along the arterial segments from proximal to distal.

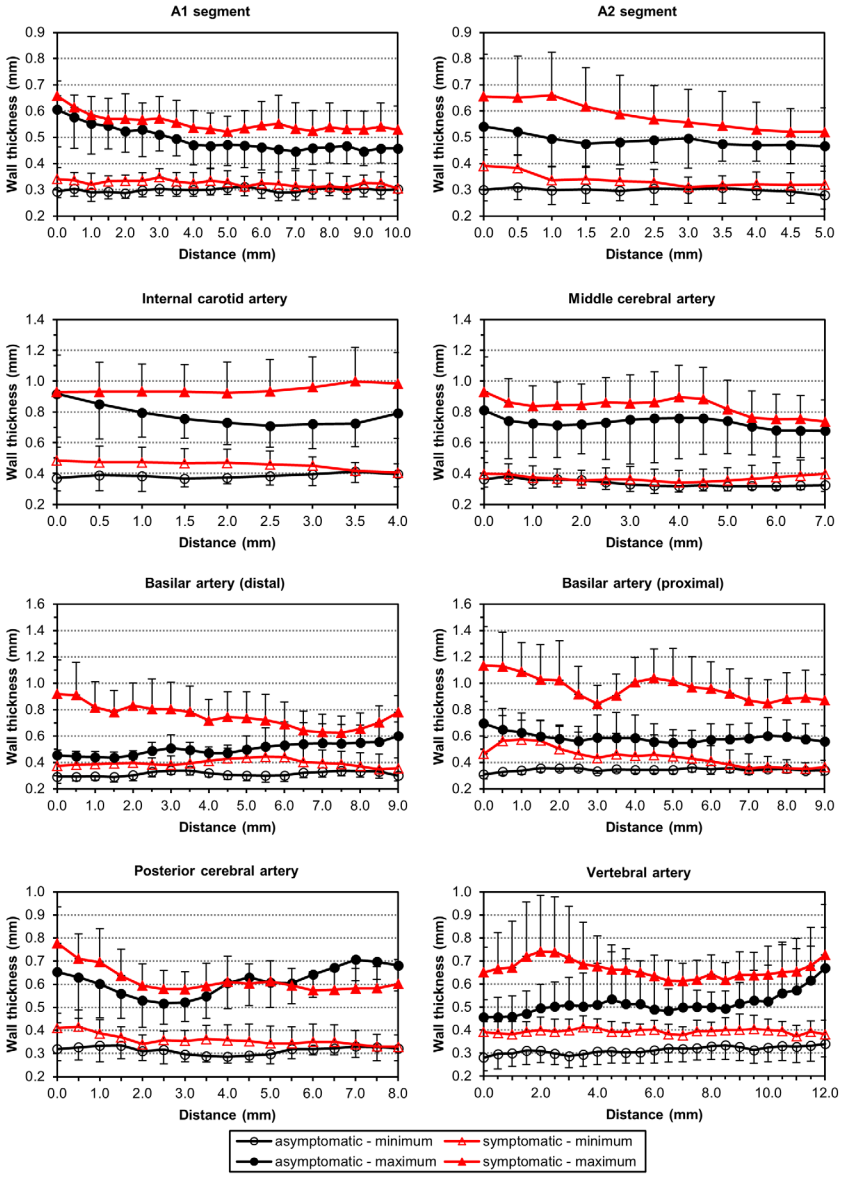

Figure 5 | Minimum and maximum vessel wall thickness MRI measurements over the fixed length of each analyzed vessel segment. Mean and standard deviation were calculated for the symptomatic (red) and asymptomatic (black) specimens separately conform Figure 4. One-sided error bars are shown for clarity. The distance represents the locations along the arterial segments from proximal to distal.

Discussion

The current study focused on vessel wall thickness measurements of the major intracranial arteries, measured using 7T MRI in both asymptomatic and symptomatic patients. The main results show that ultrahigh-resolution MRI at 7T enables accurate measurement of vessel wall thickness in *ex vivo* CoW specimens with excellent agreement with histology. Vessel wall thickness measurements over entire segments showed considerable variation both within and between arterial segments of patients. Symptomatic patients generally had thicker walls than asymptomatic patients.

The number of studies performing vessel wall thickness measurements of the intracranial arteries *in vivo* is still limited. Thus far, studies have mainly focused on performing thickness measurements in patients at the location of a stenosis in a specific arterial segment, like the middle cerebral artery[15-17] or basilar artery[18,19], or at standard locations representing common sites for intracranial atherosclerosis in healthy controls and patients[20]. Difficulties encountered during *in vivo* measurements were delineation of the outer wall at the interface between vessel wall and brain parenchyma, although this improved in patients with more CSF surrounding the arteries due to age-related brain atrophy[16]. Also, the choice of a good reference site was often stated to be difficult.[16,18] Recently, a large multicenter study by Qiao *et al*.[21] included *in vivo* quantitative measurements of several intracranial vessel segments. Measurements were performed over a longer distance for each analyzed vessel segment, instead of only focusing on a specific location (i.e. stenosis). Their measured mean vessel wall thickness ranged from 0.95 (basilar artery; average white participants) to 1.05 mm (anterior cerebral artery; average white participants). In the current study this ranged from 0.46 (anterior cerebral artery (A1 segment); average total study population) to 0.66 mm (internal carotid artery; average total study population) when taking into account vessel segments that were included in both studies.

One of the major drawbacks of *ex vivo* studies is the effect of tissue storage. Formalin used for tissue fixation causes some tissue shrinkage, which ranges from 8-20%.[22,23] This shrinkage partially covers the observed

significant difference in mean vessel wall thickness between *in vivo*[21] and the *ex vivo* measurements reported here, where the mean vessel wall thickness is ~50% smaller *ex vivo* than *in vivo*. Another important factor possibly explaining the difference between *ex vivo* and *in vivo* studies, such as that by Qiao *et al*.[21], is the spatial resolution that was used for acquisition of the vessel wall images. The reported *in vivo* acquired spatial resolution was 0.5x0.5x0.5 mm^3. To perform accurate thickness measurements, at least two full voxels without partial volume effects should represent the vessel wall (Nyquist-Shannon sampling theorem).[24,25] Taking into account the diagonal of voxels, this results in a minimum thickness of (sqrt(3) * .5 * 2 =) 1.7 mm to ensure reliable results regardless of the orientation of the vessel with respect to the voxels. Assuming the wall is parallel to one of the voxel faces, the minimum reliable thickness is still 1.0 mm. In the study by Qiao *et al*., the mean vessel wall thickness for all analyzed segments varies closely around this minimum thickness of 2 voxels (0.93-1.09 mm), while in the current post-mortem study thickness was measured with a much higher spatial resolution (0.11x0.11x0.11 mm^3) resulting in lower values with much more variation between the different vessel segments (0.44-0.73 mm). Therefore, with the currently available imaging techniques, *ex vivo* MRI with ultrahigh spatial resolution seems to be the most accurate method for now to investigate the small thickness variations that are present in the intracranial arteries. Also, *ex vivo* MRI with ultrahigh spatial resolution can be used as a complementary method to histological assessment, allowing for more viable assessment of entire arterial segments to examine total vessel wall thickening / lesion burden.[26]

Although there was considerable variation between individual patients, on average the vessel wall showed more thickening for the symptomatic group compared with the asymptomatic group for all analyzed segments. Thus far, asymptomatic and symptomatic patients have only been compared *in vivo* at the location of an MCA stenosis.[15,19] A previous autopsy study showed intracranial atherosclerosis was more frequently present in (fatal) stroke patients than in their control group (without stroke).[27], which might be an explanation for the increased wall thickness in our symptomatic group. Other vascular territories have already been studied more extensively. For instance, increased vessel wall (intima-media)

thickness in the carotid artery[28] and aorta[29] was found to be associated with future cardiovascular events. Studies in a healthy general population or without clinical cardiovascular disease showed wall thickness increases with age and varies with sex and race.[7,30] Finally, the prevalence of intracranial atherosclerosis varies depending on race-ethnicity, sex and age.[31,32] In the current study, the number of included patients was not large enough to stratify between these different characteristics to identify the driving factor of the difference in wall thickness observed between the two groups. A future study in a larger patient population with different risk factors and cerebrovascular disease burden would be an interesting next step towards a better understanding of the causes of increased vessel wall thickness of the intracranial arteries.

Several limitations exist in this study. First, image analysis was performed manually. Especially delineation of the lumen and outer wall contours over entire segments was very labor- and time intensive. Development of a tool that is capable of performing vessel wall delineation automatically, as is available for the carotid arteries and descending aorta[33], would be a prerequisite when expanding to larger patient groups. Second, the fixed length that was used for each included arterial segment in this study was determined by the excision lengths performed by the pathologist during brain autopsy. To include more data over longer distances in future studies, the variation in excision lengths between specimens should be reduced. Lastly, scan sequences with different spatial resolutions were used for the validation with histology (0.13x0.13x0.13 mm^3) and the MRI measurements of arterial segments (0.11x0.11x0.11 mm^3). Increasing spatial resolution has been shown to improve reproducibility of wall dimension measurements.[34] MRI measurements on images with the lower spatial resolution already showed excellent agreement with histology, as well as excellent interrater agreement. Therefore, using MR images with even higher spatial resolution will only improve these results.

In conclusion, ultrahigh-resolution MRI enables accurate measurement of vessel wall thickness in *ex vivo* CoW specimens, showing thickness variations over entire segments. The major arteries of the CoW showed thickness variation both within and between arterial segments of patients, as well as between asymptomatic and symptomatic patients. Considering

the relatively small thickness variations that are present, the currently used *in vivo* intracranial vessel wall MRI sequences require a higher spatial resolution for accurate measurement of vessel wall thickness in patients and to detect changes over time.

Acknowledgements

The authors would like to acknowledge Jean-Paul Aben and Chris Bouwman from Pie Medical Imaging, the Netherlands, for providing the additional MRTool software specifically designed for this study.

References

1. Dieleman N, van der Kolk AG, Zwanenburg JJ, et al: Imaging intracranial vessel wall pathology with magnetic resonance imaging: current prospects and future directions. Circulation 130:192-201, 2014.
2. Bodle JD, Feldmann E, Swartz RH, et al: High-resolution magnetic resonance imaging: an emerging tool for evaluating intracranial arterial disease. Stroke 44:287-292, 2013.
3. Resch JA, Okabe N, Loewenson RB, et al: Pattern of vessel involvement in cerebral atherosclerosis. A comparative study between a Japanese and Minnesota population. J Atheroscler Res 9:239-250, 1969.
4. Baker AB, Iannone A: Cerebrovascular disease. I. The large arteries of the circle of Willis. Neurology 9:321-332, 1959.
5. Denswil NP, van der Wal AC, Ritz K, et al: Atherosclerosis in the circle of Willis: Spatial differences in composition and in distribution of plaques. Atherosclerosis 251:78-84, 2016.
6. Lorenz MW, Markus HS, Bots ML, et al: Prediction of clinical cardiovascular events with carotid intima-media thickness: a systematic review and meta-analysis. Circulation 115:459-467, 2007.
7. Mensel B, Quadrat A, Schneider T, et al: MRI-based determination of reference values of thoracic aortic wall thickness in a general population. Eur Radiol 24:2038-2044, 2014.
8. Naqvi TZ, Lee MS: Carotid intima-media thickness and plaque in cardiovascular risk assessment. JACC Cardiovasc Imaging 7:1025-1038, 2014.
9. Macedo R, Chen S, Lai S, et al: MRI detects increased coronary wall thickness in asymptomatic individuals: the multi-ethnic study of atherosclerosis (MESA). J Magn Reson Imaging 28:1108-1115, 2008.
10. Ryoo S, Cha J, Kim SJ, et al: High-resolution magnetic resonance wall imaging findings of Moyamoya disease. Stroke 45:2457-2460, 2014.
11. Harteveld AA, Denswil NP, Siero JC, et al: Quantitative Intracranial Atherosclerotic Plaque Characterization at 7T MRI: An Ex Vivo Study with Histologic Validation. AJNR Am J Neuroradiol 37:802-810, 2016.
12. van der Kolk AG, Zwanenburg JJ, Denswil NP, et al: Imaging the intracranial atherosclerotic vessel wall using 7T MRI: initial comparison with histopathology. AJNR Am J Neuroradiol 36:694-701, 2015.

13. Petridou N, Italiaander M, van de Bank BL, et al: Pushing the limits of high-resolution functional MRI using a simple high-density multi-element coil design. NMR Biomed 26:65-73, 2013.
14. Rosero EB, Peshock RM, Khera A, et al: Agreement between methods of measurement of mean aortic wall thickness by MRI. J Magn Reson Imaging 29:576-582, 2009.
15. Xu WH, Li ML, Gao S, et al: In vivo high-resolution MR imaging of symptomatic and asymptomatic middle cerebral artery atherosclerotic stenosis. Atherosclerosis 212:507-511, 2010.
16. Zhu XJ, Du B, Lou X, et al: Morphologic characteristics of atherosclerotic middle cerebral arteries on 3T high-resolution MRI. AJNR Am J Neuroradiol 34:1717-1722, 2013.
17. Ryu CW, Jahng GH, Kim EJ, et al: High resolution wall and lumen MRI of the middle cerebral arteries at 3 tesla. Cerebrovasc Dis 27:433-442, 2009.
18. Ma N, Jiang WJ, Lou X, et al: Arterial remodeling of advanced basilar atherosclerosis: a 3-tesla MRI study. Neurology 75:253-258, 2010.
19. Huang B, Yang WQ, Liu XT, et al: Basilar artery atherosclerotic plaques distribution in symptomatic patients: a 3.0T high-resolution MRI study. Eur J Radiol 82:e199-203, 2013.
20. Qiao Y, Steinman DA, Qin Q, et al: Intracranial arterial wall imaging using three-dimensional high isotropic resolution black blood MRI at 3.0 Tesla. J Magn Reson Imaging 34:22-30, 2011.
21. Qiao Y, Guallar E, Suri FK, et al: MR Imaging Measures of Intracranial Atherosclerosis in a Population-based Study. Radiology 280:860-868, 2016.
22. Tran T, Sundaram CP, Bahler CD, et al: Correcting the Shrinkage Effects of Formalin Fixation and Tissue Processing for Renal Tumors: toward Standardization of Pathological Reporting of Tumor Size. J Cancer 6:759-766, 2015.
23. Dobrin PB: Effect of histologic preparation on the cross-sectional area of arterial rings. J Surg Res 61:413-415, 1996.
24. Kleinloog R, Korkmaz E, Zwanenburg JJ, et al: Visualization of the aneurysm wall: a 7.0-tesla magnetic resonance imaging study. Neurosurgery 75:614-622; discussion 622, 2014.
25. Bouvy WH, Biessels GJ, Kuijf HJ, et al: Visualization of perivascular spaces and perforating arteries with 7 T magnetic resonance imaging. Invest Radiol 49:307-313, 2014.
26. Westover MB, Bianchi MT, Yang C, et al: Estimating cerebral microinfarct burden from autopsy samples. Neurology 80:1365-1369, 2013.

27. Mazighi M, Labreuche J, Gongora-Rivera F, et al: Autopsy prevalence of intracranial atherosclerosis in patients with fatal stroke. Stroke 39:1142-1147, 2008.
28. van den Oord SC, Sijbrands EJ, ten Kate GL, et al: Carotid intima-media thickness for cardiovascular risk assessment: systematic review and meta-analysis. Atherosclerosis 228:1-11, 2013.
29. Maroules CD, Rosero E, Ayers C, et al: Abdominal aortic atherosclerosis at MR imaging is associated with cardiovascular events: the Dallas heart study. Radiology 269:84-91, 2013.
30. Li AE, Kamel I, Rando F, et al: Using MRI to assess aortic wall thickness in the multiethnic study of atherosclerosis: distribution by race, sex, and age. AJR Am J Roentgenol 182:593-597, 2004.
31. Caplan LR, Gorelick PB, Hier DB: Race, sex and occlusive cerebrovascular disease: a review. Stroke 17:648-655, 1986.
32. Ritz K, Denswil NP, Stam OC, et al: Cause and mechanisms of intracranial atherosclerosis. Circulation 130:1407-1414, 2014.
33. Gao S, van 't Klooster R, Brandts A, et al: Quantification of common carotid artery and descending aorta vessel wall thickness from MR vessel wall imaging using a fully automated processing pipeline. J Magn Reson Imaging, 2016.
34. van Wijk DF, Strang AC, Duivenvoorden R, et al: Increasing spatial resolution of 3T MRI scanning improves reproducibility of carotid arterial wall dimension measurements. MAGMA 27:219-226, 2014.

Supplemental Material

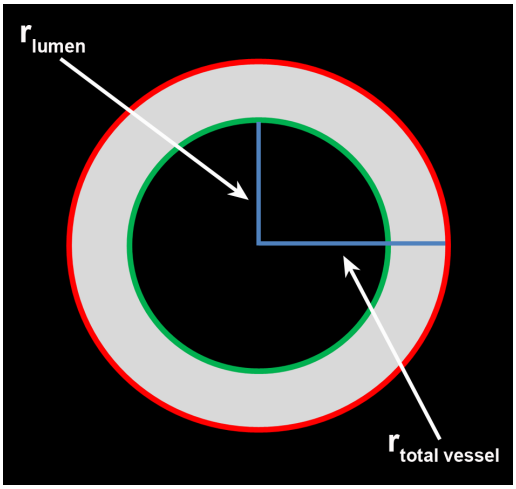

Supplemental Figure 1 | Schematic clarification of the method used for calculation of mean vessel wall thickness based on the vessel areas (Rosero *et al*. JMRI 2009). The mean vessel wall thickness is calculated by taking the difference between the radius of a circle with area equal to that enclosed by the outer wall boundary ($r_{total\ vessel}$) and the radius of a circle with area equal to that enclosed by the luminal boundary (r_{lumen}). Outer wall and luminal boundary are indicated by the red and green line, respectively.

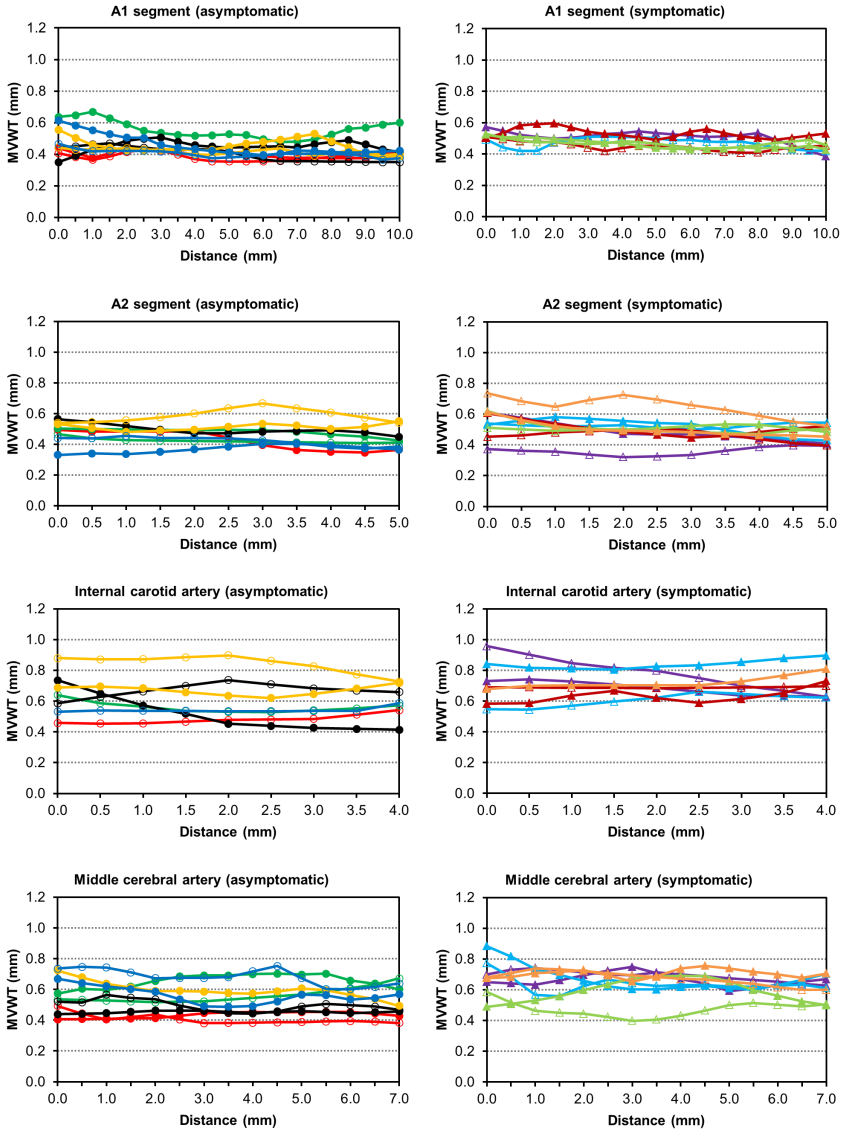

Supplemental Figure II | Mean vessel wall thickness (MVWT) MRI measurements over the fixed length of each analyzed vessel segment from the asymptomatic (graphs on the left) and symptomatic (graphs on the right) patients. For the basilar artery, the entire segment is shown. Each line color represents a different CoW specimen, where the markers indicate whether the vessel segment is located on the right (not filled) or left (filled). The distance represents the locations along the arterial segments from proximal to distal.

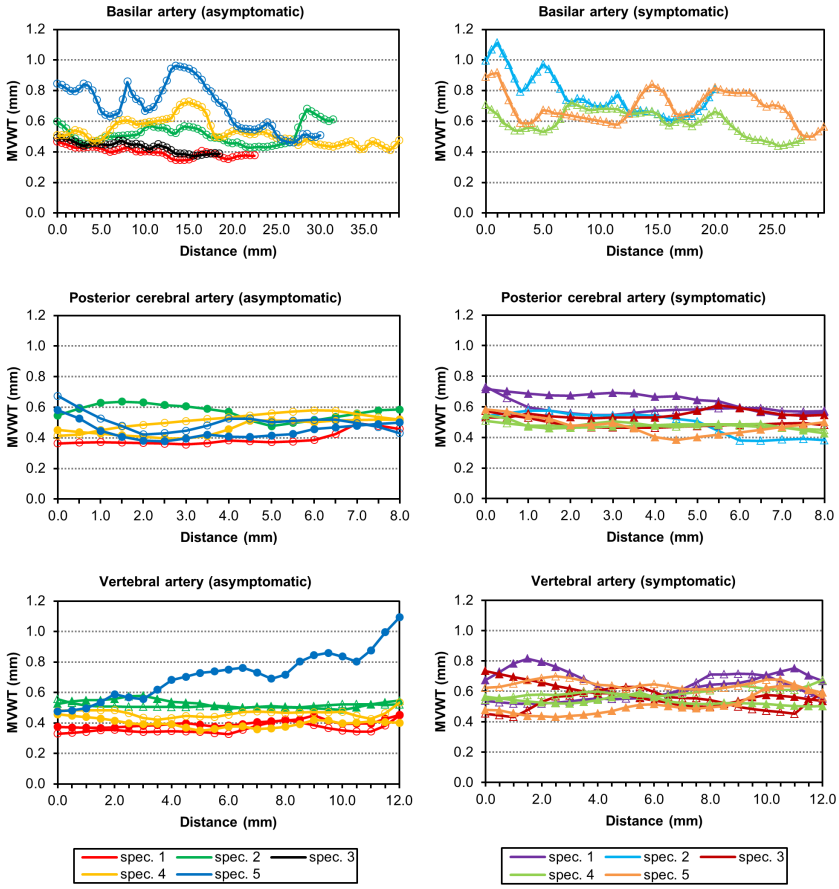

Supplemental Figure II | Continued.

Chapter 8

Summary & general discussion

Ultrahigh field MRI in cerebrovascular diseases

In the past decennia the field of MRI has expanded tremendously, resulting in many clinical applications and specialized research areas.[1] The introduction of higher field strengths (e.g. 3T and 7T) boosted possibilities of MR imaging due to the higher SNR and CNR that can be achieved. However, ultrahigh field MRI also introduced new challenges, like increased transmit field inhomogeneities causing variations in signal intensity / image contrast. Also, SAR safety limits are more easily reached, which limits freedom for protocol development.[2] One of the main application areas for 7T MRI is brain imaging for assessment of cerebrovascular diseases. In ***Chapter 2***, a comprehensive overview of key developments in the last decade of 7T MRI in cerebrovascular diseases is provided. In less than a decade, much progress has been made in the field of 7T MRI for imaging cerebrovascular diseases. Small lesions can be visualized that provide additional information, not only about the total burden of cerebrovascular disease, but also about the possible causes and prognosis of individual patients. New sequences developed and knowledge obtained at 7T MRI have been used for successful development of similar methods at lower field strengths. Several limitations of 7T MRI – like image inhomogeneity – still remain and currently hamper further technical developments. However, with the almost exponential growth in developments at 7T MRI over the last decade, these restrictions may well be partially or even totally resolved or bypassed in the near future.

MRI of intracranial arteries

Intracranial arteries are relatively small, and detailed visualization of these arteries will therefore require a high spatial resolution. This is more easily accomplished within clinically feasible scan times at (ultra)high field strengths. In the last decade, many developments have taken place in the field of MR imaging of the intracranial arterial vasculature. These can be grossly subdivided into developments in vessel lumen and vessel wall imaging (***Chapter 2***).

Vessel lumen

Multiple studies have shown the ability of 7T MRI in visualizing different perforating arteries[3-8]. Developments are ongoing to further push the limits for visualization of the smallest brain arteries using MRI.[9,10] In ***Chapter 3***, the effect on vessel lumen visualization of perforating arteries when injecting a contrast agent was evaluated. The results of this study showed that high-resolution postcontrast TOF-MRA at 7T was able to visualize multiple intracranial perforators branching off from various parts of the circle of Willis (CoW) and proximal intracranial arteries with high image contrast in patients. Some perforators could be followed over a longer trajectory with postcontrast TOF-MRA compared with precontrast images, however, no differences were found in the number of visualized perforators within the same patient. In addition, using a contrast agent for TOF imaging sometimes made it difficult to discern the arterial or venous nature of a vessel, due to the presence of venous enhancement. Further optimization of the postcontrast TOF-MRA for the new T_1 relaxation of blood (after adding contrast agent) might lead to even better image contrast with shorter acquisition times, or increased spatial resolution. This may allow for visualization of intracranial perforators which are now below the detection limit of the current sequence, possibly beneficial for e.g. tumor resection planning or identification of a distal thrombus.

Vessel wall

In the last few years, the research field dedicated to visualization of the intracranial vessel wall has seen a tremendous growth. The availability of higher magnetic field strengths was important for this developmental progress of intracranial vessel wall MRI. In recent years, several intracranial vessel wall sequences have been developed at 3T and 7T for direct visualization of the vessel wall.[11] *In vivo* imaging of intracranial arterial walls is challenging, and multiple technical requirements need to be met for proper visualization. A detailed discussion has been provided in ***Chapter 1***, and future developments will be discussed below.

Clinical evaluation of vessel wall MRI

Although intracranial vessel wall MRI is already used in clinical practice at multiple centers, research is still ongoing to further improve scan sequences and elucidate the clinical meaning of MRI findings.[12] With the higher attainable SNR and CNR at higher field strengths, it became possible to perform isotropic vessel wall imaging with a larger (whole-brain) coverage, allowing for a more overall assessment of the intracranial vasculature. This was first developed at 7T MRI[13,14], and later sequences at 3T followed[15-17]. Intracranial vessel wall imaging has its own advantages and challenges at both field strengths. The implications of these differences for the visualization of the intracranial vessel wall and detection of vessel wall lesions were still unclear, because a head-to-head comparison between different field strengths had not yet been performed. In ***Chapter 4*** of this thesis, a comparison between 3T and 7T intracranial vessel wall MRI in visualizing the intracranial vessel wall and possible vessel wall lesions was performed in asymptomatic elderly volunteers. The results of this study showed that vessel wall visibility was equal or significantly better at 7T compared to 3T for the studied arterial segments, even though there were more artefacts hampering assessment at 7T. Furthermore, more vessel wall lesions were scored on 7T images. However, surprisingly, only 71% of all 3T lesions were seen at 7T. It was concluded that despite the large variability in detected lesions at both field strengths, 7T MRI has the highest potential to identify the total burden of intracranial vessel wall lesions.

A striking secondary result of this study was that in the studied elderly asymptomatic population, a substantial amount of intracranial vessel wall lesions were found, comparable to numbers previously reported in symptomatic patients. On top of that, also many of these vessel wall lesions showed enhancement after contrast administration. Contrast enhancement of intracranial atherosclerotic plaques has been associated with acute ischemic stroke[18-20] and could be a marker of plaque inflammation or neovascularization[21], or even potentially of intracranial plaque instability and stroke risk.[20] The results of the current study in asymptomatic volunteers, however, showed that enhancing lesions are not always associated with (acute) ischemic stroke or plaque inflammation.

A direct comparison between symptomatic patients and asympto-matic healthy controls was still lacking. This comparison may further enhance our knowledge about assessment of intracranial atherosclerosis for the identification and classification of possible culprit lesions. In ***Chapter 5***, this comparison between symptomatic patients and asymptomatic healthy controls was performed. Intracranial vessel wall lesion burden and contrast enhancement were assessed in patients with recent posterior circulation ischemia using 7T MRI, and these findings were compared with age- and sex-matched asymptomatic volunteers. The main finding of this study was that overall intracranial vessel wall lesion burden and contrast enhancement were comparable between patients and matched healthy controls. Also differences between patients and controls were found, suggesting an association between posterior circulation lesion burden / enhancement and ischemic events. The results of this study point out that conclusions based on vessel wall lesions burden and contrast enhancement in patients should be made carefully, since not all lesions and contrast enhancement will be related to pathology. With the current vessel wall imaging techniques it is difficult to differentiate pathological from normal intracranial vessel wall thickening and contrast enhancement. Therefore, next to assessing the prevalence of vessel wall lesions and contrast enhancement, additional characterization of vessel wall lesions might reveal more pronounced differences between patients and healthy controls.

Validation of vessel wall MRI findings

For further development and clinical implementation of intracranial vessel wall imaging, validation of MRI findings with a gold standard (histology) is essential. However, due to the poor accessibility of the intracranial arteries, only a limited number of studies so far have addressed this important issue. Recently, a first case report[22] was published demonstrating the correlation of certain intracranial atherosclerotic plaque components visualized *in vivo* at 3T and histology of the plaque post-mortem. However, further correlations are needed to define additional plaque components, as well as to increase the number of cases. From experience within our research lab, increasing the number of cases will be difficult. We encountered only

one post-mortem case with the availability of *in vivo* intracranial vessel wall MRI within our institution since we started performing intracranial vessel wall imaging. This illustrates the difficulty of pathological validation of *in vivo* vessel wall MRI findings. Vessel wall imaging findings of this case with histological validation are shown in **Figure 1**. This case shows that locations with clear vessel wall thickening on *in vivo* vessel wall images correlated with advanced atherosclerotic plaques scored on the corresponding histological sections. Other locations with less evident vessel wall thickening on *in vivo* vessel wall images, already showed an early stage of plaque formation on the corresponding histological section. On the corresponding *ex vivo* T_1-weighted images with ultrahigh-resolution, clear focal thickening of the vessel wall could be observed in all samples. This case also nicely illustrates the big difference in spatial resolution currently achieved *in vivo* versus *ex vivo*. For identification of different plaque components *in vivo* a higher spatial resolution is required than currently feasible within clinical scan times with the large (whole brain) coverage sequences. MR sequences with higher (in plane) resolutions are available[11], however, they have a small field-of-view, only covering a limited number of identified vessel wall lesions.

A more feasible method that can be used for validation of intracranial vessel wall imaging findings, is by using merely post-mortem specimens of the CoW. Although the *ex vivo* setting has its limitations, results of using this method may serve as a starting point for further histologic validation and optimization of currently available *in vivo* intracranial vessel wall MRI sequences. Thus far, two *ex vivo* studies have been performed using 7T MRI to assess its ability in visualizing different intracranial atherosclerotic plaque components.[23,24] These *ex vivo* studies showed that 7T MRI is capable of identifying focal thickening of the intracranial arterial vessel wall, as well as distinguishing different plaque components within advanced intracranial atherosclerotic plaques with different image contrast weightings. As a next step towards validation, quantitative assessment of MR signal characteristics of specific plaque components might enable more firm conclusions regarding the ability of T_1-, T_2-, T_2^*- and PD-weighted sequences in characterizing intracranial atherosclerotic plaques. In ***Chapter 6***, a multi-parametric ultrahigh-resolution quantitative

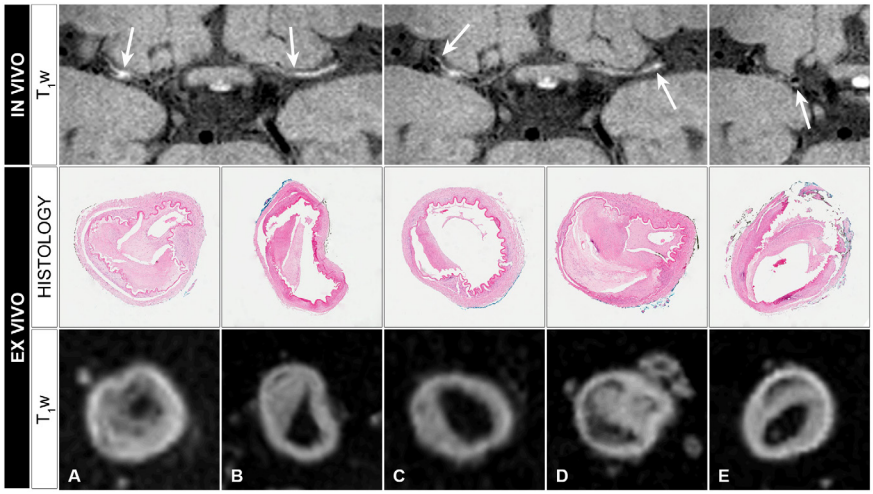

Figure 1 | Post-mortem case with *in vivo* intracranial vessel wall MRI. A 53-year-old female patient presented with ischemic stroke at multiple locations (left and right semiovale center, and in the territory of the left anterior cerebral artery). Final clinical diagnosis was Moyamoya syndrome. Histopathological assessment found variable but predominantly moderate to severe atherosclerosis, characteristic for Moyamoya syndrome. *In vivo,* intracranial vessel wall MRI was performed at 3T[17] (postcontrast only; T_1-weighted, spatial resolution 0.6x0.6x1.0 mm^3) and 7T[13,14] (not assessable due to severe motion artefacts). *Ex vivo*, the circle of Willis of this patient was scanned using an ultrahigh-resolution T_1-weighted sequence[23] (spatial resolution 0.12x0.12x0.12 mm^3), with histological validation. Arrows indicate locations analyzed *ex vivo*: (**A, C**) right middle cerebral artery, (**B, D**) left middle cerebral artery, and (**E**) right intracranial internal carotid artery. Histological sections (H&E stain) of the different samples were classified based on the modified Virmani classification[23,55] as advanced atherosclerotic lesions (**A, D**: fibrous plaques), or early lesions (**B, E**: pathological intimal thickening; **C**: intimal thickening). The locations with advanced lesions on histology **(A, D**), show clear vessel wall thickening (and contrast enhancement) on the *in vivo* vessel wall images. For the locations with early lesions on histology (**B,C,E**), vessel wall thickening on the *in vivo* images is less evident. *Ex vivo* T_1-weighted MR images show clear focal thickening of the vessel wall (intima) in all samples.

MRI protocol was performed to identify the MR signal characteristics of different intracranial atherosclerotic plaque components. Histology was used for validation of different tissue components. The results showed that primarily T_1 relaxation times were significantly different between different plaque components, the other quantitative maps (*PD, T_2 and T_2**) showed mostly non-significant differences between the individual tissue components present in the advanced intracranial plaques. Therefore,

based on these results, the most promising method for distinguishing intracranial plaque components is T_1-weighted imaging. Once it is known which plaque components can be identified with *ex vivo* MRI sequences, a translation may be made to *in vivo* intracranial vessel wall MR imaging, by developing sequences based on the NMR tissue properties of the identified atherosclerotic plaque components.

Currently, differentiation between pathological thickening and normal (age-related) vessel wall thickness variation is difficult. Autopsy studies have described the spatial distribution and severity of atherosclerosis in the intracranial arteries.[25-27] However, in contrast to vessel wall (intima-media) thickness of extracranial arteries[28-31], limited information is available on the quantitative assessment of vessel wall thickness and thickness variation over entire arterial segments of the arteries of the CoW. Therefore, in ***Chapter 7*** *ex vivo* CoW specimens were scanned with ultrahigh-resolution at 7T MRI to perform vessel wall thickness measurements of the major intracranial arteries. Histology was used for validation of the MRI measurements. Thickness measurements were performed in patients with and without cerebrovascular disease, to compare vessel wall thickness between both groups. The results showed that ultrahigh-resolution MRI enables accurate measurement of vessel wall thickness in *ex vivo* CoW specimens. Vessel wall thickness measurements over the entire length of segments showed considerable variation both within and between arterial segments of patients, and symptomatic patients generally had thicker walls than asymptomatic patients. In addition, considering the relatively small thickness variations that were present, currently used *in vivo* intracranial vessel wall MRI sequences require a higher spatial resolution for accurate measurement of vessel wall thickness in patients and to detect changes over time.

Future prospects

The research field of intracranial vessel wall MRI has gained a lot of attention in the last few years. This underlines the potential of this imaging technique as an added value to the currently available conventional imaging techniques for the intracranial arteries. Developments have led to valuable intracranial vessel wall image sequences, however, challenges

still remain. Research and development of intracranial vessel wall MRI is therefore ongoing, and it is important to further utilize this imaging technique to its full potential in clinical practice. In this thesis, studies were performed to fill certain gaps in this field, continuing on the work previously performed within our research lab dedicated to intracranial vessel wall imaging.[32,33] Also, based on the findings discussed in this thesis, potential opportunities/directions for future research of intracranial vessel wall MRI were identified.

Characterization of vessel wall lesions

Future studies should be directed towards stratifying pathological from normal vessel wall thickening and assessing the pathological substrate of contrast enhancement. With the currently available intracranial vessel wall imaging techniques aimed at identifying vessel wall lesions in multiple arterial segments, it is difficult to differentiate pathological from normal vessel wall thickening. Based on vessel wall lesion burden only, differences between patients and controls are relatively small, as discussed in ***Chapter 5***. Therefore, next to only detection of vessel wall lesions, additional characterization might reveal more pronounced differences between lesions. Ultimately, the goal would be to identify culprit lesions, or, even better, identify lesions in an early stage that have most potential to become culprit lesions.

One method, as discussed in ***Chapter 7***, might be quantitative assessment of vessel wall thickness. In other vascular territories vessel wall thickness has been studied much more extensively already.[34-37] For future application in larger patient groups, the first step would be to develop a tool that is capable of performing thickness measurements automatically, like already available for extracranial arteries[38]. To perform accurate thickness measurements, at least two full voxels without partial volume effects should represent the vessel wall (Nyquist-Shannon sampling theorem).[39,40] Direct vessel wall thickness measurements *in vivo* will therefore be difficult with the spatial resolutions currently used in intracranial vessel wall sequences. However, a different approach might be to infer wall thickness indirectly based on signal intensity differences, as has been shown previously for intracranial aneurysms[40].

Another potential method for lesion characterization could be the use of additional contrast weightings. For carotid plaque characterization it has been shown that reviewing multiple contrast-weighted images provided the most comprehensive evaluation for certain plaque components (e.g. intraplaque hemorrhage and lipid-rich necrotic core).[41,42] Intracranially, this might also aid in identifying different lesion subtypes. The most obvious way to characterize intracranial arterial plaques is by injection of a contrast agent to detect contrast uptake within the plaque. Another way is the detection of for instance intraplaque hemorrhage[43], or plaque calcifications based on their low signal intensity on high-resolution T_2^*-weighted images. However, plaque complications have been shown to be much less common in the intracranial arteries compared with for instance extracranial internal carotid artery plaques.[44] In addition, it has been described in literature that intracranial arteries show more stable lesions, develop mainly as fibrous plaques, and have some unique histological features.[44] Therefore, future studies should also be directed towards identifying imaging markers specific for intracranial arteries, since extrapolation of markers identified for extracranial plaques may not be directly applicable. Currently the scan protocol used in our *in vivo* studies only included a T_1-weighted vessel wall sequence. The results of the study described in ***Chapter 6*** showed T_1-weighted imaging to have the most promising image contrast for visualizing intracranial arterial vessel wall lesions. An additional benefit of using a T_1-weighted sequence is the possibility of contrast enhancement assessment. As we already acquire pre- and postcontrast T_1-weighted images, there is limited room for adding other image contrast weightings that will be able to include all major intracranial arteries with the required spatial resolution and proper image contrast, especially when added to a clinical protocol where also other sequences are desired like a FLAIR or TOF-MRA. Therefore, first efforts should be focused on development of faster scan sequences, to be able to include more contrast weightings.

Technical developments

Technical developments are still ongoing. A recent study[45], as well as the study discussed in ***Chapter 4***, showed that 7T provided significantly better image quality of the vessel wall and improved diagnostic confidence compared with 3T. However, the availability of 7T MRI systems is restricted. In the past period multiple efforts were made to further optimize intracranial vessel wall imaging sequences at 3T.[16,46-48]. Next to sequence optimization, future work should also be done to evaluate the relative importance of resolution versus contrast and CSF suppression.

Another interesting technical improvement is the development of dedicated multi-channel head and neck coil systems with larger longitudinal coverage and improved SNR and acceleration factors compared with a standard coil configuration[49]. Such a dedicated coil may also improve homogeneity of the magnetic field, which will especially be beneficial for the image quality at 7T MRI, where B_1^+ inhomogeneities result in a spatially varying SNR and contrast.[2,50] In the current studies at 7T, dielectric pads were placed in the upper neck region of subjects to improve imaging of the cerebellar region. This improved part of the signal loss, but did not reduce signal loss in all subjects. Furthermore, a coil that covers the head and neck region enables simultaneous imaging of the intracranial and extracranial arterial walls. Simultaneous assessment of the intracranial and carotid arteries might be an exciting development facilitating the application of vessel wall imaging in clinical diagnosis of, for instance, ischemic stroke patients.[49]

Finally, efforts should be made to reduce motion artefacts caused by movement of subjects during scanning. This is especially important for high-resolution imaging of small structures like the intracranial vessel wall (<1.0 mm thickness), and also for future developments aimed at increasing spatial resolution even further. It is often difficult for patients and elderly volunteers to lay still for a long time. In the literature, different methods have been described implementing motion-correction that substantially improve image quality for very high-resolution imaging.[51] In our current *in vivo* studies, part of the images are not assessable due to severe motion artefacts. Therefore, motion-correction may be of added value for improved visualization of the intracranial vessel wall in all subjects.

Validation of in vivo MRI findings

One of the most important issues that requires future research is the validation of *in vivo* MRI findings. Although the importance of this issue is highlighted in most articles published in this field, not many studies have tackled this topic so far. This is mainly caused by the inaccessibility of the intracranial arteries. An alternative is the evaluation of post-mortem CoW specimens enabling the combination of *ex vivo* MRI and histology as complementary methods. *Ex vivo* MRI offers the advantage of ultrahigh-resolution imaging and characterization of entire segments of the circle of Willis, where histology enables detailed assessment of a sample taken at a specific location that can be used for validation of MRI findings. Currently, *in vivo* detection of vessel wall lesions using MRI most likely only shows the 'top of the iceberg' regarding the presence of atherosclerosis (**Figure 1**). Therefore, when a vessel wall lesion is detected *in vivo*, many more will be present, similar as has been illustrated for cerebral microinfarcts.[52] *Ex vivo* imaging allows for assessment of total intracranial atherosclerosis burden, and its effect on vessel wall thickening in different stages of development. This may be used to estimate the real atherosclerotic burden based on *in vivo* vessel wall MRI findings. The first *ex vivo* validation studies were performed at 7T[23,24], and more recently also studies have been published at 3T[53] and 1.5T[54]. Hopefully, the importance of validation studies in this field will encourage other research labs to also dive into the world of *ex vivo* imaging to accelerate our knowledge in this field and enable proper translation of its results to *in vivo* imaging.

References

1. International Society for Magnetic Resonance in Medicine, in, Vol, http://www.ismrm.org/.
2. Vaughan JT, Garwood M, Collins CM, et al: 7T vs. 4T: RF power, homogeneity, and signal-to-noise comparison in head images. Magn Reson Med 46:24-30, 2001.
3. Kang CK, Park CW, Han JY, et al: Imaging and analysis of lenticulostriate arteries using 7.0-Tesla magnetic resonance angiography. Magn Reson Med 61:136-144, 2009.
4. Cho ZH, Kang CK, Han JY, et al: Observation of the lenticulostriate arteries in the human brain *in vivo* using 7.0T MR angiography. Stroke 39:1604-1606, 2008.
5. Hendrikse J, Zwanenburg JJ, Visser F, et al: Noninvasive depiction of the lenticulostriate arteries with time-of-flight MR angiography at 7.0 T. Cerebrovasc Dis 26:624-629, 2008.
6. Zwanenburg JJ, Hendrikse J, Takahara T, et al: MR angiography of the cerebral perforating arteries with magnetization prepared anatomical reference at 7 T: comparison with time-of-flight. J Magn Reson Imaging 28:1519-1526, 2008.
7. Kang CK, Park CA, Kim KN, et al: Non-invasive visualization of basilar artery perforators with 7T MR angiography. J Magn Reson Imaging 32:544-550, 2010.
8. Conijn MM, Hendrikse J, Zwanenburg JJ, et al: Perforating arteries originating from the posterior communicating artery: a 7.0-Tesla MRI study. Eur Radiol 19:2986-2992, 2009.
9. Wrede KH, Johst S, Dammann P, et al: Improved cerebral time-of-flight magnetic resonance angiography at 7 Tesla--feasibility study and preliminary results using optimized venous saturation pulses. PLoS One 9:e106697, 2014.
10. Schmitter S, Wu X, Adriany G, et al: Cerebral TOF angiography at 7T: Impact of B1 (+) shimming with a 16-channel transceiver array. Magn Reson Med 71:966-977, 2014.
11. Dieleman N, van der Kolk AG, Zwanenburg JJ, et al: Imaging intracranial vessel wall pathology with magnetic resonance imaging: current prospects and future directions. Circulation 130:192-201, 2014.
12. Mandell DM, Mossa-Basha M, Qiao Y, et al: Intracranial Vessel Wall MRI: Principles and Expert Consensus Recommendations of the American Society of Neuroradiology. AJNR Am J Neuroradiol, 2016.
13. van der Kolk AG, Hendrikse J, Brundel M, et al: Multi-sequence whole-brain intracranial vessel wall imaging at 7.0 tesla. Eur Radiol 23:2996-3004, 2013.
14. van der Kolk AG, Zwanenburg JJ, Brundel M, et al: Intracranial vessel wall imaging at 7.0-T MRI. Stroke 42:2478-2484, 2011.
15. Qiao Y, Steinman DA, Qin Q, et al: Intracranial arterial wall imaging using three-dimensional high isotropic resolution black blood MRI at 3.0 Tesla. J Magn Reson Imaging 34:22-30, 2011.

16. Yang Q, Deng Z, Bi X, et al: Whole-brain vessel wall MRI: A parameter tune-up solution to improve the scan efficiency of three-dimensional variable flip-angle turbo spin-echo. J Magn Reson Imaging, 2017.
17. Dieleman N, Yang W, van der Kolk AG, et al: Qualitative Evaluation of a High-Resolution 3D Multi-Sequence Intracranial Vessel Wall Protocol at 3 Tesla MRI. PLoS One 11:e0160781, 2016.
18. Skarpathiotakis M, Mandell DM, Swartz RH, et al: Intracranial atherosclerotic plaque enhancement in patients with ischemic stroke. AJNR Am J Neuroradiol 34:299-304, 2013.
19. Vakil P, Vranic J, Hurley MC, et al: T1 gadolinium enhancement of intracranial atherosclerotic plaques associated with symptomatic ischemic presentations. AJNR Am J Neuroradiol 34:2252-2258, 2013.
20. Qiao Y, Zeiler SR, Mirbagheri S, et al: Intracranial plaque enhancement in patients with cerebrovascular events on high-spatial-resolution MR images. Radiology 271:534-542, 2014.
21. Portanova A, Hakakian N, Mikulis DJ, et al: Intracranial vasa vasorum: insights and implications for imaging. Radiology 267:667-679, 2013.
22. Turan TN, Rumboldt Z, Granholm AC, et al: Intracranial atherosclerosis: correlation between in-vivo 3T high resolution MRI and pathology. Atherosclerosis 237:460-463, 2014.
23. van der Kolk AG, Zwanenburg JJ, Denswil NP, et al: Imaging the Intracranial Atherosclerotic Vessel Wall Using 7T MRI: Initial Comparison with Histopathology. AJNR Am J Neuroradiol, 2014.
24. Majidi S, Sein J, Watanabe M, et al: Intracranial-derived atherosclerosis assessment: an in vitro comparison between virtual histology by intravascular ultrasonography, 7T MRI, and histopathologic findings. AJNR Am J Neuroradiol 34:2259-2264, 2013.
25. Resch JA, Okabe N, Loewenson RB, et al: Pattern of vessel involvement in cerebral atherosclerosis. A comparative study between a Japanese and Minnesota population. J Atheroscler Res 9:239-250, 1969.
26. Baker AB, Iannone A: Cerebrovascular disease. I. The large arteries of the circle of Willis. Neurology 9:321-332, 1959.
27. Denswil NP, van der Wal AC, Ritz K, et al: Atherosclerosis in the circle of Willis: Spatial differences in composition and in distribution of plaques. Atherosclerosis 251:78-84, 2016.

28. Lorenz MW, Markus HS, Bots ML, et al: Prediction of clinical cardiovascular events with carotid intima-media thickness: a systematic review and meta-analysis. Circulation 115:459-467, 2007.
29. Mensel B, Quadrat A, Schneider T, et al: MRI-based determination of reference values of thoracic aortic wall thickness in a general population. Eur Radiol 24:2038-2044, 2014.
30. Naqvi TZ, Lee MS: Carotid intima-media thickness and plaque in cardiovascular risk assessment. JACC Cardiovasc Imaging 7:1025-1038, 2014.
31. Macedo R, Chen S, Lai S, et al: MRI detects increased coronary wall thickness in asymptomatic individuals: the multi-ethnic study of atherosclerosis (MESA). J Magn Reson Imaging 28:1108-1115, 2008.
32. van der Kolk AG: Intracranial vessel wall imaging at 7.0 tesla MRI. PhD thesis, Utrecht University, The Netherlands ISBN: 978-94-6259-143-1, 2014.
33. Dieleman N: MR imaging of intracranial vessel wall pathologies and parenchymal brain damage. PhD thesis, Utrecht University, The Netherlands ISBN: 978-90-393-6638-7, 2016.
34. Li AE, Kamel I, Rando F, et al: Using MRI to assess aortic wall thickness in the multiethnic study of atherosclerosis: distribution by race, sex, and age. AJR Am J Roentgenol 182:593-597, 2004.
35. Mani V, Muntner P, Gidding SS, et al: Cardiovascular magnetic resonance parameters of atherosclerotic plaque burden improve discrimination of prior major adverse cardiovascular events. J Cardiovasc Magn Reson 11:10, 2009.
36. Maroules CD, Rosero E, Ayers C, et al: Abdominal aortic atherosclerosis at MR imaging is associated with cardiovascular events: the Dallas heart study. Radiology 269:84-91, 2013.
37. van den Oord SC, Sijbrands EJ, ten Kate GL, et al: Carotid intima-media thickness for cardiovascular risk assessment: systematic review and meta-analysis. Atherosclerosis 228:1-11, 2013.
38. Gao S, van 't Klooster R, Brandts A, et al: Quantification of common carotid artery and descending aorta vessel wall thickness from MR vessel wall imaging using a fully automated processing pipeline. J Magn Reson Imaging, 2016.
39. Bouvy WH, Biessels GJ, Kuijf HJ, et al: Visualization of perivascular spaces and perforating arteries with 7 T magnetic resonance imaging. Invest Radiol 49:307-313, 2014.
40. Kleinloog R, Korkmaz E, Zwanenburg JJ, et al: Visualization of the aneurysm wall: a 7.0-tesla magnetic resonance imaging study. Neurosurgery 75:614-622; discussion 622, 2014.

41. Shinnar M, Fallon JT, Wehrli S, et al: The diagnostic accuracy of ex vivo MRI for human atherosclerotic plaque characterization. Arterioscler Thromb Vasc Biol 19:2756-2761, 1999.
42. Yuan C, Mitsumori LM, Ferguson MS, et al: In vivo accuracy of multispectral magnetic resonance imaging for identifying lipid-rich necrotic cores and intraplaque hemorrhage in advanced human carotid plaques. Circulation 104:2051-2056, 2001.
43. Moody AR, Murphy RE, Morgan PS, et al: Characterization of complicated carotid plaque with magnetic resonance direct thrombus imaging in patients with cerebral ischemia. Circulation 107:3047-3052, 2003.
44. Ritz K, Denswil NP, Stam OC, et al: Cause and mechanisms of intracranial atherosclerosis. Circulation 130:1407-1414, 2014.
45. Zhu C, Haraldsson H, Tian B, et al: High resolution imaging of the intracranial vessel wall at 3 and 7 T using 3D fast spin echo MRI. MAGMA, 2016.
46. Xie Y, Yang Q, Xie G, et al: Improved black-blood imaging using DANTE-SPACE for simultaneous carotid and intracranial vessel wall evaluation. Magn Reson Med 75:2286-2294, 2016.
47. Wang J, Helle M, Zhou Z, et al: Joint blood and cerebrospinal fluid suppression for intracranial vessel wall MRI. Magn Reson Med 75:831-838, 2016.
48. Yang H, Zhang X, Qin Q, et al: Improved cerebrospinal fluid suppression for intracranial vessel wall MRI. J Magn Reson Imaging 44:665-672, 2016.
49. Hu X, Li Y, Zhang L, et al: A 32-channel coil system for MR vessel wall imaging of intracranial and extracranial arteries at 3T. Magn Reson Imaging 36:86-92, 2017.
50. van der Kolk AG, Hendrikse J, Zwanenburg JJ, et al: Clinical applications of 7 T MRI in the brain. Eur J Radiol 82:708-718, 2013.
51. Federau C, Gallichan D: Motion-Correction Enabled Ultra-High Resolution In-Vivo 7T-MRI of the Brain. PLoS One 11:e0154974, 2016.
52. Westover MB, Bianchi MT, Yang C, et al: Estimating cerebral microinfarct burden from autopsy samples. Neurology 80:1365-1369, 2013.
53. Jiang Y, Zhu C, Peng W, et al: Ex-vivo imaging and plaque type classification of intracranial atherosclerotic plaque using high resolution MRI. Atherosclerosis 249:10-16, 2016.
54. Yang WJ, Chen XY, Zhao HL, et al: In Vitro Assessment of Histology Verified Intracranial Atherosclerotic Disease by 1.5T Magnetic Resonance Imaging: Concentric or Eccentric? Stroke 47:527-530, 2016.
55. Virmani R, Kolodgie FD, Burke AP, et al: Lessons from sudden coronary death: a comprehensive morphological classification scheme for atherosclerotic lesions. Arterioscler Thromb Vasc Biol 20:1262-1275, 2000.

Addendum

Dutch summary
(Nederlandse samenvatting)

Een herseninfarct behoort tot een van de meest voorkomende doodsoorzaken wereldwijd, en is tevens een van de belangrijkste oorzaken van invaliditeit bij volwassenen. Identificatie van de oorzaak van een herseninfarct is klinisch gezien erg belangrijk, niet alleen om te bepalen wat de beste behandelingsoptie is voor de individuele patiënt, maar ook ter voorkoming van nieuwe events. In de huidige klinische praktijk kan het soms lastig zijn de oorzaak van het herseninfarct te achterhalen, waardoor bij veel patiënten geen oorzaak geïdentificeerd kan worden. Daarom is het belangrijk dat meer methodes ontwikkeld worden die mogelijk kunnen helpen bij het vaststellen van de oorzaak.

Een van de belangrijke oorzaken voor het ontstaan van een herseninfarct of TIA is intracraniële atherosclerose. De huidige beeldvormingstechnieken die in de klinische praktijk gebruikt worden om intracraniële arteriën af te beelden (bijv. CTA en MRA), zijn allen gebaseerd op het afbeelden van het lumen van het bloedvat. Deze technieken worden gebruikt voor het detecteren van een vernauwing van het bloedvat (stenose), wat een mogelijke aanwijzing is voor een vaatwandafwijking op deze locatie. Echter, een nadeel van deze conventionele beeldvormingstechnieken is dat ze een indirecte methode zijn voor het afbeelden van de vaatwand. Hierdoor zullen vaatwandafwijkingen waarbij (nog) geen vernauwing van het lumen veroorzaakt wordt niet gedetecteerd kunnen worden, of pas in een relatief laat stadium van zijn ontwikkeling. In de afgelopen paar jaar zijn MRI-scans ontwikkeld die het mogelijk maken om direct de vaatwand af te beelden van de intracraniële arteriën. Deze MRI-scans maken het mogelijk om intracraniële vaatwandafwijkingen te detecteren, waaronder afwijkingen die nog geen vernauwing van het bloedvat hebben veroorzaakt.

Het onderzoeksveld dat specifiek is gericht op het afbeelden van de intracraniële vaatwand met behulp van MRI is in de afgelopen jaren zeer sterk gegroeid, en inmiddels wordt deze afbeeldingstechniek in een aantal centra al klinische toegepast. Desondanks moet nog diepgaander onderzoek gedaan worden naar verdere verbetering van de afbeeldingsmethode en bovenal om meer te weten te komen over de klinische betekenis van de bevindingen op deze beelden. De studies beschreven in dit proefschrift, zijn een continuering van onderzoek

verricht binnen onze onderzoeksgroep gericht op de visualisatie van de intracraniële arteriën met behulp van (ultra)hoog veld MRI, met speciale focus op het afbeelden van de vaatwand. Hoofddoelen waren de verdere histologische validatie van intracraniële vaatwand MRI en verdere klinische evaluatie van de toepassing ervan bij patiënten.

Deel I van dit proefschrift start met een overzicht van de belangrijkste ontwikkelingen in het afgelopen decennium van 7T MRI bij cerebrovasculaire ziektes (***Hoofdstuk 2***). Een van deze ontwikkelingen wordt uitgebreider beschreven in het daarop volgende hoofdstuk, waar kleine perforerende arteriën afgebeeld worden met behulp van 7T TOF-MRA na de toediening van een contrastmiddel (***Hoofdstuk 3***). Deze studie laat zien dat diverse perforerende arteriën afgebeeld kunnen worden bij patiënten met behulp van TOF-MRA na contrasttoediening. Een aantal perforerende arteriën waren na contrasttoediening zelfs zichtbaar over een langer traject van het bloedvat dan zonder contrast, maar het aantal zichtbare vaten bleef gelijk. Echter, door de contrasttoediening was het soms lastiger om venen en arteriën van elkaar te onderscheiden door de aanwezigheid van veneuze aankleuring. Door de gewijzigde T_1 relaxatietijd na toediening van het contrastmiddel, zou de scanmethode mogelijk nog verder geoptimaliseerd kunnen worden voor het verkrijgen van nog beter beeld contrast, kortere acquisitie tijd, of hogere spatiële resolutie.

Deel II en **III** omvatten studies die betrekking hebben op intracraniële vaatwand MRI. In **Deel II** worden vaatwand MRI-scans *in vivo* geëvalueerd bij patiënten en gezonde vrijwilligers. Als eerste wordt een directe vergelijking gemaakt tussen vaatwand MRI-scans toegepast op verschillende magnetische veldsterktes (3T en 7T MRI) in asymptomatische gezonde vrijwilligers (***Hoofdstuk 4***). Hierbij werd onderzocht of verschillen aanwezig zijn in zichtbaarheid van de vaatwand en detectie van vaatwandafwijkingen bij gebruik van verschillende magnetische veldsterktes. Ondanks dat er een behoorlijk grote variabiliteit was in gedetecteerde vaatwand laesies op beide veldsterktes, heeft 7T MRI de meeste potentie voor identificatie van totale vaatwand laesie burden. In de hierop volgende studie is een vergelijking gemaakt tussen patiënten met recente ischemie in de achterste cerebrale circulatie en gezonde vrijwilligers in de aanwezigheid

van vaatwandafwijkingen (***Hoofdstuk 5***). Deze vergelijking geeft mogelijk meer inzicht in de rol van intracraniële atherosclerose en de ontwikkeling hiervan bij patiënten met een herseninfarct. De resultaten lieten zien dat het totaal aantal aanwezige vaatwand laesies vergelijkbaar was tussen beide groepen, alsmede de hoeveelheid laesies die aankleuring lieten zien na contrasttoediening. Bij verder inzoomen op specifieke stroomgebieden/vaatsegmenten werden ook verschillen gevonden tussen de patiënten en controles voor zowel het aantal aanwezige laesies als contrast aankleuring. Een belangrijke bevinding van deze studie is dat voorzichtigheid geboden dient te worden indien conclusies getrokken worden op basis van vaatwand laesie burden en contrast aankleuring, aangezien niet alle laesies en contrast aankleuring gerelateerd zal zijn aan pathologie.

Om beeldvorming van de intracraniële vaatwand met behulp van MRI klinisch toe te kunnen passen, is validatie van de MRI bevindingen met een gouden standaard (histologie) een vereiste. In **Deel III** van dit proefschrift worden studies beschreven waarbij validatie van vaatwand MRI met histologie is gedaan door gebruik te maken van post mortem cirkel van Willis preparaten. In de eerste studie zijn met behulp van kwantitatieve MRI-scans MRI signaal eigenschappen van verschillende intracraniële plaque componenten geïdentificeerd (***Hoofdstuk 6***). Histologie is in deze studie gebruikt voor identificatie van de verschillende weefselcomponenten van de vaatwand. De resultaten lieten zien dat de geïdentificeerde plaque componenten voornamelijk verschilden in T_1 relaxatietijden. De volgende stap is om de bevindingen van *ex vivo* MRI voor de verschillende plaque componenten te vertalen naar *in vivo* intracraniële vaatwand MRI. In de hierop volgende studie zijn *ex vivo* cirkel van Willis preparaten gebruikt om vaatwanddikte metingen te doen met behulp van MRI-beelden met zeer hoge resolutie (***Hoofdstuk 7***). Het doel hiervan was om meer te weten te komen over wanddikte variaties van de intracraniële arteriën, om uiteindelijk in patiënten beter onderscheid te kunnen maken tussen normale en pathologische vaatwandverdikking. Histologie werd hier gebruikt voor de validatie van de MRI-diktemetingen. De vaatwanddikte metingen over gehele vaatsegmenten lieten aanzienlijke variaties zien zowel binnen elke segment als tussen de verschillende segmenten van

patiënten. Ook hadden symptomatische patiënten (met een herseninfarct/ TIA in de voorgeschiedenis) over het algemeen gemiddeld dikkere vaatwanden dan asymptomatische patiënten. Ook liet deze studie zien dat gezien de relatief kleine diktevariaties die aanwezig zijn, een hogere spatiële resolutie nodig is voor de intracraniële vaatwand MRI-scans om accuraat diktemetingen *in vivo* bij patiënten te kunnen doen.

De resultaten beschreven in dit proefschrift geven nieuwe inzichten voor interpretatie en verdere ontwikkeling van intracraniële vaatwand MRI. Voor volledige implementatie in de klinische praktijk is echter nog meer onderzoek nodig, zoals karakterisering van laesie subtypes, verdere optimalisatie van de scanmethode, en verdere validatie van MRI bevindingen.

Acknowledgements (Dankwoord)

Het onderzoek beschreven in dit proefschrift was niet tot stand gekomen zonder de bijdrage van een heel aantal mensen. Daarom wil ik iedereen die de afgelopen 4 jaar heeft bijgedragen aan dit proefschrift heel erg bedanken. Een aantal personen in het bijzonder:

Prof.dr. J. Hendrikse, beste Jeroen, dit promotietraject is allemaal bij jou begonnen. Bedankt voor het vertrouwen dat je vanaf het begin in mij had om aan dit project deel te nemen, en ook de vele mogelijkheden die je hebt gegeven voor verdere ontwikkeling. Jouw laagdrempeligheid en enthousiasme vond ik erg prettig. Ook de vrijheid en verantwoordelijkheid die je geeft, heeft ertoe geleid dat ik veel geleerd heb als beginnend onderzoeker. Bedankt voor je begeleiding in de afgelopen jaren, en ik hoop dat we in de toekomst onze samenwerking kunnen voortzetten.

Prof.dr. P.R. Luijten, beste Peter, veel dank voor de mogelijkheden die je hebt gecreëerd voor onderzoek binnen de 7T groep. De wisselwerking tussen technische methode ontwikkeling en klinisch toegepast onderzoek is een sterk punt van deze groep, en hopelijk zal dit in de toekomst in stand blijven. Ook denk ik met veel plezier terug aan onze fietsentochtjes met collega's na het werk en in Salt Lake City, waar we een gezamenlijke hobby bleken te hebben.

Dr. A.G. van der Kolk, beste Anja, wat had ik zonder jou moeten beginnen. Je was mijn 'dagelijks begeleider' tijdens dit promotietraject. Je hebt me door diverse dip(je)s heen weten te slepen, met name na mislukte overnacht-scansessies was dit soms wel nodig ;). Het was erg fijn dat ik alles met jou kon bespreken, hoe klein of groot het probleem ook was. Jouw gedrevenheid, standvastigheid en gestructureerdheid zijn een voorbeeld voor mij. Ik vond het bijzonder fijn om met je samen te werken, en wil je heel erg bedanken voor alle begeleiding en steun die je tijdens mijn promotieonderzoek hebt gegeven!

Dr.ir. J.J.M. Zwanenburg, beste Jaco, heel erg bedankt dat je mijn copromotor was. Ondanks dat je niet dagelijks betrokken was bij mijn projecten, was je bijdrage onmisbaar voor het uitvoeren van de projecten

voor dit proefschrift. De beelden hadden er een stuk minder mooi uitgezien zonder jouw hulp ☺. Erg fijn dat je altijd bereikbaar was als hulplijn tijdens scansessies, indien er weer eens onduidelijk foutmeldingen voorbij kwamen. Ook heb ik veel geleerd van jouw kritische onderzoekersblik, nauwkeurige manier van werken, en op het gebied van schrijven. Heel erg bedankt voor je begeleiding!

Leden van de leescommissie: prof.dr. N.F. Ramsey, prof.dr. R.M. Dijkhuizen, prof.dr. B.K. Velthuis, prof.dr. J.M. Rozemuller-Kwakkel en prof. dr. M.J.A.P. Daemen, hartelijk dank voor het beoordelen en goedkeuren van dit proefschrift.

Vaatwand imaging groep: Jeroen, Anja, Jaco, Jeroen S, Nikki en Arjen, bedankt voor de fijne samenwerking en het gezamenlijk uitbreiden van de kennis over intracraniële vaatwand MRI. Jeroen S, mede door jouw inzet is het gelukt om ook op 3T een intracraniële vaatwand sequentie te ontwikkelen. Ook heb je samen met Jaco ervoor gezorgd dat we voor het eerst kwantitatieve MRI hebben toegepast van de intracraniële vaatwand. Dat was in een keer een grote stap voorwaarts! Bedankt voor al je hulp bij de diverse projecten! Nikki, 'partner in crime'. Samen hebben we onze eerste echte stappen binnen de wereld van de wetenschap en vaatwand MRI gezet. Ik heb veel geleerd van onze samenwerking, en vond het fijn dat we samen nieuwe ervaringen konden delen, en konden 'sparren' over ons onderzoek. Inmiddels zijn onze wegen binnen het onderzoek meer gescheiden, maar deze zullen vast nog regelmatig kruisen binnen de MRI wereld. Arjen, de nieuwste toevoeging aan het vaatwand team. Het is altijd lastig om later in te stappen bij een lopende trein, maar dat gaat helemaal goed komen volgens mij ;). Bedankt voor je hulp bij de vele scansessies en de fijne samenwerking in de afgelopen periode!

Dr. H.B. van der Worp, beste Bart, hartelijk dank voor je betrokkenheid bij de PIVI-studie vanuit de Neurologie afdeling. Het was erg fijn dat ik altijd laagdrempelig kon overleggen over mogelijk geschikte studie kandidaten. Ook wil ik je hartelijk danken voor het meedenken en kritisch lezen van artikelen voor Deel II van dit proefschrift.

Prof.dr. M.J.A.P. Daemen, beste Mat, dank voor de samenwerking binnen het project van de histologie-MRI validatie. Het was prettig om een kritische blik vanuit pathologisch perspectief te hebben binnen dit project. Ook wil ik je hartelijk danken voor het meedenken en kritisch lezen van artikelen voor Deel III van dit proefschrift, en het plaatsnemen in de leescommissie.

Nerissa, heel erg bedankt voor je werk bij het maken van alle mooie histologische coupes voor de MRI-histologie validatie. Een erg arbeidsintensief karwei! Ik vond het erg fijn om met je samen te werken, en je hebt me veel bijgeleerd over de histologische kant van dit onderzoek. Ik hoop dat voor jou de afronding van je proefschrift ook snel zal volgen!

Afdeling pathologie UMC Utrecht: Wim S, Wim v H en Aryan, dank voor alle hulp en fijne samenwerking bij het post mortem MRI project. Wim S, dank voor jouw speciale interesse in de cirkel van Willis en het bewaren van alle preparaten. Wim v H, fijn dat je altijd bereid was om te helpen met het opsporen van een benodigde cirkel. Ondanks dat ik toch nog lichte voorkeur houd voor radiologische beelden, ben ik door jouw enthousiasme tijdens het bekijken van de histologische coupes deze beelden toch ook meer gaan waarderen ☺. Aryan, dank voor je inzet bij het uitzoeken van geschikte cirkels en voor het kritisch lezen van artikelen voor Deel III van dit proefschrift.

Alle andere co-auteurs wil ik ook graag bedanken voor hun waardevolle bijdrage aan de totstandkoming van dit proefschrift.

Alle patiënten en gezonde proefpersonen die hebben deelgenomen aan de studies beschreven in dit proefschrift wil ik nogmaals heel erg bedanken voor hun vrijwillige deelname. In het bijzonder de deelnemers aan de PIVI-studie. Zonder de deelname van deze patiënten en gezonde proefpersonen hadden de stukken in dit proefschrift nooit geschreven kunnen worden.

Alle MRI-laboranten die geholpen hebben met scannen van patiënten en gezonde vrijwilligers die hebben deelgenomen aan de studies beschreven in dit proefschrift, hartelijk dank voor jullie inzet. In het bijzonder de 7T laboranten, Guus, Gerrit, Johan, Daniel, Erik, Nikki, Myrthe en Gideon. Guus en Niels, bedankt voor jullie hulp en logistieke ondersteuning bij het opstarten en uitvoeren van de PIVI-studie op de klinische MRI systemen.

Pie Medical Imaging: Jean-Paul en Chris, dank voor de fijne samenwerking. Dankzij de software die jullie beschikbaar hebben gesteld, en specifiek hebben aangepast om met onze data te kunnen werken, werd de data analyse een stuk haalbaarder.
Secretariaat 7T/Radiologie: Sylvia, Marja en Annet, dank voor alle administratieve hulp en ondersteuning in de afgelopen periode. Erg fijn dat jullie me altijd met de meest uiteenlopende vragen konden helpen! Sylvia, fijn dat ik op een gegeven moment ook jou af en toe met dingen terug kon helpen ☺.

Trialbureau Divisie Beeld: Anneke, Shanta en Saskia, wat fijn dat jullie er zijn voor de ondersteuning van klinische onderzoeksprojecten. Heel erg bedankt voor jullie hulp bij het opzetten en uitvoeren van de klinische projecten binnen mijn promotieonderzoek.

Multimedia: Karin, Roy, en Chris, heel erg bedankt voor jullie hulp bij het maken van alle mooie figuren, posters, en flyers voor mijn promotieonderzoek (zelfs als mijn planning een beetje aan de krappe kant was..). In het bijzonder Roy, voor het maken van de lay-out voor het binnenwerk van dit proefschrift en de diverse fotoshoots van de cirkel van Willis preparaten ☺.

7T group/Q2 (former Q4)/other researchers: Dennis, Hans, Peter, Fredy, Jaco, Natalia, Jeroen, Alex, Martijn, Vincent, Sylvia, Tijl, Nikki, Jannie, Alexander, Jill, Bertine, Laura, Anja, Joep, Ronald, Vitaliy, Irene, Alessandro, Anna, Astrid, Hanneke, Alexander, Mariska, Anouk, Hugo, Nolan, Hamza, Hanke, Marlijne, Arthur, Esben, Jolanda, Niels, Rashid, Wieke, Remko, Wouter, Esther, Stefano, Matthew, Anna, Flavio, Lisa, Arjen, Maarten, Tine,

Jeanine, Tim, Frank, Janot, Oscar, Mike, Erwin, Bart, Anneloes, Sander, Ingmar, Aidin, Mark, Debra, Michel, Susanne, Hugo, Behdad, Jasper, Ilse, Simone, Tim, Koen, Doeschka, Annemarie, Björn, Anouk, Suzanne, Erika, Richard, Marjolein, Gisela, Ellis, Sophie, and all students, thanks for the good working atmosphere and collaboration in the past period and the many nice activities like bbq's, cycling, drinks, UMC estafette, 7T Winter dinner's, and ISMRM conferences. Especially all officemates: Laurens, Dhaval, Wouter, Catalina, Wybe, Alexandra, Arjan, Remco, Lennart, Deji, Lidy, and Quincy, thanks for sharing stories, highlights, frustrations, candy/cookies/chocolate, conference deadlines, funny movies, ideas, and off course helpful work related discussions ☺. Alexandra, Jill en Wieke, jullie wil ik nog specifiek bedanken voor de leuke tijd die we samen hebben gehad aansluitend aan het ISMRM congres bij het Comomeer en in Canada!

Rowbuust: Annemieke, Heleen, Hilde, Leonie, Linda, Marja, Marthe en Wietske, bedankt voor alle gezellige (sportieve) activiteiten die we de afgelopen jaren hebben ondernomen! Ik vind het mooi om te zien dat ondanks dat we inmiddels behoorlijk verspreid door NL (en daarbuiten) wonen en er nieuwe wereldbewoners bij zijn gekomen, we nog steeds tijd vinden om regelmatig af te spreken. Ik hoop dat we hier nog lang mee door zullen gaan!

Viking: na het vertrouwde Twentekanaal in Enschede te hebben verlaten, heb ik de afgelopen 4 jaar met veel plezier het roeien weer opgepakt en het Utrechtse roeiwater leren kennen. Ik wil alle ploeggenoten bedanken waarmee ik de afgelopen seizoenen heb geroeid, die voor de nodige afleiding gezorgd hebben van mijn promotieonderzoek. In het bijzonder de DVA8+ (Marjolein, Ingrid, Esther, Dewi, Margreet, Suzan, Suzanne, Maartje, Loes, Marijke, Selma, Sannerijn en Carel), de Elfstedentocht-dames, en mijn huidige ploeggenoten van de Zoennami-8 (Maartje, Anne Wietske, Marije, Annemieke, Lotte, Marja, Marian, Janneke en Jeroen). Ook de BikeBabes (Marije, Esther, Lotte, Margreet, Inge en Anne Wietske) wil ik bedanken voor de gezellige rondjes Lekdijk met taartstop, en andere mooie fietstochten en -weekendjes.

Monique, ik ben blij dat we elkaar beter hebben leren kennen in Nijmegen tijdens ons afstudeerjaar bij de Nucleaire Geneeskunde. Inmiddels ben ik jou ook weer gevolgd naar Utrecht ☺. Bedankt voor alle bios bezoekjes, fietstochten, hardlooprondjes en borrels in de afgelopen jaren. Fijn dat we 's avonds na een drukke dag al onze belevenissen konden bespreken, en ik hoop dat we onze vriendschap nog lang zullen voortzetten.

Leonie, het maakt niet uit hoe lang we elkaar niet zien door wereldreizen, of dat we wat verder bij elkaar vandaan wonen. Zodra we elkaar weer zien, is het direct weer vertrouwd. Eigenlijk vanaf het eerste moment dat we in dezelfde projectgroep begonnen bij TG, zijn we bevriend geraakt. We hebben inmiddels al veel samen gedaan en meegemaakt. Ik vind het erg fijn dat we alles met elkaar kunnen bespreken, en dat je altijd voor me klaar staat. Bedankt voor alle activiteiten die we samen ondernomen hebben in de afgelopen periode ter afleiding en ontspanning van mijn promotieonderzoek. Ik hoop dat we nog veel leuke activiteiten zullen ondernemen samen!

Tot slot wil ik mijn familie bedanken. Als eerste mijn ouders, dankzij jullie ben ik gekomen waar ik nu ben. Zonder de mogelijkheden die jullie gegeven hebben, was dit nooit gelukt. Mam, bedankt dat je er altijd voor me bent, en dat je me onvoorwaardelijk steunt bij elke keuze die ik maak. Pap, ook al is niet altijd even duidelijk waar ik allemaal mee bezig ben, ik weet dat je trots op me bent. Henri, bedankt voor jouw interesse die je altijd toont in wat ik doe en specifiek voor mijn promotieonderzoek in de afgelopen jaren. Mijn sissies, Linda en Ria, wat ben ik trots dat jullie bij de verdediging van mijn proefschrift naast mij staan. Ik vind het mooi dat ik dit moment zo intensief met jullie kan delen. Heel erg bedankt voor jullie luisterend oor bij zowel de ups en downs tijdens dit promotietraject. Tijdens drukke periodes was ik niet altijd even gezellig, maar bij jullie weet ik dat dit kan. Bedankt voor jullie begrip ;) Ik hoop dat we naast deze mijlpaal nog vele mooie momenten zullen meemaken samen!

Curriculum Vitae

Anita Harteveld was born on February 28, 1985 in Rotterdam, the Netherlands. After obtaining her pre-university diploma at the Caland Lyceum Rotterdam in 2003, she moved to Enschede to study Technical Medicine at the University of Twente. In 2006 she obtained her Bachelor's degree, and continued with the Master's program (track 'Robotics & Imaging'). In the second year of the Master's, she completed clinical internships at different hospital departments (Intensive Care Unit of the Canisius-Wilhelmina Hospital in Nijmegen, department of Aneasthesiology of the Canisius-Wilhelmina Hospital in Nijmegen, department of Pedriatic Urology of the Wilhelmina Childen's Hospital in Utrecht, and department of Nuclear Medicine of the Leiden University Medical Center in Leiden). In the third year of the Master's, she performed her Master's thesis at the department of Nuclear Medicine of the UMC St. Radboud in Nijmegen, which was focused on the optimization of SPECT image acquisition and reconstruction in clinical and preclinical applications. In 2010 she graduated from the Master Technical Medicine. Afterwards, she worked for a year as a research assistant at the Donders Centre for Cognitive Neuroimaging of the Radboud University Nijmegen, and travelled to Australia, New Zealand and Indonesia for six months. In October 2012, she started working as a PhD student at the department of Radiology of the University Medical Center Utrecht. Her research, of which the results are presented in this thesis, focused on *ex vivo* validation and *in vivo* evaluation of intracranial vessel wall MRI under the supervision of prof. J. Hendrikse, prof. P.R. Luijten, dr. A.G. van der Kolk, and dr.ir. J.J.M. Zwanenburg. Upon completion of her PhD in 2017, she will continue to work at the University Medical Center Utrecht as a post-doctoral researcher. This research will be focused on the development and clinical implementation of perfusion measurement methods in the body using arterial spin labeling MRI, under the supervision of dr. C. Bos and dr. M. van Stralen.

List of publications

Peer-reviewed publications

Harteveld AA, van der Kolk AG, van der Worp HB, Dieleman N, Siero JC, Kuijf HJ, Frijns CJ, Luijten PR, Zwanenburg JJ, Hendrikse J: High-resolution intracranial vessel wall MRI in an elderly asymptomatic population: comparison of 3T and 7T. Eur Radiol 27:1585-1595, 2017.

Harteveld AA, van der Kolk AG, Zwanenburg JJ, Luijten PR, Hendrikse J: 7-T MRI in Cerebrovascular Diseases: Challenges to Overcome and Initial Results. Top Magn Reson Imaging 25:89-100, 2016.

Harteveld AA, Denswil NP, Siero JC, Zwanenburg JJ, Vink A, Pouran B, Spliet WG, Klomp DW, Luijten PR, Daemen MJ, Hendrikse J, van der Kolk AG: Quantitative Intracranial Atherosclerotic Plaque Characterization at 7T MRI: An *Ex Vivo* Study with Histologic Validation. AJNR Am J Neuroradiol 37:802-810, 2016.

Dieleman N, van der Kolk AG, Zwanenburg JJ, Brundel M, **Harteveld AA**, Biessels GJ, Visser F, Luijten PR, Hendrikse J: Relations between location and type of intracranial atherosclerosis and parenchymal damage. J Cereb Blood Flow Metab 36:1271-1280, 2016.

Siero JC, Hartkamp NS, Donahue MJ, **Harteveld AA**, Compter A, Petersen ET, Hendrikse J: Neuronal activation induced BOLD and CBF responses upon acetazolamide administration in patients with steno-occlusive artery disease. Neuroimage 105:276-285, 2015.

Harteveld AA, De Cocker LJ, Dieleman N, van der Kolk AG, Zwanenburg JJ, Robe PA, Luijten PR, Hendrikse J: High-resolution postcontrast time-of-flight MR angiography of intracranial perforators at 7.0 Tesla. PLoS One 10:e0121051, 2015.

Dieleman N, van der Kolk AG, van Veluw SJ, Frijns CJ, **Harteveld AA**, Luijten PR, Hendrikse J: Patterns of intracranial vessel wall changes in relation to ischemic infarcts. Neurology 83:1316-1320, 2014.

Dieleman N, van der Kolk AG, Zwanenburg JJ, **Harteveld AA**, Biessels GJ, Luijten PR, Hendrikse J: Imaging intracranial vessel wall pathology with magnetic resonance imaging: current prospects and future directions. Circulation 130:192-201, 2014.

Cousijn H, Rijpkema M, **Harteveld AA**, Harrison PJ, Fernández G, Franke B, Arias-Vásquez A: Schizophrenia risk gene ZNF804A does not influence macroscopic brain structure: an MRI study in 892 volunteers. Mol Psychiatry 17:1155-1157, 2012.

Visser EP, **Harteveld AA**, Meeuwis AP, Disselhorst JA, Beekman FJ, Oyen WJG, Boerman OC. Image quality phantom and parameters for high spatial resolution small-animal SPECT. Nucl Instrum Meth A, 2011.

Harteveld AA, Meeuwis AP, Disselhorst JA, Slump CH, Oyen WJ, Boerman OC, Visser EP: Using the NEMA NU 4 PET image quality phantom in multipinhole small-animal SPECT. J Nucl Med 52:1646-1653, 2011.

Submitted manuscripts

Harteveld AA, van der Kolk AG, van der Worp HB, Dieleman N, Zwanenburg JJ, Luijten PR, Hendrikse J. Detecting intracranial vessel wall lesions with 7T MRI: patients with posterior circulation ischemia vs healthy controls.

Harteveld AA, Denswil NP, Van Hecke W, Kuijf HJ, Vink A, Spliet WG, Daemen MJ, Luijten PR, Zwanenburg JJ, Hendrikse J, van der Kolk AG. Vessel wall thickness measurement of the circle of Willis using 7T MRI.

Lindenholz A, **Harteveld AA**, Zwanenburg JJM, Siero JCW, Hendrikse J. Comparison between 3T intracranial vessel wall MRI sequences.

Lindenholz A, van der Schaaf IC, van der Kolk AG, van der Worp HB, **Harteveld AA**, Kappelle LJ, Hendrikse J. High-resolution MR vessel wall imaging after intra-arterial treatment for acute ischemic stroke.

Dieleman N, van der Kolk AG, Frijns CJM, **Harteveld AA**, Zwanenburg JJM, Kuijf HJ, Lindenholz A, Kappelle LJ, Luijten PR, Hendrikse J. Intracranial vessel wall imaging in suspected cerebral vasculitis: diagnostic value and treatment effects at 3T & 7T MRI.

Conference presentations (first author only)

Harteveld AA, van der Kolk AG, van der Worp HB, Dieleman N, Luijten PR, Zwanenburg JJM, Hendrikse J. Detection of intracranial vessel wall lesions using 7T MRI: patients with posterior circulation ischemia versus healthy controls.

- *Oral power pitch presentation, 25th Annual Meeting International Society for Magnetic Resonance in Medicine 2017, Honolulu, Hawai'i, USA. ISMRM magna cum laude merit award.*

Harteveld AA, van der Kolk AG, Denswil NP, Siero JCW, Kuijf HJ, Vink A, Spliet WGM, Luijten PR, Daemen MJ, Zwanenburg JJM, J. Hendrikse. Vessel wall thickness measurements of the circle of Willis using 7T MRI.

- *Oral presentation, 24th Annual Meeting International Society for Magnetic Resonance in Medicine 2016, Singapore. ISMRM summa cum laude merit award.*

Harteveld AA, van der Kolk AG, van der Worp HB, Dieleman N, Siero JCW, Kuijf HJ, Frijns CJM, Luijten PR, Zwanenburg JJM, Hendrikse J. High-resolution intracranial vessel wall magnetic resonance imaging in an elderly asymptomatic population: comparison of 3T and 7T.

- *E-poster presentation, 24th Annual Meeting International Society for Magnetic Resonance in Medicine 2016, Singapore. ISMRM summa cum laude merit award.*
- *Poster presentation, 8th Annual Meeting ISMRM Benelux Chapter 2016, Eindhoven, the Netherlands.*

Harteveld AA, van der Kolk AG, van der Worp HB, Dieleman N, Visser F, Luijten PR, Zwanenburg JJM, Hendrikse J. Detection of intracranial vessel wall lesions in an elderly asymptomatic population using 7T MRI.

- *Poster presentation, 17th International Symposium on Atherosclerosis 2015, Amsterdam, the Netherlands.*
- *Oral presentation, 23th Annual Meeting International Society for Magnetic Resonance in Medicine 2015, Toronto, Canada.*
- *Power poster presentation, 7th Annual Meeting ISMRM Benelux Chapter 2015, Ghent, Belgium.*

Harteveld AA, Denswil NP, Siero JCW, Zwanenburg JJM, Vink A, Spliet WGM, Dieleman N, Luijten PR, Daemen MJ, Hendrikse J, van der Kolk AG. Quantitative MR imaging of *ex vivo* intracranial atherosclerotic plaques at 7.0 tesla.

- *Poster presentation, 23th Annual Meeting International Society for Magnetic Resonance in Medicine 2015, Toronto, Canada.*
- *Oral presentation, 26th International Workshop on Magnetic Resonance Angiography 2014, Rome, Italy. MRA Student Travel Award.*

Harteveld AA, Denswil NP, Siero JCW, Zwanenburg JJM, Vink A, Spliet WGM, Dieleman N, Luijten PR, Daemen MJ, Hendrikse J, van der Kolk AG. Ultrahigh-field quantitative MR imaging of ex vivo intracranial atherosclerotic plaques.

- *Poster presentation, 22th Annual Meeting International Society for Magnetic Resonance in Medicine 2014, Milan, Italy.*
- *Poster presentation, 6th Annual Meeting ISMRM Benelux Chapter 2014, Maastricht, the Netherlands.*
- *Poster presentation, 6th International Conference on Intracranial Atherosclerosis 2013, Houston, Texas, USA.*

Harteveld AA, Dieleman N, De Cocker LJ, Frijns CJ, Visser F, Luijten PR, Hendrikse J, van der Kolk AG.
High-resolution 7.0 tesla pre- and post-contrast time-of-flight MRA of intracranial perforators.

- *Poster presentation, 21th Annual Meeting & Exhibition International Society for Magnetic Resonance in Medicine 2013, Salt Lake City, Utah, USA. Nominated for 'Poster Prize Competition' at the High Field Study group meeting.*
- *Poster presentation, ISMRM Workshop on Ultra High Field MRI 2013, Noordwijk aan Zee, the Netherlands.*